Surface Science Studies of Adsorption and Reactivity of Pd (111) and Au-Pd (111)

Jonathan David Peter Counsell

School of Chemistry

Cardiff University

2010

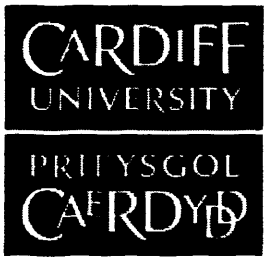

ProQuest LLC
789 East Eisenhower Parkway
P.O. Box 1346
Ann Arbor, MI 48106-1346

DECLARATION

This work has not previously been accepted in substance for any degree and is not concurrently submitted in candidature for any degree.

Signed ..... (candidate) Date 3/3/2010

STATEMENT 1

This thesis is ~~being~~ submitted in partial fulfilment of the requirements for the degree of PhD.

Signed ..... (candidate) Date 3/3/2010

STATEMENT 2

This thesis is the result of my own independent work/investigation, except where otherwise stated.

Other sources ~~are~~ acknowledged by explicit references.

Signed ..... (candidate) Date 3/3/2010

ACKNOWLEDGEMENTS

Firstly I would like to thank Professor Mike Bowker of Cardiff University for his assistance and insight throughout the course of my studies. His experience and enthusiasm for the subjects of surface science and industrial catalysis have been invaluable. Thanks also goes to Dr Albert Carley for his technical support and advice regarding UHV problems.

I would also like to thank BP Chemicals for providing the CASE award that helped to fund this project. The advice and support I received from my industrial supervisors Dr. Malcolm Cunnington and Dr Cliff Williams is also greatly appreciated, particularly in discussing the history of vinyl acetate synthesis, and the significance of gold in catalyst performance. In addition, this project was funded by the EPSRC and I am grateful for their support.

Props to everyone I shared -1.63(B) with; Marco, Dan, Dave, Bishop, Theo, Kareem and Lee. I will sorely miss the many and varied erudite discussions regarding love, life and surface science.

I also thank my Mum and Dad for the support and advice they have bestowed upon me for the past 26 years. Were it not for them, I would never have written this thesis. For housing and feeding me for the last nine months, a special thanks goes to Andy, Viv and David.

Lastly, I thank my darling wife Rhian. Her never-ending support, love, encouragement and belief in me made the experience a whole lot easier!

ABSTRACT

The adsorption, reaction and decomposition of a series of molecules (oxygen, ethylene, acetic acid, carbon monoxide and acetaldehyde) associated with vinyl acetate synthesis were investigated using a combination of ultra-high vacuum surface science techniques, including molecular beam sticking, x-ray photoelectron spectroscopy and temperature programmed desorption. The single crystal Pd (111) surface, bimetallic Au/Pd (111) surfaces prepared by metal vapour deposition and an alloyed $Au_{30}Pd_{70}$ (111) crystal were used in these studies. All the molecules investigated adsorbed onto the Pd (111) surface across a wide temperature range. Mechanisms for the reactions of each with the surface were suggested. The carbonaceous organic molecules all decomposed to deposit carbon at the surface at room temperature and above, blocking active sites to adsorption. Above a specific temperature, this carbon went subsurface and no longer inhibited subsequent adsorption of molecules. The deposited carbon could often be removed in a facile manner by oxygen treatment

Contents

Chapter Sections and their associated page numbers are described on the contents page at the beginning of each chapter.

1. Introduction

"History proves abundantly that pure science, undertaken without regard to applications to human needs, is usually ultimately of direct benefit to mankind"

Irving Langmuir

1.1 General Overview

The purpose of this chapter is to explain the importance of catalysis and its relationship with surface science. An introduction to surface properties and reactivity is described which should make the following chapters more accessible to those outside the surface science community. The motivation behind the research carried out concerns the industrial production of vinyl acetate. A background of its production and the various mechanistic theories related to its formation are detailed. Questions still remain concerning the true nature of its synthesis, highlighting the need for the subsequent studies.

1.2 Surface Science and Heterogeneous Catalysis

The role of surfaces in chemistry is fundamental and therefore plays a role in many aspects of modern life. A wide range of fields from semiconductors to photography employ surface science investigative techniques; however, this area has mainly developed in tandem with catalysis due to its importance in the chemical industry. The rates of chemical reaction can be accelerated by means of a catalyst. When a catalyst is introduced into a chemical process, it affects the kinetics of a reaction without having an effect on its equilibrium. It lowers the activation energy level for the reaction but does not have a significant effect on the overall energy of reaction. The catalyst is not consumed during the reaction process but is regenerated at the end. A reaction pathway scheme showing energy as a function of reaction coordinate, for the same reaction with and without a catalyst is shown in figure 1.1.

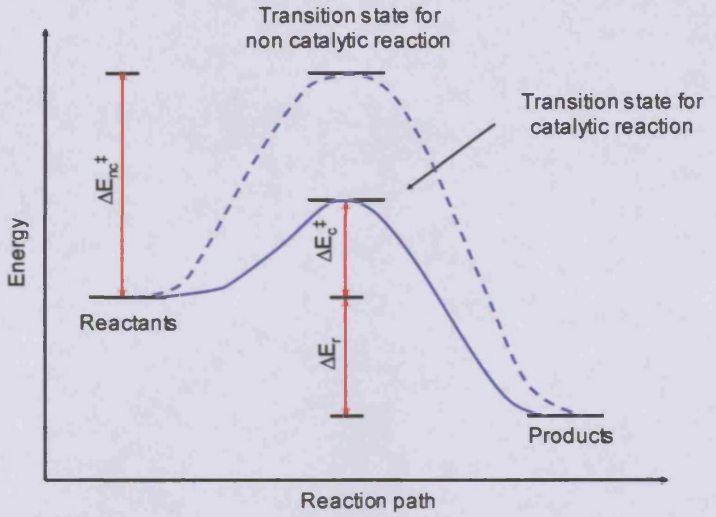

Figure 1.1 The effect of a catalyst is to lower the activation energy of a reaction

Catalysts can broadly be labelled as being either homogeneous or heterogeneous in nature. Surface science studies predominantly concern the latter whereby the reactants are in a different phase to the catalyst, which is a solid. The first applications of heterogeneous catalysis can be dated back to the beginning of the nineteenth century when Dőbereiner used a platinum surface to catalyse the reaction of H_2 and O_2 to create a source of light[1]. Another important early application of heterogeneous catalysis involved the development of the miners' safety lamp by H. Davy[2]. Davy carried out many studies regarding the reaction of coal gas and oxygen mixtures on hot platinum wires. A significant observation was that deactivation of the platinum catalyst occurred upon the formation of a carbide film on the wire. In more modern times, heterogeneous catalysts have been employed to manufacture simple molecules of industrial importance. One such example is the Haber process which uses finely divided iron as its catalyst[3]. Another example is in the production of margarine *via* the hydrogenation of vegetable oils using a nickel catalyst. Another significant catalytic development has been to reduce air pollution caused by car engines. Catalytic converters are now fitted as part of a car's exhaust and help to cut

down on polluting emissions *via* a three-way process. A single monolith supporting platinum, palladium, rhodium and ceria enables the system to oxidise CO to CO_2, reduce NO_X to N_2 and oxidises any remaining hydrocarbons, forming CO_2 and H_2O.

The focus of research in surface science has reflected the advances in the disciplines of ultra-high vacuum (UHV) and solid state physics over the past hundred years. Langmuir performed the first investigations on tungsten filaments and greatly improved the diffusion pump which lead the way towards the creation of ultra high-vacuum chambers. He also carried out experiments regarding atomic and molecular adsorption, relating the surface coverage of adsorbed gas and gas pressure at a given temperature - the Langmuir isotherm[4]. Langmuir also defined dissociative chemisorption[5] and developed the Langmuir-Hinshelwood mechanism for the bimolecular reaction of adsorbates[6,7]. Further developments followed including the Rideal-Eley mechanism and the definitions of physisorption, chemisorption and activated adsorption[8-11]. These early developments, amongst others, allowed the foundations of surface science to be built. The impressive extent of advances in this field has allowed scientists to study model surfaces such as single crystals and nano-particulate arrays on an atomic scale. Surface science techniques have been used to complement macroscopic analysis of catalytic activity, selectivity and durability by yielding useful information regarding molecular and atomic processes on the surface. Processes such as adsorption and desorption, reaction and decomposition, and diffusion of surface species have helped explain macroscopic phenomena. Surface studies have been carried out on a wide range of different catalytic systems. The nature of the Haber process on the molecular level has been investigated from a surface science perspective helping elucidate the reaction mechanism and pinpoint the dissociation of adsorbed N_2 as the rate-determining step[12-14]. Our knowledge of

molecular processes has helped improve various other systems including the catalytic converter and has explained the role of chlorine in ethylene oxidation[15].

Much of the history of the twentieth century would have been very different if it were not for the developments in heterogeneous catalysis. Both the Haber and Fisher-Tropsch processes allowed Germany to mass produce explosives and liquid fuel in World War I and II respectively. In fact, many historians believe both wars would have been considerably shortened if it was not for the development of these new technologies. Despite this unfortunate history, the benefits have been extensive. Much less energy is now consumed in the production of heavy chemicals and automotive pollution has been greatly reduced. Since nowadays more than 90% of all chemical manufacturing uses catalysts, it is more important now than ever to investigate the fundamental surface processes taking place.

1.3 Reactions on Surfaces

In order to understand surface adsorption and reactivity, it is important to understand the nature of the clean surface. It is possible to grow many metals and semiconductors as single crystals, and when these crystals are cut in specific orientations, surfaces of very high crystallographic order can be revealed. These surfaces contain specific binding sites which allow investigations into how molecules bind in certain orientations. With respect to catalysts, this may seem an over simplification; however when metal nanoparticles form on the surface of a catalyst, terraces of ordered low energy faces tend to be exposed. The atoms in a metal are normally arranged in the form of a cubic structure. The most common structures are presented below in figure 1.2. For metals such as platinum, copper and palladium, the

normal crystal structure is face-centred cubic (fcc). Each atom in this configuration has twelve nearest neighbours. Metals such as iron adopt a more open body-centred cubic (bcc) structure with each atom having eight neighbours.

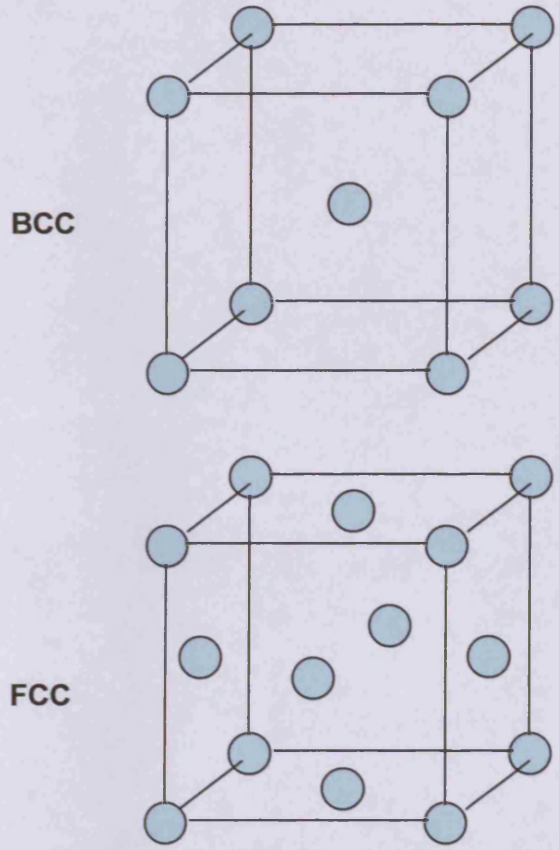

Figure 1.2 A representation of the fcc and bcc structures

When a bulk crystal undergoes cleavage, a particular surface plane is exposed. In order to define the exposed surface face, miller indices are used which are directly related to the positions of the atoms in the bulk lattice. Surface studies are commonly carried out on low indexed faces as they have the most ordered structures and offer the fewest number of adsorption sites therefore providing the simplest and flattest systems for analysis. The three most commonly studied surfaces are the (100), (110) and the (111) surface. These low-index planes are displayed in figure 1.3 for both the

fcc and bcc lattices.

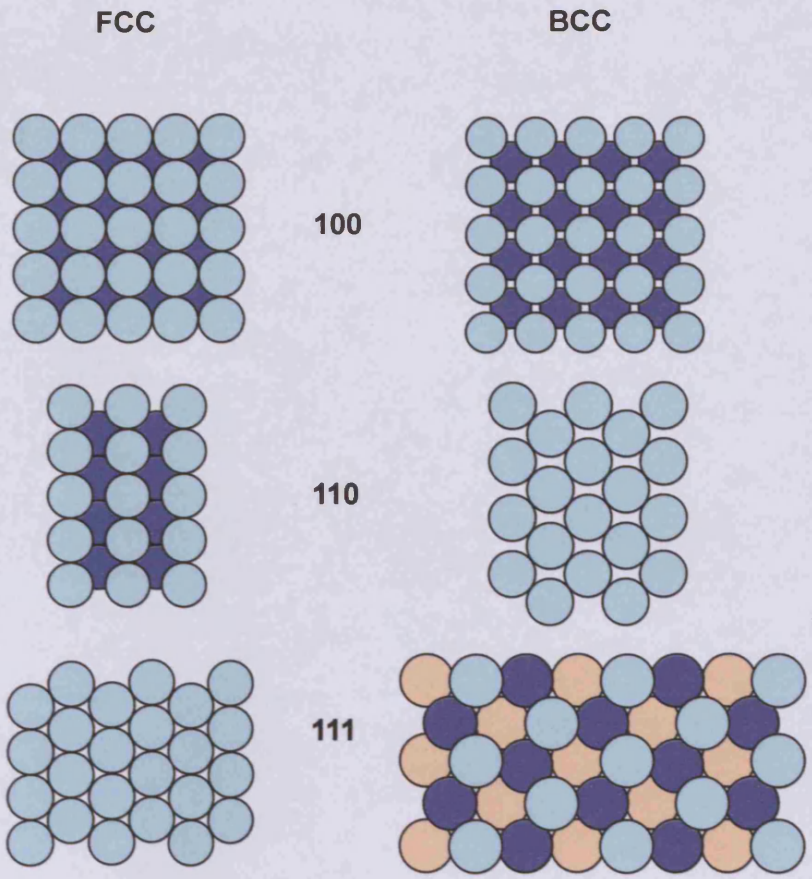

Figure 1.3 (100), (110) and (111) surface configurations for (a) fcc and (b) bcc crystal structures

For the surfaces of fcc crystals, it is possible to see several different binding sites for adsorbing molecules. On the (100) surface, bonding may occur on top of an atom (one-fold), bridging two adjacent atoms (two-fold) or in a hollow (four-fold). The bonding number denotes the number of surface atoms the adsorbate is coordinated to. Similarly on the (111) surface, one two and three-fold bonding may occur. The (110) surface displays two different types of two-fold bonding, one between atoms in the same row, another longer site between atoms in adjacent rows. Due to the occurrence of different sites, the way in which molecules bond and behave

changes from one surface to another. Thus, the arrangement of atoms on a surface has a direct effect on the activity, reactivity and selectivity of a reactant. For the bcc system the (111) surface is the most open and consequently the most reactive however for the fcc system the opposite is the case.

When an atom or molecule collides with a surface, several different processes may occur. It may rebound off the surface, being either elastically or inelastically scattered, or it may be retained. When the species is retained by the surface, it may be held in a weakly bound state known as physisorption or in a much stronger chemically bonded state known as chemisorption. Physisorption is based upon the balance between weak attractive van der Waals forces between the surface and adsorbate and repulsive forces due to close contact. The electron density of the two species, the molecule and the surface, remains separate with no exchange of electrons between the gas molecule and the surface, therefore no chemical bond is present. When a molecule undergoes physisorption, the interactions between adsorbates is often more significant than the between adsorbates and the surface. When chemisorption occurs, electrons are exchanged between the adsorbate and the surface. This results in the formation of strong bonds which are stable to elevated temperatures. Due to these greater surface interactions, chemisorption displays much more surface specificity resulting in different adsorption strengths depending on what face is exposed.

Chemisorption of a molecule may result in either dissociative or non-dissociative adsorption. Non-dissociative adsorption involves the formation of surface -substrate bonds with all interatomic bonds still intact whereas dissociative adsorption describes the process whereby the adsorbate bonds break up upon bonding to the surface. Dissociative chemisorption may occur in two forms either activated or non-activated. Figure 1.4 shows the potential energy curve for a molecule as a

function of the distance between the surface and the adsorbate. As the molecule approaches the surface it becomes physisorbed into a chemisorption precursor state. A potential energy barrier exists between this precursor and the chemisorbed state due to the deformation of the adsorbate bond and rearrangement of the substrate atoms. Non-activated chemisorption occurs when the energy barrier between the precursor and the chemisorbed state is below the energy zero reference axis, meaning the process is likely to be rapid (figure 1.4a). This is because no additional energy is needed for the system to pass into the dissociated chemisorbed state. For activated chemisorption the energy barrier (E_a) is large enough to lie above the zero energy axis (figure 1.4b) resulting in a slower reaction due to the absence of sufficient energy.

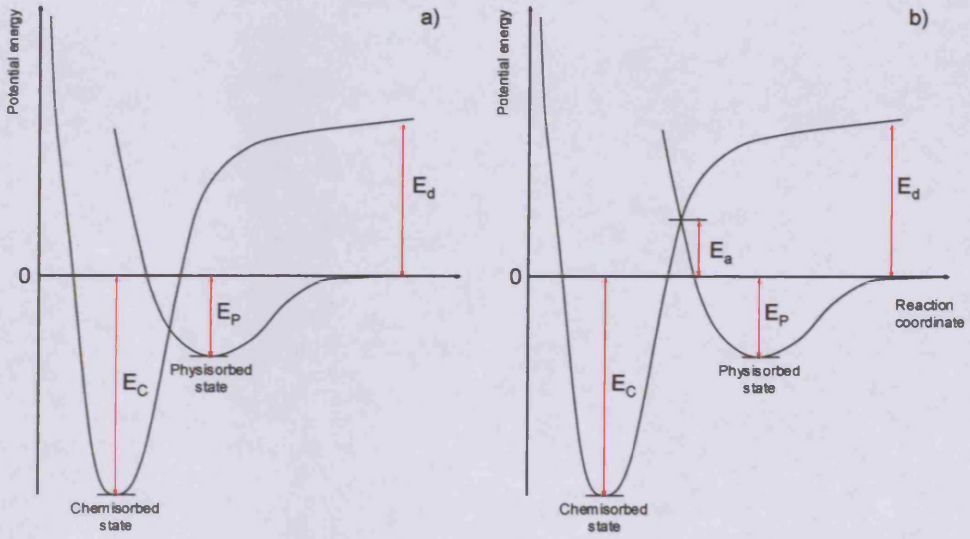

Fig 1.4 Potential energy *vs* reaction coordinate diagrams for a) non-activated chemisorption and b) activated chemisorption processes

1.4 Background of Vinyl Acetate synthesis

Vinyl acetate is an unsaturated ester with the chemical formula $CH_3COOCH{=}CH_2$. It is a versatile and economically important chemical with a wide variety of industrial and commercial applications. It is commonly referred to as VAM (vinyl acetate monomer) since it is widely used in the polymer industry. It homopolymerises readily to form polyvinyl acetate (PVA) when treated with light or free radicals. VAM is also used with other organic compounds such as ethylene, acrylate, vinyl alcohol, vinyl ester and vinyl chloride to produce copolymers. These polymers have a variety of commercial applications including the production of building materials, adhesives, cosmetics, pesticides and even as a constituent for chewing gum bases[16]. VAM is also used in the synthesis of several drugs and as an agent in some acetylation reactions. Examples of polymers derived from VAM and their uses are shown below in figure 1.5. In 2007, 5 million metric tonnes of VAM was synthesised utilizing 78% of global capacity. Polyvinyl acetate accounted for over 45% of global VAM consumption. The production of polyvinyl alcohol also consumed around 38% of VAM with and ethylene-vinyl acetate copolymers using around 9%. Market development of VAM is growing at a rate of ~3% per year and is expected to continue until at least 2014 due to the demand in the far east[17].

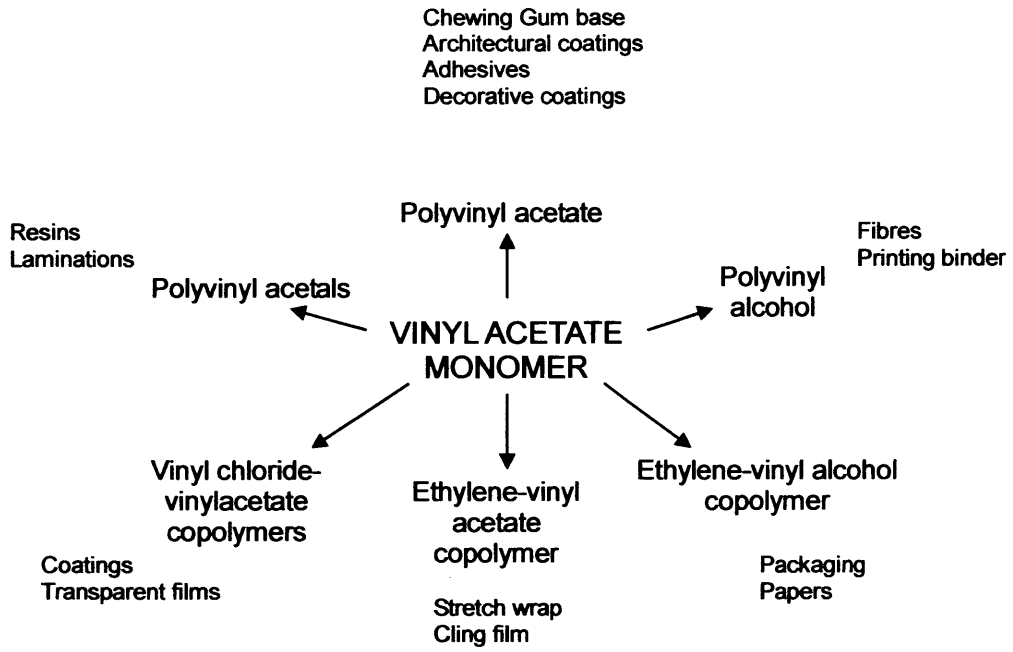

Figure 1.5 Spider diagram showing the main polymers derived from VAM with their industrial and commercial uses

VAM was initially synthesised by the reaction of acetylene and acetic acid[18]. This was originally developed by Klatte in a homogeneous liquid phase reaction using Hg sulphate[19]. This process was developed by Wacker using Zn acetate on a carbon support[20], and was found to be cheap and easy to control with a very high selectivity and a VAM yield of 97%. In more recent times, VAM has been produced *via* the acetoxylation of ethylene with acetic acid[21-23]. Due to the lower feedstock and conversion costs of ethylene derived from natural gas, this reaction has become much more favourable industrially. The various reactions are summarised below in figure 1.6

Method	Description
Klatte (1912)	Acetylene + Acetic Acid → VAM Mercurous Sulphate / Acid solution 333 - 373K Low Yield
Moiseev (1960)	Ethylene + Acetic Acid + Oxygen → VAM + Water Homogeneous Liquid Phase 30:70 Ethylene : Oxygen Acetic Acid / Na or K Acetate / Cu (I) : Cu (II) slurry 353 - 423K 70 - 90% Yield
Vapour Phase (1968)	Ethylene + Acetic Acid + Oxygen → VAM + Water Heterogeneous Pd/C catalyst Vapour Phase ~423K 5 atm 91 - 95% Yield CO and Acetaldehyde main by-products

Figure 1.6 The three known methods for VAM synthesis

The latter reaction is of interest to this thesis and was first performed by Moiseev[21]. It involved a 'Wacker-like' liquid phase synthesis of VAM using Pd (II) and Cu (I) and (II) chlorides in the presence of a sodium acetate promoter. The equations below show the role of Pd and Cu in the process.

$$Pd^{2+} + 2CH_3COO^- + C_2H_4 \rightarrow CH_3COOCH{=}CH_2 + Pd\ (0) + CH_3COOOH$$

$$Pd\ (0) + 2Cu^{2+} \rightarrow 2Cu^{+} + Pd^{2+}$$

This process had a 90% selectivity towards VAM with acetaldehyde and ethylidene diacetate as the major by-products. Chloride free catalysts were later developed which improved the overall reactivity by overcoming by-product poisoning and catalyst corrosion problems caused by chloride ions[24]. Since then, a more favourable and simpler heterogeneous 'solid-gas phase' has been developed which

minimises by-product formation and catalyst corrosion.

The heterogeneous process usually uses Pd metal as the catalyst, sometimes alloyed with Au or Cd, and is the primary method for producing VAM today[25-26]. Numerous studies have been carried out alloying Pd with various other metals such as Pt, Ni, Ag, Ru and Rh. However Au has been shown to be the most favourable due to its greater selectivity towards VAM synthesis[27-29]. Most industrial fixed bed reactors operate at around 440K and 4-11 atmospheres overpressure[30-31]. The reactant composition is normally 65% ethylene, 35% acetic acid, 8% oxygen and 2% nitrogen. The reason for the inert gas and low oxygen composition is due to the explosive nature of the oxygen-ethylene mixture. The lower explosion limit may however be increased by adding methane into the feed stream, allowing oxygen to be increased, thereby increasing the space-time yield of VAM[32]. This system is highly selective towards VAM synthesis with a yield of between 90 – 96%. The main by-products have tended to be carbon dioxide, acetic anhydride and acetaldehyde.

Pd/Au catalysts were developed by Bayer and Hoescht[26,33] and later by DuPont[34] and consisted of 'egg-shell type' Pd/Au nanoparticles. The weight loading is usually 0.5 – 2% Pd; 0.2 – 1.2% Au and 1 – 4% potassium acetate, with these metals dosed on a metal oxide support. Various different supports have been studied including silica[33,34], alumina[35], titania[36] and metal silicates[37,38]. The most favourable of these supports is silica used in the form of small pellets of high surface area. Its popularity is partly due to its relatively inert chemical behaviour. The added Au and potassium acetate act as moderators and promoters to the catalytic reaction, improving factors such as catalyst durability, selectivity and activity towards VAM synthesis[39].

The exact nature of the relationship between Pd, Au and potassium acetate is not fully understood, nor is the surface environment of the surface of the catalyst.

1.5 Mechanistic Theories

The synthetic mechanism of how VAM forms *via* the acetoxylation of ethylene is still not fully understood. There have been many studies carried out in recent times concerning this system, most of which have tried to answer some of the questions listed below:

- What surface intermediates are present in the mechanistic cycle?
- How does Au affect the catalytic properties of Pd?
- How are by-products formed in these mechanisms?
- What is the oxidation state of the Pd catalytic particles?
- What is the nature of the active catalytic sites with respect to size and structure?

Most of the research carried out has been undertaken on 'real' systems under conditions similar to those found in the industrial manufacturing process. These studies have involved the use of Pd supported catalysts with and without Au doping. There have also been studies carried out on model single crystal surfaces looking at the fundamental interactions between different reactant molecules and the metal. Unfortunately none of these studies have successfully managed to conclusively produce VAM under UHV conditions. Two basic schools of thought exist regarding the overall mechanism. These can be described by their disagreement over the exact phase in which catalysis occurs. In the first proposed mechanism, the Pd metal

particles remain metallic in nature throughout. This involves Pd atoms staying in the (0) oxidation state and can be described as occurring in the solid-gas phase i.e. heterogeneous. The other opposing theory includes the formation of Pd acetate particles as catalytic centres. This process can be described as being in a pseudo-liquid phase *i.e.* homogeneous in nature. The oxidation states of the Pd atom centres has been proposed to be either (0), (I) or (II). Despite the apparent differences between the three states, other mechanisms have been proposed which propose a mixture of the all three oxidation states. Each hypothesis will be briefly discussed in order to give a general overview of the current theories.

1.5.1 *Solid-Gas phase mechanism:*

Moiseev reported that the active site consisted of Pd metal centres that remained in the same oxidation state throughout the mechanism[21]. The rate determining step was activation of a C-H bond in ethylene producing a vinyl intermediate which reacts rapidly with an adsorbed acetate surface species to produce VAM. A simple schematic of this process is displayed below in figure 1.7

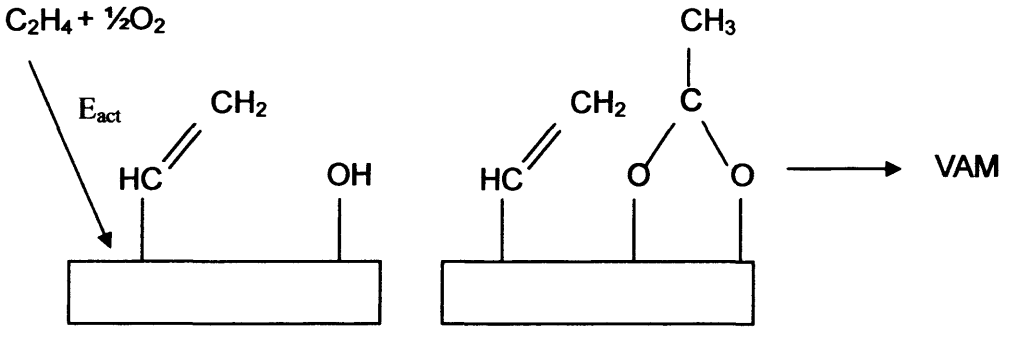

Figure 1.7 Diagram showing VAM formation via a heterogeneous mechanism first proposed by Moiseev[21]

1.5.2 *Pseudo-liquid phase mechanism:*

Nakamura initially investigated the gas phase reaction of propene, oxygen and acetic acid on metallic Pd[40,41]. Their results implied that a Pd (II) 'pseudo-liquid phase' mechanism was occurring involving the formation of iso-propenyl acetate, n-propenyl acetate and allyl acetate. However, in the gas phase reaction, allyl acetate is the only product. This led them to propose the following mechanism for VAM synthesis. In this mechanism, the active intermediate would seem to be a Pd (I) acetate complex:

$C_2H_4 + 2Pd \leftrightarrow CH_2\text{-}CH\text{-}Pd + PdH$

$O_2 + 2Pd \leftrightarrow 2Pd\text{-}O$

$CH_3COOH + Pd \leftrightarrow Pd\text{-}CH_3COOH$

$Pd\text{-}CH_3COOH + Pd\text{-}O \leftrightarrow Pd\text{-}O\text{-}COCH_3 + PdOH$

$Pd\text{-}O\text{-}COCH_3 + CH_2\text{-}CH\text{-}Pd \leftrightarrow Pd\text{-}CH_2CHOCOCH_3 + Pd$

$Pd\text{-}CH_2CHOCOCH_3 \leftrightarrow Pd + CH_2CHOCOCH_3$

$Pd\text{-}OH + Pd\text{-}H \leftrightarrow Pd\text{-}OH_2 + Pd$

$Pd\text{-}OH_2 \leftrightarrow Pd + H_2O$

This mechanism suggests that dissociatively adsorbed ethylene and acetic acid combine to give Pd-vinyl and Pd-acetate species which form vinyl acetate in the gas phase. Both starting materials dissociate by H abstraction and are thus active. In the case of acetic acid this requires the presence of dissociated oxygen. Potassium from K acetate acts as a promoter by facilitating the abstraction of H from acetic acid, and reducing the chemisorption strength in Pd acetate. Secondary reactions producing combustion products from vinyl and acetate groups have also been devised showing

the production of CO_2 and H_2O by-products:

$$Pd\text{-}O + Pd\text{-}O\text{-}COCH_3 \rightarrow Pd\text{-}OH_2 + Pd\text{-}O\text{-}CO + CH$$

$$Pd\text{-}OH_2 + Pd\text{-}O\text{-}CO \rightarrow 2Pd + H_2O + CO_2$$

Nakamura also stated that Pd (II) acetate only formed during this mechanism when both an excess of acetate was present with respect to ethylene and the reaction was carried out at low temperatures[41]. The presence of Pd (II) acetate was thus considered to be a poison of the Pd catalyst and had no role in VAM production. The nature of ethylene adsorption was also considered. Previous studies of acetylene on VAM synthesis catalysts have shown a surface species to decompose causing poisoning of the catalyst. This is thought to occur after acetylene binds to the surface as a bidentate Pd-CH=CH-Pd adsorbate[42]. Since ethylene was not seen to poison the VAM catalyst even after 100hrs of exposure, it was proposed that it binds instead as a monodentate vinyl group rather than in a bidentate fashion.

Another theory proposed by Samanos[43] and Zaidi[44] suggests that Pd in fact exists in the Pd (II) oxidation state in the active catalyst. This is in principle very similar to the Pd salt catalysed 'Wacker-like' homogeneous process mentioned previously[20,21]. It is not totally clear how VAM was produced in this homogeneous process, however the following mechanism has been suggested[45,46]

$$C_2H_4 + PdCl_2 + HCl \rightarrow [C_2H_4PdCl_3]^- + H^+$$

$$[C_2H_4PdCl_3]^- + AcOH \rightarrow [C_2H_4PdCl_2(OAc)]^- + Hcl$$

$$[C_2H_4PdCl_2(OAc)]^- \rightarrow [C_2H_4PdCl(OAc)]^- + Cl^-$$

$$[C_2H_4PdCl(OAc)]^- \rightarrow CH_2CH\text{-}OAc + Pd + HCl$$

In this system, Pd^{2+} is provided by Pd (II) chloride. However, in the heterogeneous synthesis it was proposed that the oxidation of finely divided Pd metal to Pd (II) acetate provided the Pd^{2+}:

$$Pd + \tfrac{1}{2}O_2 + 2CH_3COOH \rightarrow Pd\text{-}(OOCCH_3)_2 + H_2O$$

$$Pd\text{-}(OOCCH_3)_2 + OOCCH_3^- \rightarrow Pd\text{-}(OOCCH_3)_3^-$$

$$Pd\text{-}(OOCCH_3)_3^- + 2C_2H_4 + \rightarrow VAM + CH_3COOH + CH_3COO^-$$

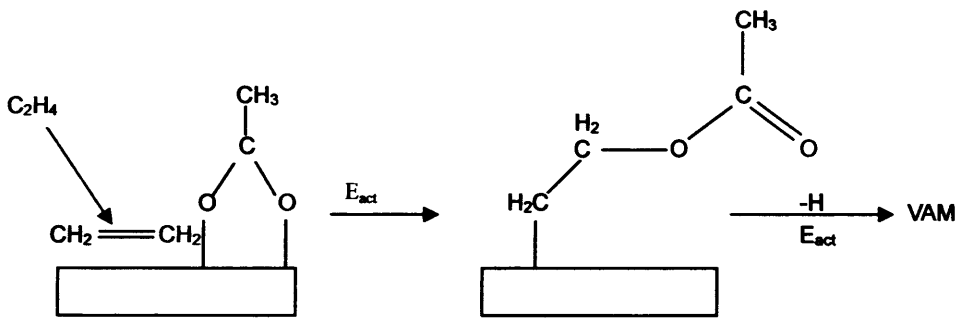

Figure 1.8 Coupling of ethylene with chemisorbed acetate

Figure 1.8 above shows mechanism proposed by Samanos for VAM production[43]. This reaction scheme differs from that which was proposed by Nakamura because Pd (II) acetate reacts with gaseous ethylene to produce VAM rather than reacting with a Pd-vinyl intermediate. Much evidence has been reported showing the existence of a thick multilayer of adsorbed acetic acid on the surface of the catalyst under reactor conditions[43,47]. A 3ML thick layer was also seen using isotopic transient kinetic studies and TPD on Pd/Cd and Pd/Au silica supported catalysts[48]. The presence of alkali metal acetate has been shown to enhance the adsorption of acetic acid[49]. KOAc forms a dimer with acetic acid which immobilises it. This has been shown to lower the activation energy for VAM formation, increasing

the overall rate of production. Under these conditions, it is unlikely that adjacent Pd metal sites would be available for the mechanism proposed by Nakamura to occur. Studies using DRIFTS-MS have also indicated Pd (II) acetate to be present as a reaction intermediate[47]. Using a KCl matrix, this intermediate was seen to react with oxygen and ethylene to give VAM and acetic acid at 413-443K. Kinetic studies also showed the order of reaction with respect to acetic acid to be zero, suggesting it is in much greater excess. This differs from previous studies carried out by both Samanos[43] and Nakamura[40]. DFT has also been employed to study this mechanism, examining the interactions of VAM reactants with Pd-18[50]. VAM production was seen to be feasible and produced data regarding the energies of reaction which was very similar to real reactor data. The RDS in this model seems to be the cleavage of the C-H bond via the β-hydride mechanism to form VAM. This involves the reaction of Pd-O surface species with the cleaved H atom to form Pd-OH. This is different to the RDS proposed earlier by Samanos who thought the RDS was the insertion of ethylene into the acetate intermediate[43].

Other studies also support the existence of only gas phase ethylene stating that in the oxidising conditions present, residence times of ethylene would be very short[47]. C-H stretches due to ethylene were not observed in DRIFTS spectra for VAM synthesis on silica supported Pd. Dissociative adsorption of ethylene is unlikely to occur in VAM synthesis, as in UHV, since it would be readily oxidised to combustion products with co-adsorbed oxygen[51].

1.5.3 *Combination of both mechanisms*

Catalytic studies on Pd/α-Al_2O_3 catalysts reported that the ratio of VAM product to catalyst is less than 1 in 40 indicating that most Pd metal atoms do not take part in the reaction[47]. Also, somewhat surprisingly, the activity of the catalyst was found to be at a maximum when the Pd is metallic in nature, and hence not very well dispersed[43]. In fact, minimum activity was found in the regions of lowest metallic nature. It was thus proposed that in fact the active phase is a combination of Pd (0-2) in the form of Pd (I) and Pd (II) islands on Pd (0) metal and Pd oxide.

1.6 Bimetallic Catalysis with Gold

All of the above theories regarding the formation of VAM relate to a monometallic system. In the industrial process however, the production of VAM relies on a bimetallic catalyst. The addition of Au to the already catalytically active Pd introduces valuable new properties, including improved selectivity, longevity and activity. These changes occur *via* the modification of surface electronic properties (ligand effect) or geometric properties (ensemble effect). Not all catalyst particles form alloys in bimetallic cluster systems - Ru/Au supported catalysts were found to be immiscible[52]. However the Au/Pd system employed here has been found to be miscible even at comparatively low temperatures[53]. In a bimetallic alloy, the surface composition can be very different to that in the bulk. This can have a direct effect on the catalysed adsorption and surface reactions. The component with the lower surface free energy and sublimation energy will tend to segregate to the surface and enrich the top few atomic layers. In the case of Au/Pd, in which the metals have similar atomic

radii, Au has the lower surface free energy and would be expected to enrich the surface. This has indeed been confirmed using a variety of techniques[54,55].

The addition of Au, which has a low activity as a bulk metal, to an active metal ensemble can reduce the activity. These changes may be positive or negative depending on the system. The oxidation of ethylene on Pd and Pd/Au alloys is a good example of Au suppressing surface reactivity[56,57]. On clean Pd, ethylene undergoes complete oxidation to CO_2 and H_2O on two adjacent Pd atoms. The addition of Au dilutes the concentration of Pd sites improving the partial oxidation pathways to acetic acid, acetaldehyde and acetic anhydride, which only requires isolated Pd atoms.

Model catalyst studies carried out on Pd/Au (100) and Pd/Au (111) surfaces by Goodman *et al* have shown that the main role of Au is to isolate Pd monomer sites[58]. These isolated Pd monomer sites were found to be more active for the acetoxylation reaction compared to contiguous sites. The rate of formation of VAM was examined for both surfaces at 453K with pressures of acetic acid, ethylene and oxygen of 4, 8 and 2 torr respectively[59]. The Pd/Au (100) surface was seen to be the most active, with a maximum rate of production (TOF) at 0.07ML coverage indicating that a pair of non-contiguous Pd atoms is the most catalytically effective configuration. The rate of VAM production was seen to decrease as the Pd coverage increased on Pd/Au (111). By modelling the adsorption of both ethylenic species and acetate on Pd sites, the optimum distance between two atoms for the coupling reaction to take place was calculated to be ~3.3Å. On the Pd/Au (100) and (111) surfaces, the spacing between two neighbouring monomers was seen to be 4.08Å and 4.99Å respectively. For the (100) surface, this distance was considered acceptably close for the coupling reaction to take place. The distance on the (111) surface is much greater than the ideal value of

3.3Å and was therefore deemed less effective at VAM production[60]. These studies indicate the role of Au in the industrial catalyst to be to isolate Pd atoms into certain geometries which promote the coupling of adsorbed acetic acid and ethylene. By isolating this reaction, the formation of other undesirable surface species and by-products is also suppressed. The effect of Au on the coupling of acetylene to benzene on the Pd (111) surface has also shown up a significant ensemble effect[61]. A surface composition of ~85% Pd was shown to be the most active catalytically, indicating that the activity does not correlate with the number of single Pd atoms. This implies that the activity is dominated by the presence of Pd_7 and Pd_6Au ensembles. A major role of Au was also to lower the desorption temperature of benzene, a rate-limiting step in this system.

The effect of ageing Pd-Au-K/SiO2 catalysts has also been investigated with a variety of techniques[62]. A fresh catalyst showed Pd to exist in both a highly dispersed form and as a alloyed particle alloyed with Au. After using the catalyst, sintering of the Pd/Au particles was observed as was the presence of a Pd acetate compound. Since there was no change in the composition of the Pd/Au particles, it was assumed that the Pd acetate species played no role in the sintering process. Fixed bed and TAP reactors have been used to study the effect of Au and KOAc on the reaction pathways associated with VAM synthesis[39]. Au was seen to suppress the combustion of acetic acid to CO and enhance the formation of VAM.

There are also several schools of thought as to the electronic behaviour of Pd/Au alloys. Bulk Au has a filled d-band and a half filled valence s-band, and it had been proposed that the Pd 4d-band overlaps with the Au 6s-band to form an alloy composite structure[63]. Also it has been suggested that in excited states Pd metal has a

partially occupied d-band containing 0.6 holes per Pd atom[53]. In the alloy, Au s-electrons will shift to the unoccupied states in the Pd d-band. Hence it might be expected that at an Au: Pd ratio of about 3:2, the d-band will be filled and the catalytic properties would alter markedly. This hypothesis was supported in experiments involving conversion of para- to ortho-hydrogen on such surfaces[64]. However, the surface and bulk compositions can be very different, and the alloy composition and structure may change considerably during treatment and analysis. Hence models which consider both the surface and bulk were proposed[65]. However, it has been suggested that there is not a direct correlation between extent of d-band occupancy by Au content, and catalytic activity. Also, the electronic structure of the Pd and Au atoms may remain virtually unchanged in the alloys, implying only local electronic effects in these systems[66].

1.7 Thesis Synopsis

The experiments described in this thesis primarily deal with the adsorption, decomposition and reaction of small organic molecules related to the production of vinyl acetate. The overall aim is to develop a greater understanding of the molecular processes taking place on the surface of the industrial catalyst. This can be done by characterising possible surface intermediates and developing reaction mechanisms. Using surface science techniques and UHV conditions, the aim is to study the effects of gold on the reactivity palladium surface.

This chapter has provided an overview of heterogeneous catalysis and surface science. The history of vinyl acetate synthesis and the various theories considering the role of Au in the catalyst has also been provided, hopefully providing sufficient

background knowledge to enable the reader to fully appreciate the following chapters. Chapter 2 describes the nature of the UHV chamber used in theses studies and the reasons why such low experimental pressures are necessary. Background theory of the different surface techniques is also discussed highlighting both their uses and limitations. Chapter 3 will examine the reactivity of the clean Pd (111) surface towards various molecules related to vinyl acetate production including starting materials and by-products. Different surface temperatures are studied as well as oxidation reactions. Chapter 4 deals with the nature of the growth of Au as it is deposited onto the clean surface. The effect of heating on deposited Au over-layers and the change in their composition is discussed. These studies have particular relevance to chapter 5, where the effect of Au on the surface reactivity of Pd (111) is explored. The change in surface reactivity was studied at a number of different Au coverages for all the molecules examined in chapter 3. Chapter 6 gives a summary and general conclusion to the findings of chapters 3 to 5.

1.7 References

1. J. W. Döbereiner, *Ann. Phys.*, **72** (1822) 193
2. H. Davy, *Phil. Trans. R Soc.*, **107** (1817) 77
3. F. Haber, *Nature.* **111** (1923) 101
4. I. Langmuir, *J. Chem.Soc.*, **38** (1916) 2221
5. I. Langmuir, *J. Chem. Soc.*, **34** (1912) 1310
6. I. Langmuir, *Trans. Faraday. Soc.*, **17** (1922) 607 & 621
7. C. N. Hinshelwood, *Annual Reports Chemical Society London*, **24** (1928) 335

8. D. D. Eley, E.K. Rideal, *Nature.*, **146** (1940) 401

9. D. D. Eley, E.K. Rideal, *Proc. R. Soc.*, **A178** (1941) 429

10. H. S. Taylor, *J. Am. Chem. Soc.*, **53** (1931) 578

11. J. E. Lennard-Jones, *Trans. Faraday. Soc.*, **28** (1932) 333

12. F. Bozso, G. Ertl, M. Grunze, M. Weiss. *J. Catal.*, **49** (1977) 18

13. R. Imbihl, R. J. Behm, G. Ertl, W. Moritz. *Surf. Sci.*, **123** (1982) 129

14. G. Ertl, S. B. Lee, M. Weiss *Surf. Sci.*, **114** (1982) 515

15. C. T. Campbell, *Appl. Surf. Sci.*, **19** (1984) 32

16. US Patent No. 5837302 (1998)

17. SRI Consulting Report (2009)

18. Ullman's Encyclopedia of Industrial Chemistry, 40 vols, 6th edition, Wiley. VCH, New York.

19. F. Klatte, US Patent No. 1084581 (1914)

20. S. J. Wacker, *J. Am. Chem.. Soc.*, **60** (1938) 440

21. I. I. Moiseev, M. N.Vargaftic, Y. K. Syrkin, *Dokl. Akad. Nauk. SSSR.*, **133** (1960) 377.

22. Imperial Chemical Industries Co. Patent Nos. 964001, 969162, 975683, 75709, 1026594, 1061788. Also *Chem. Week* **101** (1967) 73.

23. W. D. Shaeffer, Union Oil Co. of California, US Patent Nos, 3260739, 3253020.

24. W. D. Shaeffer, US Patent No. 3221045

25. British Patent No. 1521652, US Patent No. 3775342

26. British Patent No. 1220180, US Patent No. 3658888

27. British Patent No. 1146731

28. British Patent Nos. 1103125, 1107495, 1235632, US Patent No. 34322544

29. L. A. Sokolova, N. M. Popova, V. K. Eritsyan, B. S. Mukanova, V. K. Boyadzhyan, S. S. Khachatryan, *Izv. Akad. Nauk Kaz. SSR, Ser. Khim.* **28** (1978) 57.

30. US Patent No. 4902823

31. EP Patent No. 403950

32. G. M. Severs Jr. *Ger. Offen.* 2 3 61 098 (1974)

33. *World Pet. Cong. Proc.* **5** (1968) 41

34. US Patent No. 4048096

35. National Distillers, Ger. Offen. 1 9 44 933 (1970)

36. Grace & Co. Corp., British Patent No., 1183672 (1967)

37. T Saito, M. Takano, S. Moriyama, H. Murayama, *Jap. Kokai*, **73** (1973) 711

38. British Patent No., 1128993

39. W. D. Provine, G. W. Mills, J. J. Lerou, *Studies in Surface Science & Catalysis*, **101** (1996) 191.

40. S. Nakamura, T. Yasui, *J. Catal.*, **17** (1970) 366.

41. S. Nakamura, T. Yasui, *J. Catal.*, **23** (1971) 315.

42. L. H. Little, N. Sheppard, P. J. C. Yates, *Proc. Roy. Soc*, **242** (1960) A259.

43. B. Samanos, P. Boutry, R. Montarnal, *J. Catal.*, **23** (1971) 19

44. S. A. H. Zaidi, *Appl. Catal.*, **38** (1988) 353

45. C. R.Reilly, J. J. Lerou, *Catal. Today.*, **41** (1998) 433

46. G. S. Grover, R. V. Chaudharu, *Chem. Eng.*, **32** (1986) 93.

47. S. M. Augustine, J. P. Blitz, *J. Catal.* **17** (1970) 366

48. E. A. Crathorne, D. Macgowan, S. R. Morris, A. P. Rawlinson, *J. Catal.* **149** (1994) 254

49. Handbook of Chemistry and Physics, 48th ed., Chemical Rubber Company,

1967

50. M. Neurock, W. D. Provine, D. A. Dixon, G. W. Coulston, J. J. Lerou, R. A. van Santen, *Chem. Eng. Sci.*, **51** (1996) 1691.

51. R. J. Madix, E. M. Stuve, *Surf. Sci.*, **160** (1985) 293

52. J. H. Sinfelt, *J. Catal.*, **29** (1973) 233

53. E. G. Allison, G. C. Bond, *Cat. Rev.*, 7 (1972) 233

54. G. Maire, L. Hilaire, P. Legare, F. G. Gault, A. O'Cinneide, *J. Catal.*, **44** (1976) 293.

55. Jablonski, S. H. Overbury, G. A. Somorjai, *Surf. Sci.*, **65** (1977) 578

56. H. R. Gerberich, N. W. Cant, W. K. Hall, J. Catal., **16** (1970) 264

57. H. R. Gerberich, W. K. Hall, *Nature.*, **213** (1967) 1120

58. M. Chen, D. W. Goodman, *Chinese. J. Catal.*, **29** (2008) 1178

59. M. Chen, D. Kumar, C. W. Yi, D. W. Goodman, *Science.*, **310** (2005) 291

60. D. Kumar, M. Chen, D. W. Goodman, *Catal. Today.*, **123** (2007) 77

61. C. J. Baddeley, M. Tikhov, C. Hardacre, J. R. Lomas, R. M. Lambert, *J. Phys. Chem.*, **100** (1996) 2189

62. N. Macleod, J. M. Keel, R. M. Lambert, *App. Catal. A.*, **261** (2004) 37

63. N. F. Mott, H. Jones, '*Theory of the Properties of Metals and Alloys*' (OUP, London, 1936) Chapter 6.

64. A. Couper, D. D. Eley, *Disc. Farad. Soc.*, **8** (1950) 172.

65. L. Whalley, D. H. Thomas, R. L. Moss, *J. Catal.*, **22** (1971) 302.

66. J. A. Nicholson, J. D. Riley, R. C. G. Leckey, J. G. Jenkin, J. Liesegang, *J. Electron Spectrosc. Related Phenomenon.*, **15** (1979) 95.

2. *Experimental Chapter*

2.1 Introduction

Despite constant advancements in surface science, no single technique has been developed which can characterise a surface's structure and reactivity completely. When a variety of techniques are combined they may be capable of giving useful information on the adsorbate structure, electronic and physical properties, oxidation states and chemical composition of the surface. This chapter is designed for the reader to understand the experimental procedure and the workings of the equipment used. A general overview on the Ultra High Vacuum (UHV) system and the reasons for using UHV conditions for surface science studies are discussed. Attention is addressed to the UHV system used, presenting a general overview on it. Single components as well as the different techniques used during the experimental sessions are presented with their relevant characteristics.

In order to study metal-adsorbate interactions effectively, the use of a clean UHV environment is necessary. Three reasons dictate this:

1. When carrying out photoemission spectroscopy, the electrons travelling from the surface to the analyser should encounter as few molecules as possible. A vacuum $<10^{-6}$mbar is sufficient.
2. A suitably high vacuum is required to prevent electrical discharge between an x-ray anode and an electron analyser.
3. Although a high vacuum will suffice for points one and two, the need for atomically clean surfaces requires UHV.

Following on from point three, the rate of impingement (F) of a gas molecule on a surface is governed by the Hertz-Knudsen equation;

$$F = P / (2\pi mkT)^{1/2} \qquad \ldots(2.1)$$

P =pressure (Nm^{-2}), m =mass (Kg), K =Boltzmann constant and T =Temperature (K). At a pressure of 1 x 10^{-6} mbar at 298K, the bombardment rate of CO on the surface will be 2.88 x 10^{14} molecules cm^{-2} s^{-1}. Assuming a sticking probability of one, then a surface consisting of 1.5 x 10^{15} atoms cm^{-2} will be covered with a monolayer of surface contamination after only a 5s exposure. If the surface is exposed to the same background gas at a pressure of 1 x 10^{-10}mbar, saturation will take >8 hours.

2.2 System design and operation

A schematic of the stainless steel chamber used is shown below in figure 2.1.

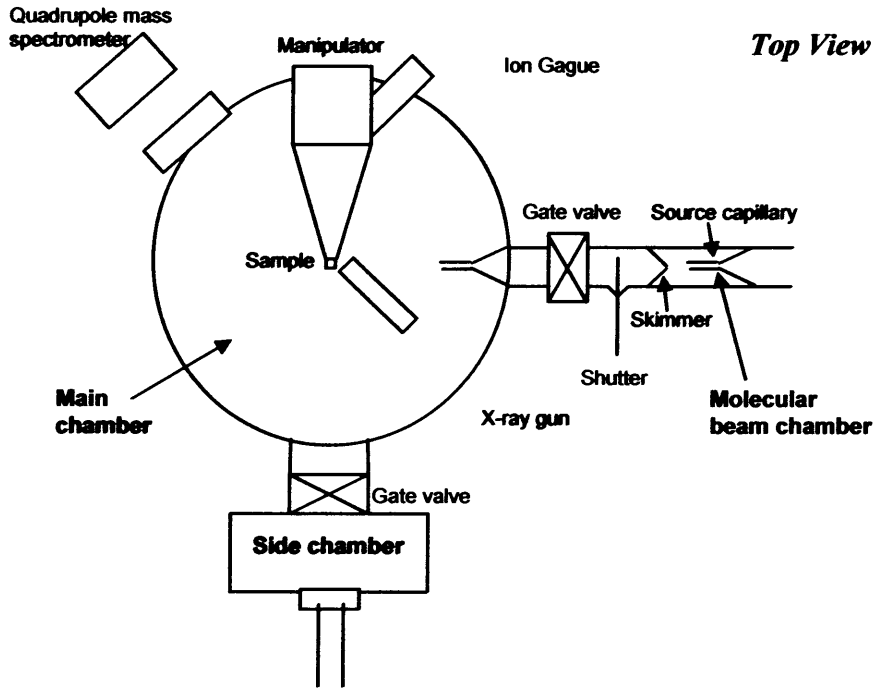

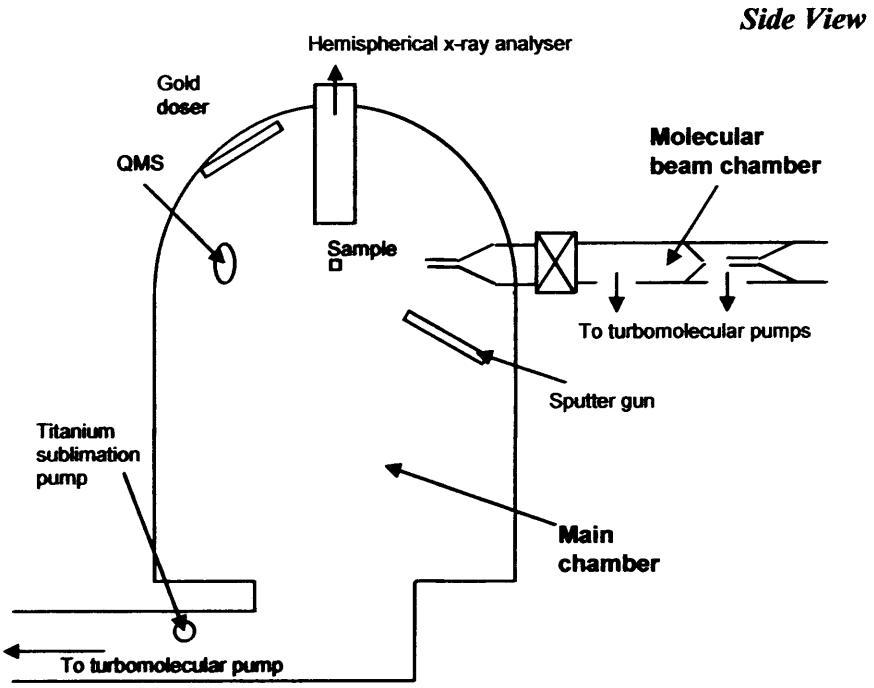

Figure 2.1 Schematic representation of the Molecular Beam/XPS system

The system consists of a main stainless-steel chamber separated from a secondary chamber (side chamber) by a gate valve. The pressure in the chamber is kept constant in the order of 10^{-10} mbar thanks to a pumping system. The main chamber is kept under ultra-high vacuum conditions using a Leybold turbomolecular pump. Figure 2.2 below shows the core features of any turbomolecular pump. It consists of a rotor fitted with blades that spin at the same order of magnitude as the velocity of the gas molecules moving in the chamber[1]. This type of pump operates best under molecular flow conditions. Under these conditions, gas molecules collide with the blades and are physically removed from the chamber. In order for the turbomolecular pump to operate, a backing pump is required in order to exhaust the expelled gas to atmosphere.

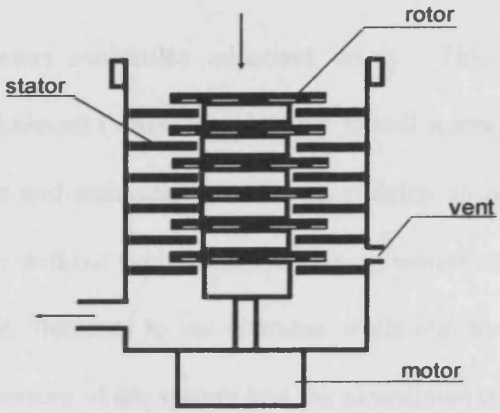

Figure 2.2 Schematic of a turbo pump operation. The arrows indicate the direction of flow of gas molecules.

To achieve a very low base pressure of ~$1x10^{-10}$mbar, an additional titanium sublimation pump (TSP) was employed. The sublimation pump used contains three titanium/molybdenum alloy hairpin style filaments which, when heated, produce a titanium vapour which condenses on the surrounding chamber walls. This layer reacts with residual active gases to form stable compounds. The pump is only used for short periods to prevent ageing of the filaments. Often it is necessary to bring the system up to atmospheric pressure in order to carry out maintenance work. After the system has been vented and all repairs carried out, the system is then gradually pumped down, firstly by a rotary pump and then by the turbomolecular pump. Once this has been done, it is necessary to heat the whole chamber in order to obtain UHV conditions and to get rid of all the contaminants (especially water). This process is called bakeout and is a long process that takes up to 2 days to complete. The chamber is insulated in a fibreglass tent and heated to approximately 140°C. Degassing is carried out in order to remove contaminants from filaments after bakeout. This is a practice common to all the ionising filaments present in the system. It consists of gradually increasing the current passing through the filament from the minimum value, to the maximum (usually the operating current), thus inducing thermal

desorption of gaseous molecules adsorbed on it. This is normally carried out immediately after bakeout (while the chamber is still warm) allowing the removal of those contaminants and reducing the amount sticking to the walls of the chamber. Using the filaments without preliminary degassing would result in the removal of the impurities from the filaments to the chamber walls and to the sample surface. This would affect the pressure of the system and the cleanliness of the sample.

The pressure inside the chamber is measured using two different types of gauge. A pirani gauge can measure pressure from 1bar to a limit of 10^{-3}mbar. This gauge was mainly used on the gas line and for monitoring the pressure when pumping down the main chamber. At lower pressures, thermoionic ionisation gauges were employed which have been shown to be sensitive as low as 10^{-11}mbar. The apparatus consists of a filament emitting electrons, a cylindrical open mesh grid and an ion collector. The electrons generated are accelerated inside the grid and oscillated back and forth. Some of the electrons collide with gas molecules present in chamber and ionise them. These ions are attracted to the central earthed filament, the collector, and produce a current directly proportional to the pressure of the gas molecules in the gas phase. When the number of gaseous molecules becomes too low, the ion gauge reaches its limit because the ions produced are not numerous enough to generate a current on the collector filament. A problem with using ion gauges is the desorption of residual gases, such as H_2, CO and CO_2, from the filament. Because of this, degassing is essential.

2.3 Sample preparation

The Pd (111) crystal was mounted on and heated resistively by two tungsten wires which passed through grooves in the edges of the crystals. The temperature was measured using a chromel-alumel thermocouple which was attached directly to the sample via a small hole drilled in the side. The Pd(111) was cleaned by flashing to 1200K, sputtering with 500eV Ar^+ at 700K, flashing to 1200K again and finally annealing in O_2 whilst the sample cooled down to 800K. This temperature was maintained until all O_2 had been pumped away upon which a final flashing to 1200K was carried out. The major elemental impurity in the Pd(111) sample, carbon, was removed during the sputtering cycles. The absence of the C 1s (284eV) peak was an indication of a clean surface. Another effective alternative to spectroscopy to check for surface cleanliness involved beaming O_2 at > 500K and checking i) if CO or CO_2 were evolved and ii) if the sticking probability for oxygen was as expected for the clean Pd surfaces.

2.4 Reactant Preparation

The gaseous chemicals used in these experiments: argon, oxygen, carbon monoxide and ethylene were used in lecture bottles provided by Argo Ltd, with purities of 99.999%, 99.6%, 99.5%, and 99.5% respectively. The liquid chemicals used in these experiments: acetic acid and acetaldehyde were all of analytical reagent grade i.e. >99% purity. In spite of this, these samples contained trace impurities from isomerisation by exposure to UV radiation in sunlight. Thus they were in covered

glass vials fitted with Youngs taps when used on the gas line, and below 273 K when in storage. Before any experiment, liquid samples were subjected to rotary pumping and freeze-pump-thaw cycles to remove gaseous and high vapour pressure contaminants. Samples were checked regularly by mass spectrometry for air leaks and isomerised contaminants. 'Multiplex' i.e. simultaneous monitoring of several masses by mass spectrometry was required for most TPD and MBS experiments.

2.5 Quadrupole Mass Spectrometry: QMS

Quadrupole mass spectrometry is a technique used to identify the residual gas composition of the chamber atmosphere. This technique is useful for analysing the purity of gasses introduced into the chamber prior to and during experiments. It is also very useful when leak checking. The quadrupolar mass analyzer, (figure 2.3), consists of four conducting rods. Two opposite bars are connected to the positive pole of a variable DC generator, while the other two are connected to the negative pole[1]. An AC RF voltage, out of phase of 180°, is also applied to each couple of bars. This setting allows bars to have the same tension in modulus $|U+V\cos(\omega t)|$, but opposite in sign and to invert their polarity with every 2ω. The result is the production of a complex electromagnetic field between the bars. The applied voltages affect the trajectory of ions traveling down the flight path centered between the four rods. For given dc and ac voltages, only ions of a certain mass-to-charge ratio pass through the quadrupole filter and all other ions are thrown out of their original path.

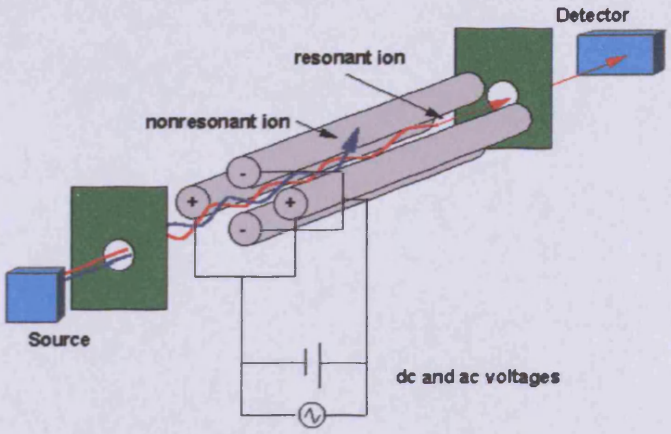

Figure 2.3 Schematic of a quadrupole analyzer

A mass spectrum is obtained by monitoring the ions passing through the quadrupole filter as the voltages on the rods are varied. The quadrupole analyzer is a relatively low resolution mass filter compared to magnetic sector mass spectrometers, but is more suitable for residual gas analysis in UHV. The chamber is equipped with one ThermoVG QMS capable of monitoring multiple masses simultaneously. This allows for the monitoring of reactant and product desorption during TPD experiments. It is also sensitive enough to analyze product evolution during molecular beam experiments and to observe the reactivity of the incident beam on the surface.

2.6 Temperature Programmed Desorption (TPD)

Temperature programmed desorption (TPD) is a valuable technique for determining kinetic and thermodynamic parameters of desorption and decomposition. It is used on model and real catalysts to investigate both surface coverages of adsorbates and the strengths of surface-adsorbate interactions. Behaviour such as rate mechanisms and activation energies of desorption can be obtained. The sample is

predosed with an exposure (measured in Langmuir) of a molecule that is stable at the starting temperature. A linear temperature ramp (usually between 1 and 100 Ks^{-1}) is then applied by measuring the amount of adsorbate desorbed vs. temperature. The amount of adsorbate desorbed can be measured in a variety of ways, but in these experiments it was monitored by quadrupole mass spectrometry. The temperature of evolution of desorbed species relates directly to their chemisorbed or physisorbed bond strength. Also, the temperature where maximum desorption occurs (Tp) relates to the maximum desorption rate. TPD can be used to investigate decomposition reaction mechanisms by monitoring the masses of several products at once by mass spectrometry, and this requires consideration of where products desorb with respect to temperature. This technique is often called temperature programmed reaction (TPR)

2.7 The Molecular Beam Reactor

2.7.1 The System

Molecular beams have been used widely since 1915 in a variety of different applications[3,4]. With regards to chemistry, they have been very useful in providing information regarding the adsorption of molecules on surfaces. Studies regarding the reaction kinetics and structure of surfaces have been possible. This is due to the unique way in which the beam molecules undergo interactions only with the surface analyzed and are not influenced by the external environment. Intermolecular collisions are minimal because of the high flux of the molecules towards the surface across a pressure gradient. Molecules therefore arrive intact on the surface and the

evolved products are not a result of a side reaction either in the gas phase or on walls or supports inside the reaction chamber. Simplistically, there are only two possible routes for the incident reactant molecules. They either undergo adsorption onto the surface, through physisorption or chemisorption or are reflected back into the gas phase. This allows the molecules to be assessed closely and the possible product formation to be monitored. It is also possible to investigate surface reaction kinetics including the sticking probabilities of different molecules on the surface. This information provides an insight into the reaction mechanism as step by step product formation can be observed.

The thermal nozzle source molecular beam system used is described below in figure 2.4[5,6]. The beam housing consists of two stainless steel six way cross junctions and one four way cross junction. The four way cross is backed by a rotary pump and is attached to the gas line. This allows for the introduction of beam gases and acts as a source chamber. Attached to it, a six way cross acts as a beam production chamber, the other six-way junction defines the beam. Both six way crosses are backed by Leybold turbomolecular pumps, which in turn are differentially backed by two Edwards rotary pumps. The pumping speed of the turbomolecular pumps has been calculated[7] to be around 18 l/s, reduced by the connective piping from the manufacturer's value of 50 l/s. The entire beam housing is bolted to the main chamber via a fast acting gate valve, allowing either region to be isolated from the other.

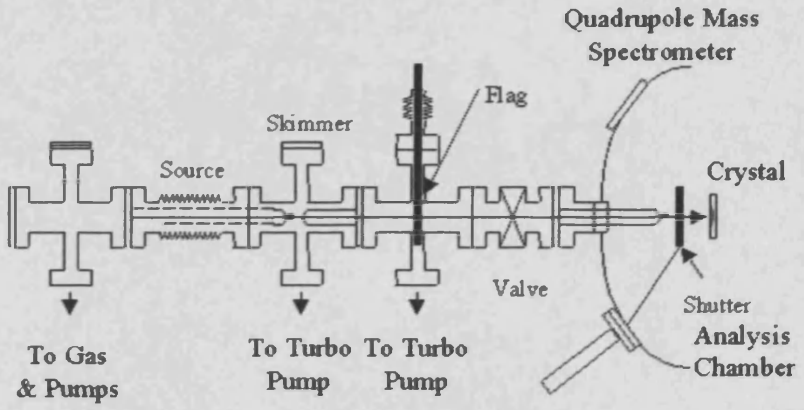

Figure 2.4 Schematic of the molecular beam reactor

In order to produce a beam, gas enters the source chamber from the gas line up to a pressure of 40 mbar in all experiments. The source chamber pressure was monitored using a baratron gauge and was maintained by a 5L glass reservoir. The gas effuses through a quartz capillary (nozzle) mounted at the end of the source chamber. It is possible to change the capillary temperature using a platinum heater coiled around the end of the capillary however this was not used in these experiments. The xyz position of the capillary can be manipulated to maximise beam alignment and flux in the analysis chamber using mass spectrometry and argon as a sample gas. The beam production chamber contains a conical skimmer with a central hole between the two six-way junction crosses. This collimates the beam, removing out-of-axis scattered molecules. The beam definition stage contains a 'beam flag' which can block the beam path in an infinitesimal time. Also in this stage a Pyrex tube acts as the final beam collimator. Its exit is 50 mm from the centre of the analysis chamber and the crystal sample. An ion gauge is also placed in this final section to measure the pressure in this region. In the main chamber, between the crystal surface and the Pyrex tube, is a 'chamber flag' which can block the beam directly in front of the crystal face.

2.7.2 Background and Theory

Molecular beams are divided into two types of system 'thermal' and 'supersonic'. Thermal molecular beams are named as such because the beam obtains the temperature of the walls of the source orifice. Supersonic beams are labelled such due to the very high velocities of the molecules in the beam. Supersonic beams are able to explore the energy thresholds of highly activated adsorption processes unlike the thermal beams. In order to explain a molecular beam, it is important to discuss the parameters that define it. Figure 2.5[8] below shows a plot of conductance down a capillary as a function of pressure behind the capillary. At low pressure, the flow is of the 'Knudsen' type i.e. molecular flow is occurring. In this regime, the flux of molecules is directly proportional to the beam pressure. As the pressure increases, the molecules exhibit laminar flow with higher speeds in the flow direction. In this region, the conductance becomes a function of pressure. In all the experiments in this thesis, flow was of the molecular (Knudsen) type.

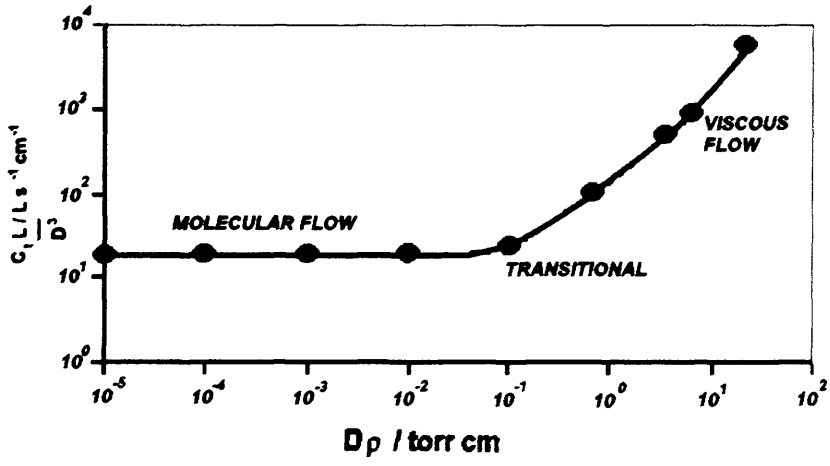

Figure 2.5 Conductance dependence of average pressure across a capillary

The beam of molecules enters the chamber through an aperture which defines the shape of the beam profile at the surface. In order to obtain good sticking measurements for varying surface coverage, it is essential that the molecular beam has a well defined solid angle of flux i.e. a sharp umbra (a few mm wide) of constant flux and a small penumbra where the flux falls off with increasing distance from the umbra. If the penumbra is too large (approximately greater than or equal to half the umbra width) then sticking measurements will not be accurate enough. In figure 2.6, beam 1 would generate more precise data than beam 2 because the umbra : penumbra is more favourable. The penumbra can be minimised by i) reducing the ratio of collimator-sample and source-sample distances or ii) reducing the nozzle or source aperture width. Thus it is important to have a good beam design, and to keep the sample as close to the collimator as possible.

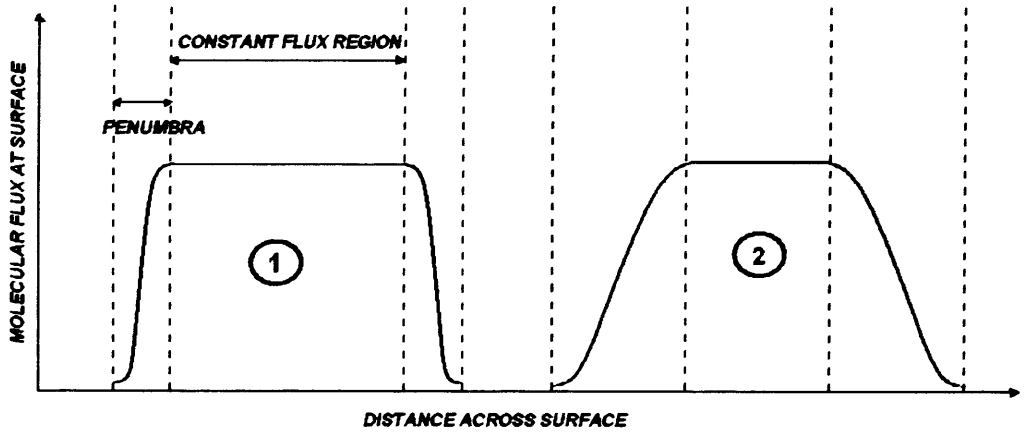

Fig 2.6 Umbra and penumbra distances vs. flux for two different beams.

2.7.3 Sticking Probability Measurements

A valuable piece of information available from molecular beam systems is the ability to measure the adsorption, sticking or reaction probability of a molecule onto a surface and its dependence of coverage. The sticking probability (S) is the tendency of a particular surface type to adsorb a particular incident molecule type. S also depends on a variety of factors, including the surface structure, its coverage and temperature. The sticking probability is defined as follows:

$$S = \frac{\text{Rate of adsorption of particles on the surface}}{\text{Rate of collision of particles with the surface}}$$

Kings and Wells have described previously how to obtain sticking measurements using the molecular beam flag[9,10]. Figure 2.7 shows a typical beam profile for O_2 on clean Pd at 373K and the experimental procedure which allows sticking measurements to be obtained. The initial sticking probability is related to the two pressure P1 and P2.

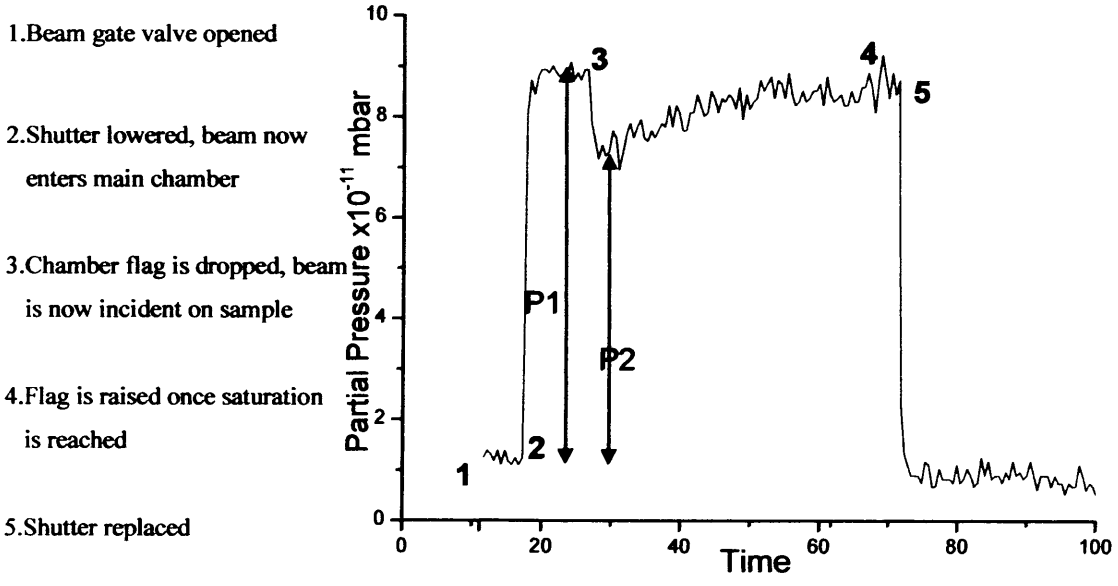

Figure 2.7 Typical molecular beam profile for O_2 on Pd (111) at 373K with protocol explained

The changes between P1 and P2 are due to the beam being turned 'on' and 'off' by manipulation of a chamber flag. The surface behaves as a pump, as some of the molecules adsorb to the surface they are removed from the chamber. This is why the partial pressure decreases as the surface is exposed. Through time the surface becomes saturated and so the sticking of an incident molecule becomes less probable until the surface is fully saturated. The sticking probability at any given time can be calculated by the equation:

$$S_{(t)} = (P_1 - P_2)/P_1$$

The coverage of the surface is directly related to the sticking probability such that;

$$\text{Surface coverage} = \theta(t) = N\int S(t)\,dt \qquad \text{Where N = beam flux}$$

This information can then be converted to a plot of S versus coverage. This information allows adsorption trends of surface temperatures or molecule and/or surface types to be compared. In cases where there is an activation barrier to adsorption, S will be small. By varying the beam temperature, the value of this activation barrier, which may arise from the cleavage of bonds in the incident molecules, can be calculated. However, for all molecules investigated in the following chapters, the sticking probabilities were sufficiently high to be measured at beam temperatures of 298 K, and the effect of beam temperature on S was not investigated.

Molecular beams can also be used to investigate reactions between adsorbing molecules, either by i) preadsorbing known coverages of one reactant then beaming with another, or ii) by simultaneously beaming reactants that are already mixed in the

gas line. In both cases, the rate of adsorption of starting molecules and emission of products can be monitored by quadrupole mass spectrometry. Thus, for a more complex reaction of the type X(g) + Y(a) → Z(g) + A(g) where Z and A are products and X and Y are reactants, three possibilities may arise:

i) X adsorbs on the surface and reacts with adsorbed Y.

ii) X does not adsorb onto the surface but reacts with adsorbed Y

iii) Both of the above occur.

2.8 X-ray Photoelectron Spectroscopy: XPS

2.8.1 Background and theory

XPS is based upon the principle of the photoelectric effect, a phenomenon whereby electrons are emitted from matter after the absorption of electromagnetic radiation[11]. Einstein was awarded the Nobel Prize in Physics for his paper which explained that the effect was due to the absorption of discrete quanta of light[12]. Siegbhan and co-workers first used the principle of the photoelectric effect practically by developing x-ray photoelectron spectroscopy in the 1960's[13]. X-ray photoelectron spectroscopy is a powerful analytical technique used widely in surface science and catalytic studies. It can provide useful quantitative and qualitative information regarding the surface of a sample. It is possible to determine the elemental composition and the chemical state of the different species present on the surface of the sample. This is carried out by irradiating the surface with soft x-rays and measuring the kinetic energy of the photoelectrons emitted after the interaction (figure 2.8).

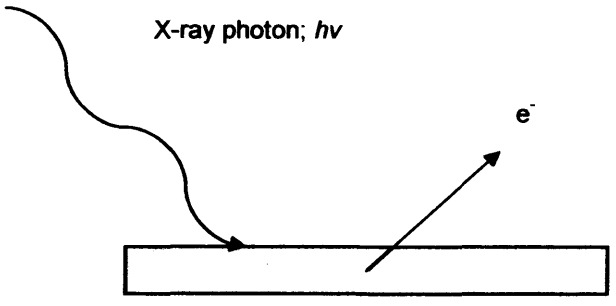

Figure 2.8 Schematic representation of the photoelectric effect

When a surface is irradiated with energetic photons, the ejection of a photoelectron occurs with a characteristic kinetic energy (KE) directly proportional to its initial binding energy (BE). This can be represented by the equation:

$$h\nu = \mathrm{BE} + \mathrm{KE} + \Phi \qquad \ldots(2.2)$$

In the above equation, $h\nu$ is the energy of the incident photon and BE is equal to the ionisation energy with respect to the Fermi level. The Φ part of the equation is a correction factor known as the work function. In this case the work function takes into account not only the energy necessary to remove an electron from the highest occupied energy level in the solid, the Fermi level, to the vacuum level. It also takes into account the electrostatic environment in which the electron is generated and measured and some instrumental correction factors specific to the spectrometer used. A schematic description of the process is shown below in Fig 2.9.

An important characteristic of the excited electrons is their limited escape depth making XPS a surface specific technique. Although the soft x-rays will penetrate the sample by a few millimetres, the measured photoelectron signal originates from the surface region. This is due to the inelastic scattering of the emitted electrons within the sample. The inelastic mean free path of an electron (IMFP, λ) is a measure of the average distance travelled by an electron through a solid before it is inelastically scattered. The IMFP of an electron from a material is dependent on the energy of the photoelectron and is described by "universal" curve[14] (figure 2.10). If electrons of KE's between 10 – 1500 are monitored, only the top 10 surface monolayers are observed i.e. the surface region.

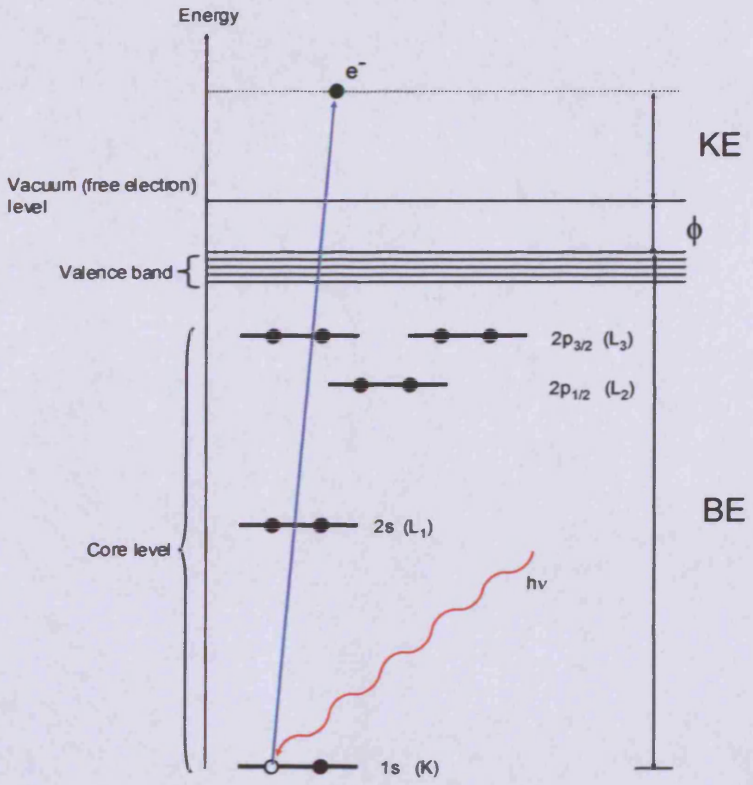

Figure 2.9 Schematic representation of photoemission described in eqn 2.1

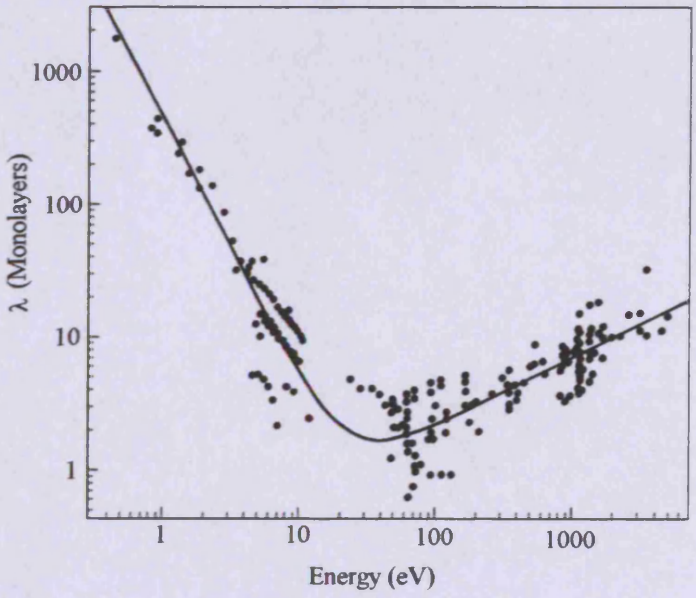

Figure 2.10 The "universal" curve;

After photoemission, the material is left in an excited state with a negative charge missing (the core hole). The system stays in this excited state for a very short time ($\Delta E_n \sim 10^{-15} - 10^{-16}$ sec), than relaxes to rearrange the charge distribution by filling the core hole with an electron from an outer shell. This may happen in the two different ways shown in figure 2.11:

1) X-Ray fluorescence: the electron relaxation from an outer shell to the core hole releases energy in the form of an X-Ray photon. The released photon has an energy equals to the difference between the two energy levels where the transition occurs.
2) Auger electron emission: a more energetic electron relaxes to the core hole. The excess energy is dissipated by ionisation of an outer orbital. This emits a secondary electron known as the Auger electron, resulting in a doubly ionised system.

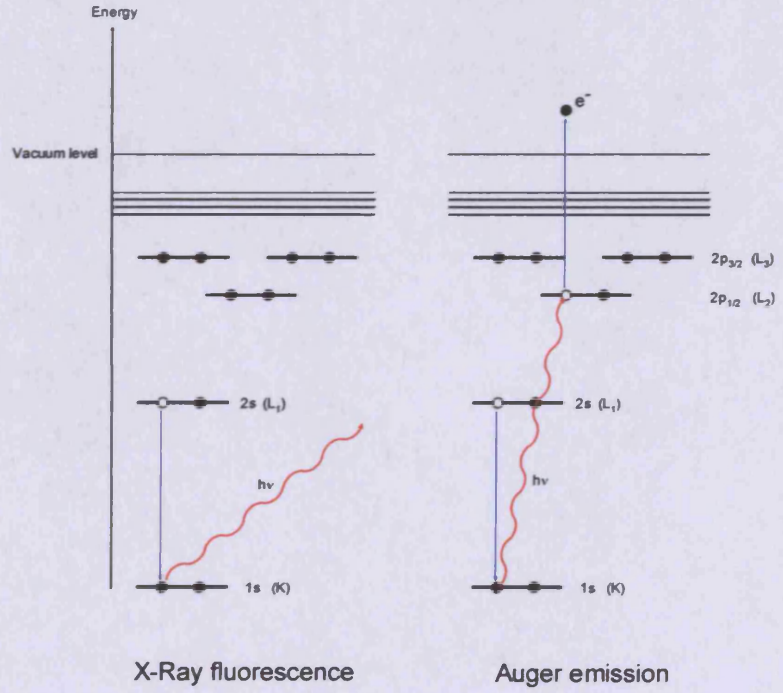

Figure 2.11 a) X-ray fluorescence energy diagram and b) Auger emission energy diagram.

A XPS spectrum is represented by a series of discrete peaks of different shape and intensity emerging over a background. A typical broad spectrum of the Pd (111) sample is shown below in figure 2.12. The background signal increases from low to high binding energy. The background signal is mainly due to inelastic scattering of the photoelectrons emerging from the sample and from Bremsstrahlung radiation generated by a non monochromatic X-Ray source. The background contribution from Bremsstrahlung radiation is significant at high binding energies. The peaks are characterised by their BE position (eV), full width at half maximum FWHM (eV) and intensity (Counts per second, CPS). The BE position is related to the orbital from which the photoelectrons have originated. The FWHM is related to a contribution of different parameters such as the analyser resolution and the width of the x-ray radiation used.

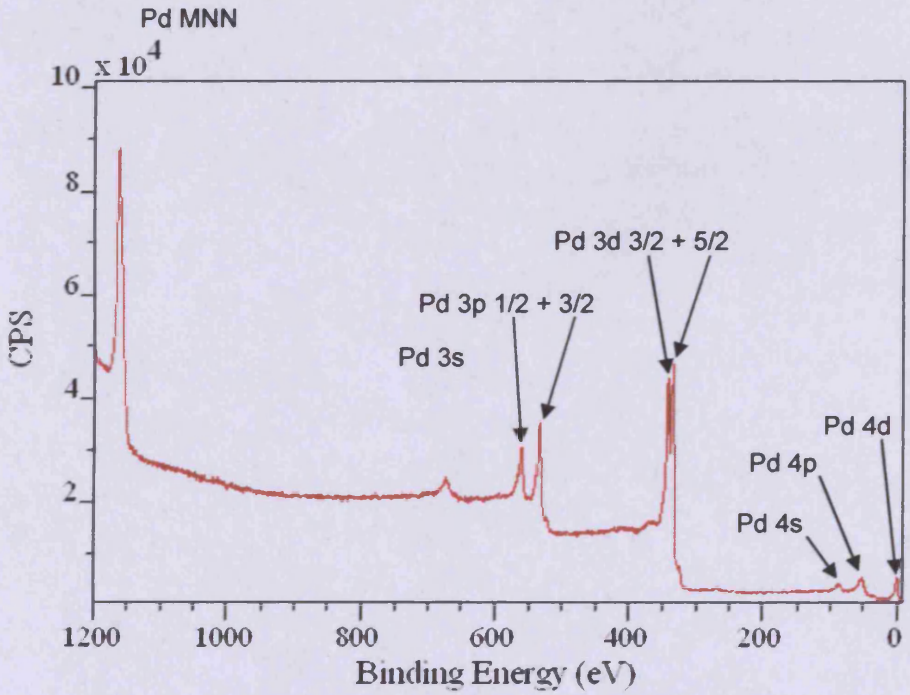

Figure 2.12 A typical broad spectrum of a "clean" Pd (111) crystal

The peaks are labelled according to the following notation: to the principal quantum number n followed by the symbol s, p, d, or f depending upon the value of the angular quantum number I. A subscript of the value of the total angular momentum J is also shown,

The Auger peaks are labelled with respect to the shell where the initial core hole was localised, the outer shell from which the electron relaxes to fill the hole in the inner shell and the shell from where the ejected electron is generated. The letters used are K, L, and M corresponding to the quantum number n. When I>0, the magnetic coupling between the spin of an unpaired core electron with its angular momentum induces splitting known as spin-orbit splitting. Following photo-ionisation, an unpaired electron remains which has a spin vector parallel or anti-parallel to its orbital angular momentum vector (I). For a one-hole configuration this resolves the degenerate hole state into two components, where the total orbital quantum number, $J = L \pm S$. For the Pd (3p) spectrum, I = 1 and s =1/2. This give rise to two components indicated as Pd (3p3/2) for the anti parallel configuration and Pd (3p1/2) for the parallel configuration. The respective intensities of these final states are given by (2J + 1), resulting in a Pd (2p3/2): Cu (2p1/2) intensity ratio of 2:1. Lab based X-Ray sources also produces satellite lines at lower binding energies, with intensity and spacing characteristic of the X-Ray anode material, generated from less probable transitions. This gives rise to additional features in the XP spectrum. The pattern of these additional lines is presented in the following table:

Emission peak	$\alpha_{1,2}$	α_3	α_4	α_5	α_6	β
Mg displacement /eV	0	8.4	10.1	17.6	20.6	48.7
Relative height /%	100	8.0	4.1	0.6	0.5	0.5
Al displacement /eV	0	9.8	11.8	20.1	23.4	69.7
Relative height /%	100	6.4	3.2	0.4	0.3	0.6

2.8.2 Instrumentation

The instruments used in the acquisition of XP spectra include an x-ray gun and a hemispherical electron analyser. The X-Ray gun is a twin anode source, providing both Mg Kα (1253.6 eV) or Al Kα (1486.6 eV) radiation. The advantage of a twin anode source is represented by the possibility to switch between sources to resolve any interference which can occur between the photoelectron and the Auger electron signals. The KE of Auger electrons is independent of the photoelectron energy, therefore only the signal from the photoelectrons is affected by changing the anodes. Therefore, on the KE scale, photoelectron peaks will be shifted by 233 eV because of the difference in energy between the two anode sources. A schematic of the head of the x-ray source can be seen below in figure 2.13.

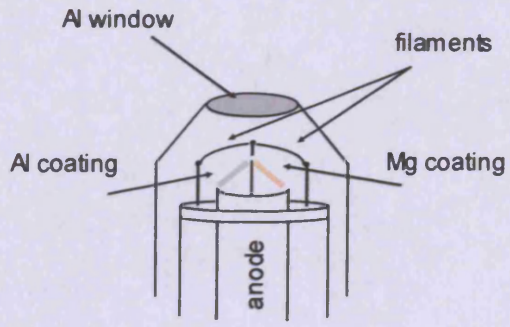

Figure 2.13 Schematic of X-ray gun head

A heated ThO_2-Ir filament bombards the selected anode which is at a high positive potential. The high potential difference between the filament and the anode is necessary to accelerate the electrons. By switching the filament used, the other face of the anode can be excited. The Al window shields the sample from stray electrons, heating effects and approximately 80% of Bremsstrahlung radiation. The analyser consists of two hemispherical, oppositely charged, surfaces positioned concentrically. Upon entering the analyser, photoelectrons encounter a retarding potential. By varying the retarding potential, it is possible to vary the KE of the photoelectrons passing through to be analysed.

2.8.3 Quantification and Qualification

When depositing atoms or molecules onto the sample surface, it is important to know what the surface concentration is. By careful analysis of XP spectra, it is possible to accurately calculate the surface coverage. Since the magnitude of a photoelectron peak is relative to the species' abundance, its area must be obtained. By removing the background, the peak area is measured by integrating the intensity between two points above a fitted baseline. After obtaining the peak areas of the substrate and adsorbate, the values can be applied to the Eq 2.3[15,16] to calculate the surface concentration, as follows;

$$\sigma = \frac{I_A KE_A \mu_S \rho_S N_A \lambda_S \cos\phi}{I_S KE_S \mu_A M_S} \qquad \ldots(2.3)$$

Where; σ = surface concentration; A = adsorbate; S = substrate; I = integrate peak intensity; KE = kinetic energy; μ = modified photoionisation cross-section; ϕ = photoelectron take-off angle; N = Avogadro's number; λ_s = escape depth of photoelectrons through substrate; M_s = molar mass of substrate; ρ_s = substrate density. The photoemission cross-section is a parameter which governs the relative intensities of core level peaks. Values of μ have been directly calculated and have also derived from x-ray mass absorption coefficients[17]. Values for the escape depth of electrons of different energies were obtained from previously calculated data tables[18]. Many of the terms in equation 2.3 remain constant allowing it to be simplified where A is a constant for a particular system (eqn 2.4)

$$\sigma_A = (I_A / I_S) \times A \qquad \ldots(2.4)$$

The Carley-Roberts equation makes the assumption that the surface adsorbate does not attenuate the signal. For coverages >1ML this needs to be taken into account. Equation 2.5 estimates the depth of the adsorbate based on the attenuation of the substrate signal.

$$d = \frac{\lambda(\ln I - \ln I_0)}{-\cos\phi} \qquad \ldots(2.5)$$

d = film thickness; I_0 = integrated intensity of clean substrate; I = integrated substrate intensity after deposition; λ = IMFP of the substrate photoelectrons through adsorbed species.

When collecting XP spectra, it is most important to observe the positions of the relevant photoemission peaks since a shift in position may yield important information regarding the oxidation state of the species. A shift to higher BE implies the species is more positively charged, i.e. it has lost electrons and vice versa. For instance, a C1s peak for clean carbon would have a BE of ~285eV. If the surface carbon formed carbide, a shift would be observed to 282eV. Conversely if the carbon were to be oxidised, the 1s peak would shift to a higher BE.

The various techniques detailed here are yield information regarding different aspects of surface chemistry. The molecular beam reactor can tell us about adsorption and desorption products and the reactivity of the surface towards different molecules. This is useful in determining the nature of surface processes and reaction mechanisms. Quantitative analysis of the surface species and their electronic and chemical environments can be carried out using XPS. By the combination of different surface techniques, a broader understanding of surface processes can be obtained.

2.9 References

1. A. Chambers, R. K. Fitch, B. S. Halliday, Basic Vacuum Technology *2nd Edition*,; ISBN 0-7503-0495-2
2. ST22 Titanium sublimation pump cartridge – Operating instructions, Fisons Instrument Vacuum Generators, 1994.
3. M. Knudsen, *Ann. Phys.* **48** (1915) 1113.
4. R. W. Wood., *Philos. Mag.* **30** (1915) 300.
5. M. Bowker, *Appl. Catal. A: General* **160** (1997) 89.

6. D. A. King, M. G. Wells, *Surf. Sci.*, **29** (1972) 454

7. M. Bowker, P. D. A. Pudney, C. J. Barnes, *J. Vac. Sci. Technol.* A **8 (2)** (1990) 816.

8. A. Roth, Vacuum Technology *3rd edition.*; ISBN 0-444-88010-0

9. D. A. King, M. G. Wells, *Surf. Sci.*, **29** (1972) 454

10. P Alnot, A. Cassuto, D. A. King, *Farad. Disc. Chem. Soc.*, **87** (1989) 219.

11. H. Hertz, *Ann. Physik.* **31** (1887) 983

12. A. Einstein, *Ann. Physik.* **17** (1905) 132

13. K. Siegbahn, Et. Al., *Nova Acta RegiaeSoc.Sci., Ser. IV*, **20** (1967)

14. D. P. Woodruff, T. A. Delchar, Modern Techniques of Surface Science.; ISBN 0521424984

15. A. F. Carley, M. W. Roberts. Proceedings of the Royal Society; *London A*, **363** (1978) 403

16. T. E. Maddey, J. T. Yates, N. E. Erickson. *Chem. Phys. Letts.* **19** (1973) 487

17. J. H. Scofield. *J. Electron. Spectrosc. Relat. Phenom.* **8** (1976) 129

18. D. R. Penn. *J. Electron. Spectrosc. Relat. Phenom.* **9** (1976) 29

3. *The reactivity of the Pd (111) surface towards VAM related molecules*

3.1 Introduction

This chapter is concerned primarily with the reactivity of various different molecules related to the heterogeneous production of VAM via the acetoxylation of ethylene. In order to investigate the effect of Au on the reactivity of the Pd surface, thorough studies must firstly be carried out on clean Pd in order for a direct comparison to be carried out. The molecules studied include the three starting materials, oxygen, ethylene and acetic acid. Also studied are two molecules, carbon monoxide and acetaldehyde, which have exhibited interesting chemistry with palladium previously and have been found to have significance in the decomposition of VAM. The basic nature of these molecules allows simple studies to be carried out without the need for complicated interpretation.

On Pd surfaces, these molecules chemisorb and may decompose to produce new products or recombine when heated to high temperatures. The Pd (111) surface was chosen for these studies as a direct comparison to those carried out on the (110) surface previously. Since the catalytically active metals Pd, Rh and Pt all exhibit an fcc structure, the (111) plane corresponds to one of the close-packed layers on which the structure is based. The surface atoms in the (111) plane are equivalent and have a relatively high coordination number of nine. This makes the surface the least reactive of the 3 most commonly studied. The surface generally allows three different binding sites; on-top, bridging two atoms and 3-fold-hollow sites.

3.2.1 Oxygen on Pd (111)

3.2.1.1 Background – O_2 adsorption on different Pd surfaces

Any fundamental investigation regarding the synthesis of VAM requires studies regarding the feedstock chemicals. Oxygen, a simple diatomic molecule has been studied previously on platinum group metals and was shown to dissociate at room temperature[1,2]. This can be attributed to its relatively low dissociation energy (498kJ/mol)[3]. By contrast, CO doesn't dissociate at room temperature because of a much higher energy of dissociation. Low temperature studies have shown oxygen to adsorb molecularly on Pd (110) at 120K forming a (2x1) array[4,5]. Dissociation occurred after heating above 200K forming an ordered 2x4 LEED pattern by 470K. Milun et al carried out TPD experiments on the O_2/Pd system and found two states of desorption by 800K arising from the recombination of oxygen atoms on the surface[6]. Most TPD spectra in the literature agree that the two β desorption states occur at around 690K and 770K. The shapes of the peaks imply second order kinetics, often seen with associative desorption[7,8]. The lower temperature (β_1) state was attributed to desorption of oxygen in the subsurface region and was observed at oxygen coverages >0.5ML[9,10]. XPS and TPD studies have shown that the Pd (110) surface readily absorbs oxygen into the bulk at 400K. Since no observable shift in the O1s binding energy was observed after exposures of 10^8L, it was supposed that the absorbed oxygen molecules diffuse deep into the subsurface Pd layers to a depth greater than 15-20Å[7]. Molecular beam, XPS and TPD experiments determined S_0 to be ~0.44 at room temperature decreasing to 0.33 +/- 0.02 at 700K[11]. This relatively small change in sticking probability agrees with studies carried out by Yagi et al who suggest the

mechanism of dissociation is precursor-trapping and that S_0 is independent of temperature[12]

The reactivity of oxygen has also been studied on the more close-packed Pd (111) surface. The dissociative adsorption of oxygen at 300K was shown to produce a well-defined (2x2) superstructure in the LEED pattern indicating a saturation coverage of 0.25ML[13]. Low temperature investigations showed oxygen to adsorb molecularly at 100K to a saturation coverage of 0.61ML[14,15]. TPD of oxygen dosed at this temperature resulted in three molecular desorption processes at 125K, 150K and 200K. As on Pd (110), O_2 was seen to dissociate above 200K on (111). An associative desorption process was observed around 800K with E_d = 53kcal/mol[15]. The maximum coverage of dissociated oxygen after heating from 100K was 0.17ML, 32% lower than saturation (0.25ML). This indicates that only 27% of surface species dissociate, the remainder desorb. STM studies of low temperature oxygen adsorption showed the fcc threefold hollow site to be the stable binding position[16]. Dissociation was observed above 160K with the atoms typically separated by approximately 0.5nm. Molecular beam studies of O_2 have shown S_0 to decrease linearly with surface temperature and the probability of the molecule being captured in the precursor state was noted as being ~0.5[17]. Uvdal et al determined the S_0 with a supersonic molecular beam to be 0.63 at 0.083eV and 0.58 at 0.69eV translational energies at 300K[18]. Thermal molecular beam studies found S_0 to be 0.27 +/- 0.02 at room temperature which decreased linearly with coverage falling to 0.2 +/- 0.01 at 465K[11].

Oxygen migration into the subsurface region has also been observed at temperatures >500K[19]. Both the use of strong oxidants such as NO_2 and dosing O_2 at high pressures have resulted in different surface structures[20]. These changes in

structure have been attributed to the formation of palladium oxide (Pd_xO_y). A metastable "Pd_5O_4" phase was observed at high O_2 partial pressures (>10^{-3}mbar) at 430K, or after long exposures at 10^{-6}mbar between 500-600K[21]. TPD of oxygen dosed Pd (111) attributed desorption at 1100K to desorption of oxygen dissolved in the palladium bulk[13]. Other studies have dismissed bulk diffusion and instead suggest the formation of a surface oxide[21].

3.2.2 O_2 on Pd (111)

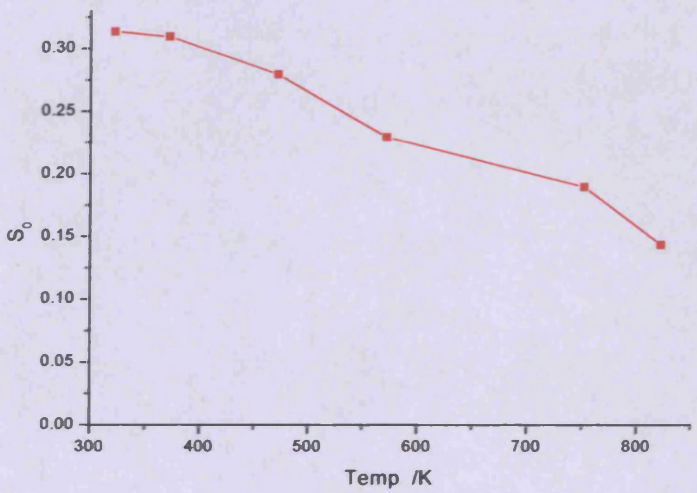

Figure 3.1 Initial sticking probability of oxygen on Pd (111) at different surface temperatures

Figure 3.1 above shows the relationship between the initial sticking probability of O_2 on clean Pd (111) and the surface temperature over a range of 323K to 823K. At 323K, S_0 was observed to be 0.31 +/- 0.02 and at 823K S_0 was 0.15 +/- 0.02. The S_0 can also be seen to decrease linearly with respect to surface temperature

which agrees with previous studies carried out by Engel et al[17]. A decrease in S_0 as temperature increases can be attributed to a decrease in the residence time for the molecule. The less time a molecule resides in a precursor state, the less probable it is to undergo an energy exchange (thermalization) process with the surface needed for chemisorption to occur. Although the initial sticking decreases at higher surface temperatures, the change is not as significant as other molecules such as NO studied on this surface[22].

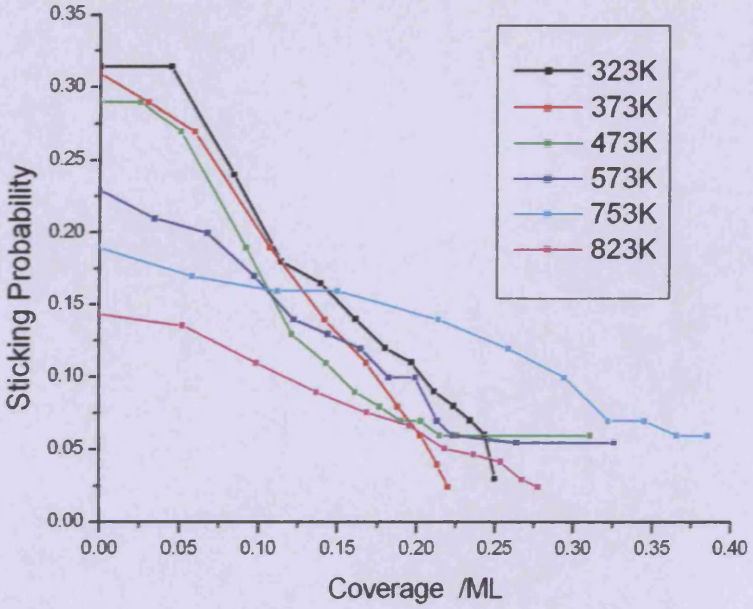

Figure 3.2 Sticking probability of O_2 on clean the clean Pd (111) surface as a function of surface coverage for different surface temperatures.

Figure 3.2 shows the relationship between the sticking probability and coverage for O_2 over the temperature range 323K to 823K and agrees well with previous studies on this system[11]. The saturation coverage of 0.25ML at 323K was assigned from previous LEED studies carried out on the (111) surface. Saturation coverage for the different temperatures is relatively uniform indicating a stable

0.25ML oxygen uptake across this temperature range. This is also different to other molecules studied such as NO which show a decrease in uptake coverage as the surface temperature rises[22]. Oxygen uptake on the Pd (110) surface has also been shown previously to be independent of surface temperature in this temperature range[11]. At temperatures above 573K, a linear relationship between sticking probability and coverage can be seen. At 473K, steady-state sticking of 0.06 +/- 0.02 can be observed. Since no CO or CO_2 production was recorded due to carbon contamination, it can be concluded that the oxygen atoms are migrating subsurface. This observation is similar to those found >500K using either high pressures of O_2 or strong oxidants such as NO_2[19]. Similar steady-state sticking can also be seen at 573K once saturation of the stable 0.25ML surface has occurred. At 753K, O_2 sticking probability decreases more slowly as surface coverage increases, indicating a greater migration of oxygen atoms into the subsurface region even at low coverage. Steady-state sticking is therefore probably reached once the near surface region is saturated and uptake is limited by the slow diffusion of oxygen atoms into the bulk At 823K, the overall uptake of oxygen is still 0.25ML, however steady-state uptake of the molecule was difficult to observe accurately because of low sticking probability. This is due to associative desorption processes occurring in this temperature range[14,15]. Similar observations of oxygen migration have also been seen on Rh (111) where oxygen penetration was observed to occur between 390 and 800K, below the onset of desorption[23].

3.2.2 Carbon Monoxide on Pd (111)

3.2.2.1 Background

CO is an important molecule when considering the acetoxylation of ethylene due to the fact that along with acetaldehyde, it is one of the major by-products of the industrial process[24-26] . In fact CO has been shown to be an important molecule in various catalytic systems involving Pd. The formation of polyketones via the Pd catalysed copolymerisation of CO and ethylene has attracted much interest both in academic studies and industrial applications[27,28]. A similar area of recent interest has also been the selective electrochemical carbonylation of methanol to dimethyl carbonate using Pd[29,30]. CO has also been shown to not only be a by-product of VAM production but also as a feedstock compound for VAM synthesis via methanol[31]. All of these reactions are homogeneous in nature and therefore differ somewhat from the seemingly heterogeneous acetoxylation of ethylene.

The oxidation of CO has been of significant interest over the years due to its relevance to the automotive industry. Environmental concerns and stricter legislation have demanded lower CO and NO_x emissions, increasing the need to develop more efficient catalytic converters. Recently, the use of Pd in catalytic converters has increased due to its cheaper costs on the world metals market compared to Pt and Rh. This increases the need for detailed studies related to CO oxidation on Pd. The adsorption of CO with various transition metal surfaces has been studied and certain cases have shown CO dissociative adsorption on Pt, Ni and Rh catalysts[32-34].

Because it is a small, simple molecule, its common usage is that of a probe for the surface. The additional significance of CO as a surface probe can be found with regard to IR spectroscopy, where the C=O vibrational frequency is simple to analyse in a variety of chemical and structural environments. CO reactivity and binding structure has been observed with many precious metal surfaces. Its binding and oxidation on Pt[35,36] and Au[37,38] surfaces have been investigated using a variety of techniques and have yielded interesting results highlighting the importance of surface morphology.

The CO/Pd (111) system has been studied extensively with LEED[39-42], XPS, TPD[41,43-45], molecular beam measurements[39,46-49], RAIRS and IRAS. At 300K, well ordered island growth has been observed at 0.33ML, indicated by a sharp $\sqrt{3}$ x $\sqrt{3}$/R 30° LEED pattern[39,40]. This is due to weak attractive interactions between the molecules. CO bonding at this low coverage is thought to occur at three-fold coordinated fcc sites, showing a band at 1849cm^{-1}. As CO coverage increases up to 0.5ML, the observed LEED pattern changes to an ordered c(4x2). Subsequent LEED patterns such as c($\sqrt{3}$x5) are also seen at 0.6ML coverage and a (2x2) pattern is seen at a 0.75ML coverage. The absorption band also shifts to 1918cm^{-1}, indicating a change in CO bonding from the fcc triple coordinated site to a bridging conformation[41]. At room temperature the saturation coverage is 0.5ML. Work function studies also show similar changes in bonding arrangements as CO coverage increases[50]. In order to obtain higher coverages, low temperature conditions are needed, e.g. 0.66ML at 200K and 0.75ML at 90K[51]. It has been shown that the isoteric adsorption energy for CO on Pd (111) is constantly 34 kcal/mol up to coverages of 0.66ML[42]. This agrees with the notion of weak interactions between CO molecules <0.5ML. However, studies have also indicated a link between CO

adsorption temperature and desorption activation energy with respect to coverage[41]. The formation of large ordered domains at low temperatures (87K) and smaller domains at higher temperatures (200K) goes some way in explaining this phenomenon. Investigations have also shown a relationship between CO adsorption structures and adsorption pressure for temperatures <250K, however above this temperature range, no such correlation was found[52].

Using a back scatter CO flux technique, the sticking probability has been found to be about ~1.0, and is independent of temperature[47]. Using the more direct molecular beam approach, S_0 has been determined to be 0.45 and the saturation coverage as 0.55ML at 300K[48,49]. The sticking coefficient was found to decrease at higher temperatures, similar to a trend observed on Rh[53]. Molecular beam studies have concluded that the bimolecular surface reaction between CO and O_2 proceeds via the Langmuir-Hinshelwood (LH) mechanism[39,46,54]. This mechanism denotes that CO_2 formation takes place via interaction of both CO and O_2 in their chemisorbed state. Unfortunately it has not been possible to write an equation for the rate of CO_2 formation as a product of the coverages and rate constant. This is due to the complicated nature of CO and O_2 interactions on the surface. CO has been shown to both inhibit O_2 adsorption at coverages >0.06ML and compress adsorbed oxygen islands at higher coverages, reducing the activation energy for the reaction. At temperatures >500K, the reaction takes place between rapidly diffusing CO molecules and stationary oxygen islands. All these factors have an effect on the rate of reaction under different conditions. A simple rate equation was produced, however it was only found to apply in the case of both low CO and oxygen coverages.

3.2.2.2 Molecular Beam and TPD Experiments CO/Pd (111)

Molecular beam CO/Pd (111) experiments all produced beam profiles of similar shape, the only differences being the initial sticking probability and the overall uptake of CO on the surface. A beam profile for CO/Pd (111) can be seen below in figure 3.3. The beam pressure was 40mbar.

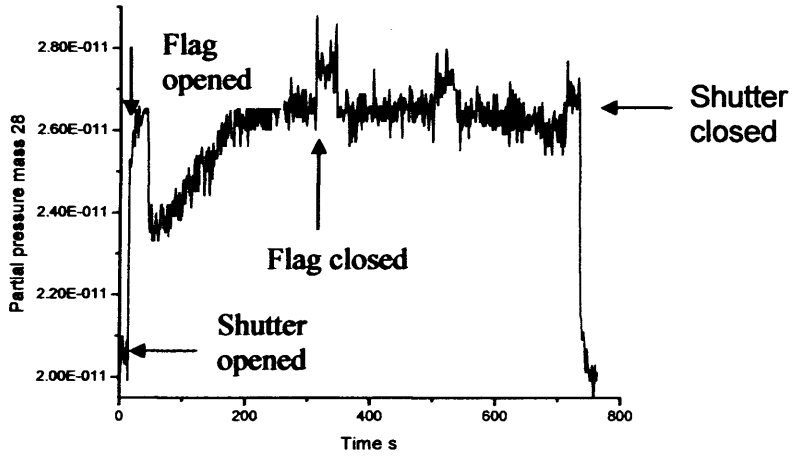

Figure 3.3 An example of a beam profile for CO/Pd (111) at 315K. The partial pressure of mass 28, the molecular mass of CO, is monitored vs time.

Sticking measurements by molecular beam for the CO/Pd (111) were carried out at a variety of sample temperatures. Figure 3.4 be shows the sticking probability variation with respect to coverage. The initial sticking probability is 0.52 at 298K. With reference to previous LEED studies on CO uptake, the saturation corresponds to 0.5ML, associated with a c (4x2) CO/Pd (111) unit cell. S_0 starts to decrease significantly above 397K due to desorption of CO above this temperature. The CO saturation coverage also falls as substrate temperature increases, to 0.15 at 420K and 0.04 at 453K. This is also due to the prevalence of CO desorption competing with

adsorption at these temperatures as can be seen from TPD. Similar results have been observed on Pd(110)[49].

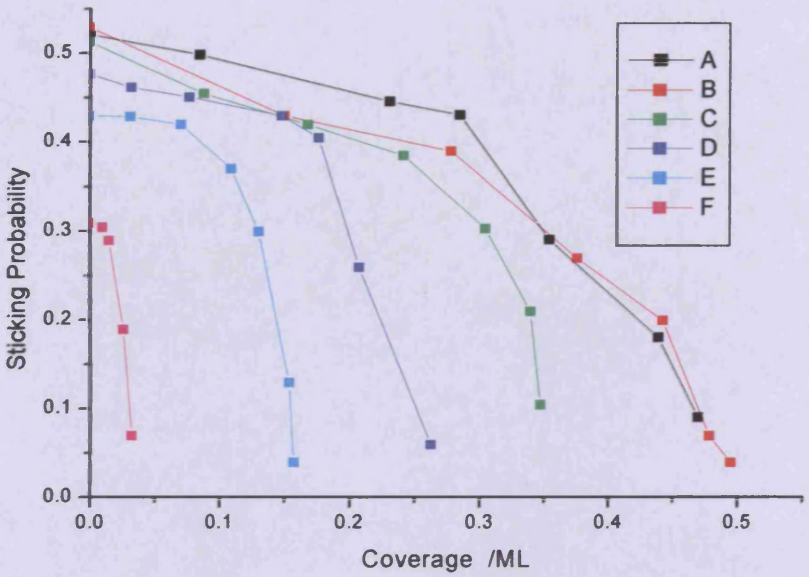

Figure 3.4 Sticking probability vs coverage curves for carbon monoxide on Pd (111) across a range of temperatures. Gas line source pressure was 40 mbar in each case. Results were calibrated from LEED data in literature where saturation was found to be 0.5ML at 298K. A: 298K; B: 318K; C: 353K; D: 397K; E: 420K; F: 453K

Figure 3.5 below shows a typical TPD plot from exposures of 10L and 0.1L on CO/Pd(111). This behaviour is similar to other data found in the literature which have shown there to be various adsorption states depending on exposure and temperature[41,43]. The peak observed after dosing 0.1L occurs at 454K and can be attributed to the β_2 adsorption site[43] . At the higher coverage, there is a peak shift down the temperature scale to 424K. This is thought to be caused by an increase in repulsive interactions between adjacent CO molecules. The high CO coverage TPD

spectrum also exhibits a broad shoulder on the low temperature slope. The existence of a β_1 binding site has been noted previously in the literature[44]. Other desorption states have also been observed from low temperature TPD, α_3 at 330K, α_2 at 250K and α_1 at 160K [45]. The results presented here concerning the interaction of CO with the Pd (111) surface are in excellent agreement with previous studies carried out on this system.

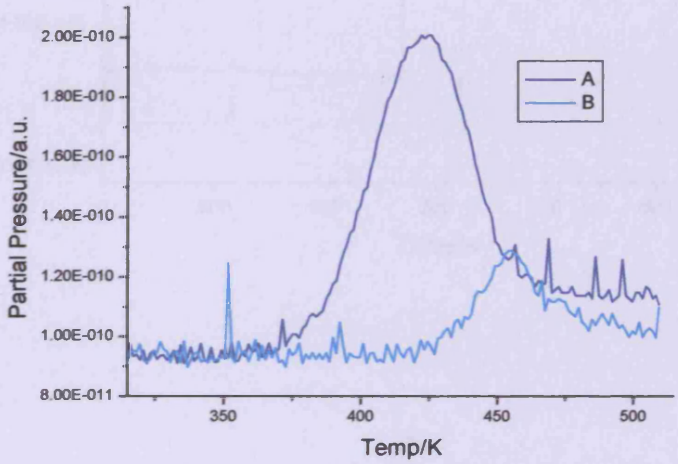

Figure 3.5 TPD spectra for carbon monoxide desorption from Pd (111) at different initial coverages; A: 10L, B: 0.1L. The ramp rate was ~0.1K/s

3.2.2.3 CO Oxidation Reactions

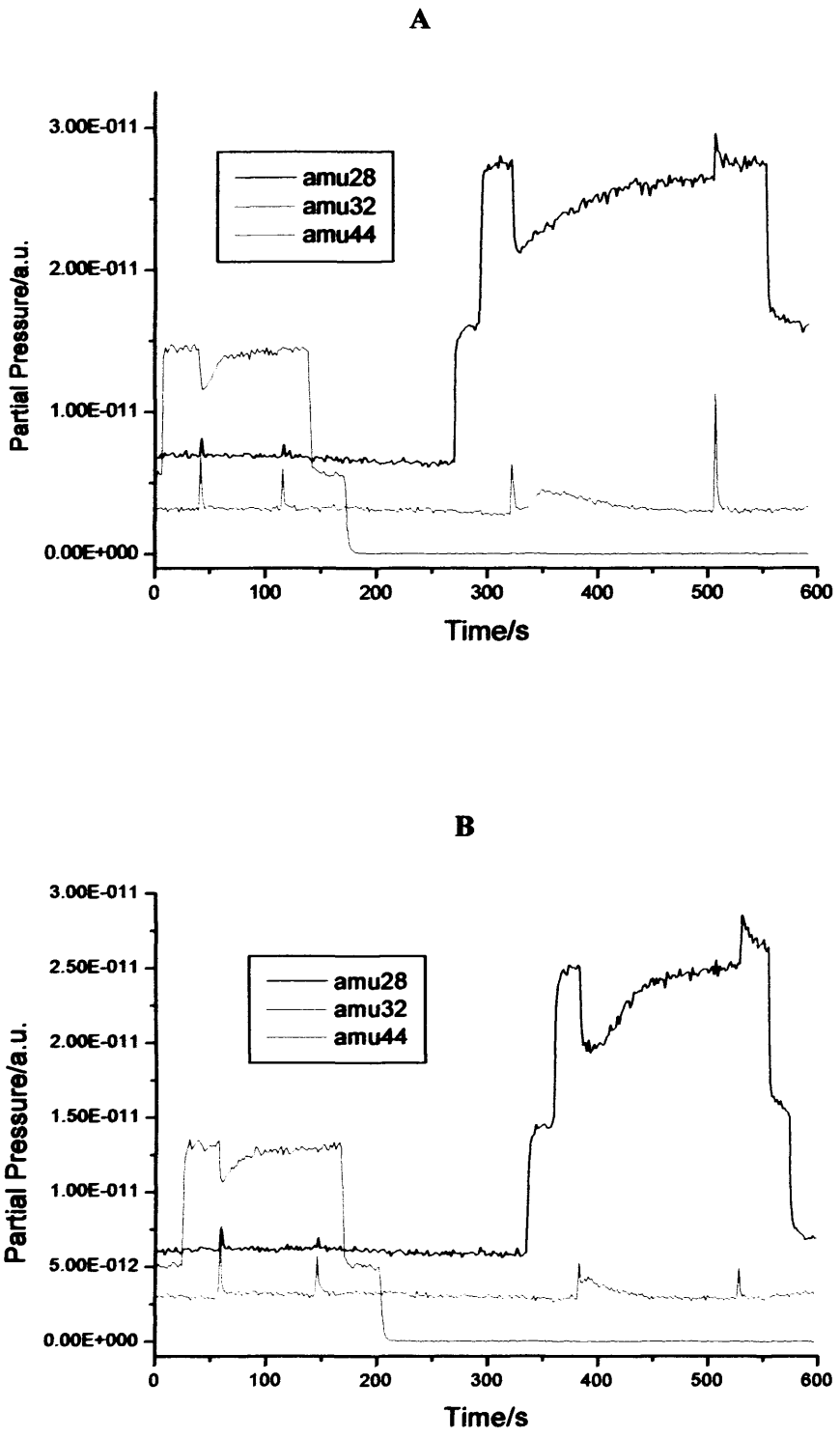

Figure 3.6.A. Molecular beam profile of O_2 followed by CO at 313K. **B.** Repeated at 373K. CO, O_2 and CO_2 monitored from masses 28, 32 and 44 respectfully

Pd(111) was beamed with oxygen at 333K resulting in an initial S(t) of 0.31, typical for a clean Pd(111) surface at this temperature. Once S(t) ~ 0, the flag was shut and O_2 was pumped away. CO was then introduced to the beam and the flag was once again opened to allow CO to interact with the substrate at 313K. CO stuck to the surface with an initial S(t) of 0.5. Initially, there was no CO_2 production observed, however after ~10s, CO_2 began to evolve. This is due to the gradual build-up of surface CO molecules. When CO molecules bind to the surface initially, there are sufficient free sites for the species to reside without oxidation occurring. As the concentration builds up, the rate of oxidation increases.

$$CO_{(g)} \longrightarrow CO_{(a)}$$

$$CO_{(a)} + O_{(a)} \longrightarrow CO_{2(g)}$$

Figure 3.6A below shows the beam profile for O_2 followed by CO at 313K. Figure 3.6B is the profile for the experiment repeated at 373K. The behaviour of CO and O_2 doesn't change greatly over this temperature range. There is however a noticeably quicker evolution of CO_2 at the higher temperature. This is due to greater mobility of surface species at this elevated temperature and a higher affinity for CO_2 desorption. N.B. Spikes occurring in the mass 44 trace are due to the mechanical desorption of CO_2 when the flag is moved. The Pd (111) surface was beamed with CO at 323K with an initial S(t) of 0.5 until saturation had occurred (0.5ML). Figure 3.7A shows the CO beaming and sticking profile. This was followed by O_2 beaming at the same temperature, seen in figure 3.7B. Initially no O_2 sticking was observed and no CO_2 evolution occurred. This is due to the preferential occupation of binding sites by CO molecules, inhibiting O_2 adsorption and reaction. Once the sample is

heated, the partial pressure of O_2 in the chamber was seen to decrease indicating surface adsorption taking place. This can be attributed to the desorption of surface CO molecules freeing up sites for O_2 adsorption, Sticking occurs in tandem with the CO desorption peaking at 425K. Concurrently there is a peak in mass 44 indicating CO oxidation occurs once enough CO has desorbed to allow O_2 to stick to the surface.

$$O_{2(g)} \longrightarrow 2O_{(a)}$$

$$2O_{(a)} + 2CO_{(a)} \longrightarrow 2CO_{2(g)}$$

This produces CO_2 which desorbs, freeing up yet more surface sites for O_2 sticking. This gives rise to the catalytic ignition of CO oxidation, visible by the sharp CO_2 peak. As the temperature rises further, all the CO is used up and Oxygen starts to poison the surface.

A

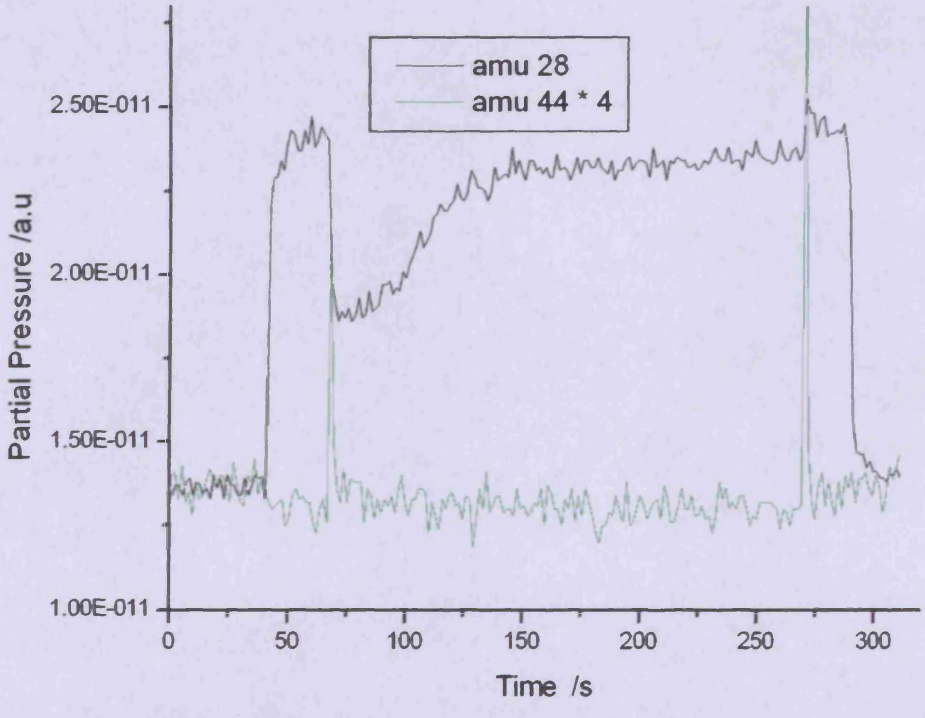

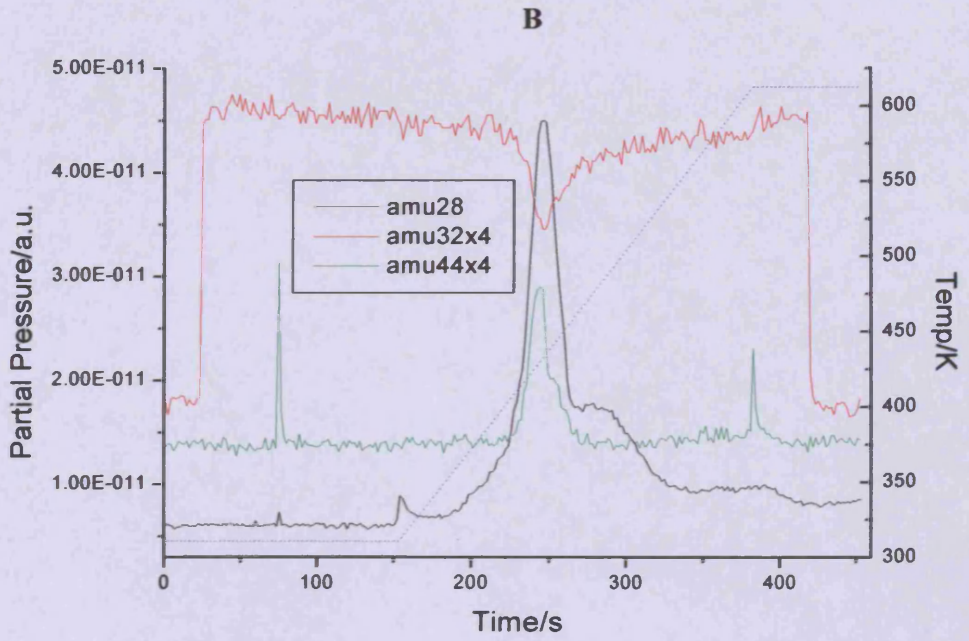

Figure 3.7.A. CO beamed on Pd(111) surface at 323K. **B.** Oxygen beamed on after CO followed by heating. O_2, CO and CO_2 monitored from masses 32, 28 and 44 respectfully. Temperature indicated by dotted line.

3.2.2.4 CO-O_2 Mixed Beam

The previous experiments carried out studying the oxidation of CO are of a transient nature. In the catalytic system in which VAM is manufactured, a more dynamic steady-state environment exists. This can be replicated by co-beaming two reactants in a mixed beam which can shed light on the catalytic turnover. A mixed beam of CO and O_2 of ratios 1:4 was dosed onto the sample at two different starting temperatures of 323K and 383K. The sample temperature was increased at a constant heating rate to observe the effect of heating on surface reactivity. The mixed beam profiles for masses 28, 32 and 44 can be seen below in figure 3.8A.

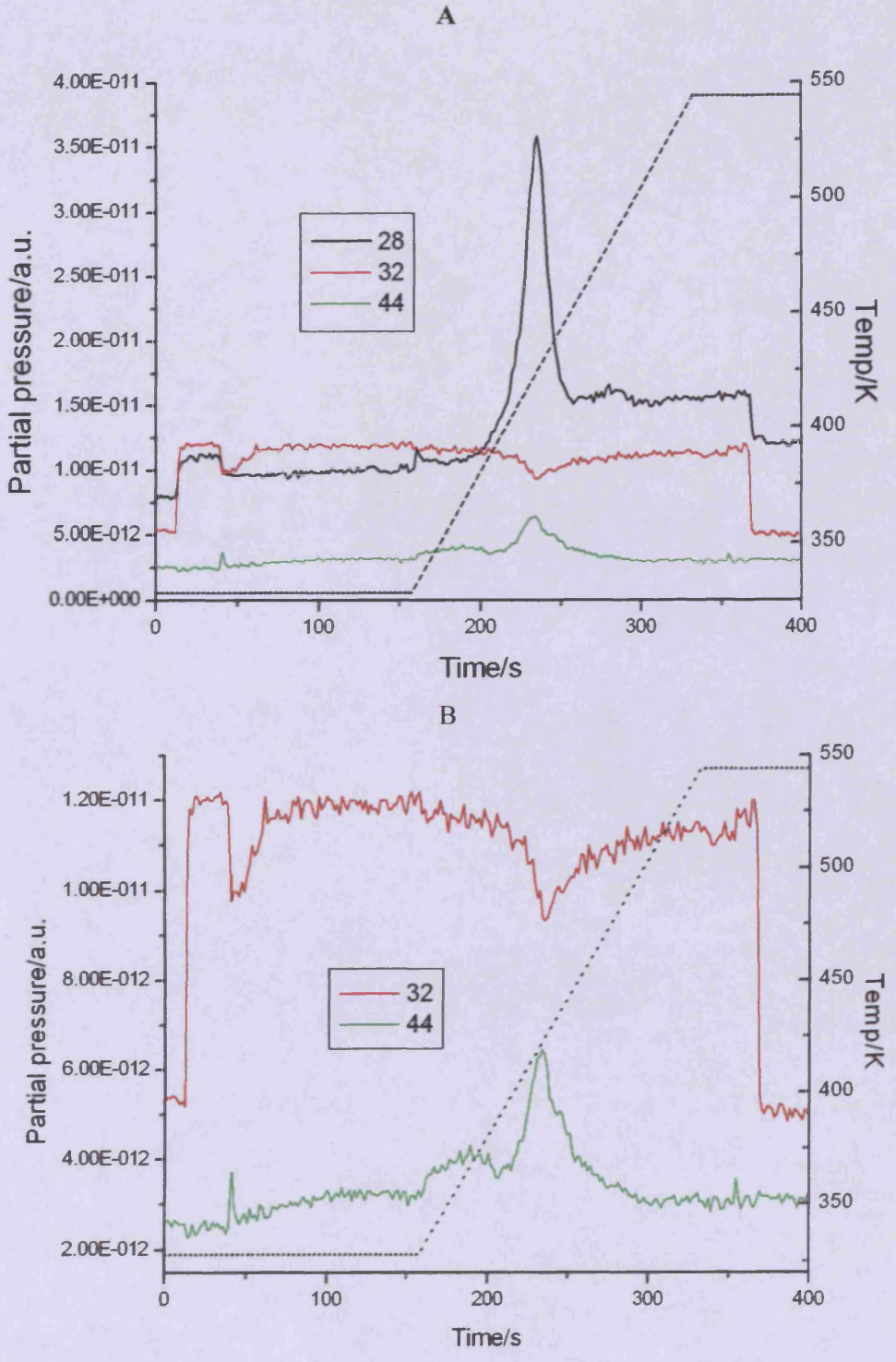

Figure 3.8.A. Mixed beam experiment initial temperature 323K ; O_2 : CO ratio 4:1 showing masses 28,32 and 44. ***B.*** Enlarged mass 32 and 44 signal plot. The temperature can be obtained from the dotted line.

Figure 3.8B shows masses 32 and 44 in greater detail. From the plot it is simple to observe the rate of production of CO_2 against time and the effect of temperature. Immediately once the beam flag is opened, CO_2 production commences observable by the slow increase of mass 44. Initial sticking probability of O_2 is 0.34 which drops off to zero after 25s. The initial sticking of CO was 0.5 and remains constant until heating. As the temperature increases, CO S(t) apparently decreases as CO starts to desorb. There is also an increased production of CO_2 which initially peaks at 370K, possibly due to the oxidation of the β_1 CO bonding state. At ~400K, CO starts to undergo rapid desorption. This allows O_2 molecules to stick to the surface and oxidise CO, observable by an increased CO_2 signal. CO desorption peaks at 425K, the same temperature at which CO_2 production peaks and O_2 sticking reaches a maximum of 0.42. As CO is gradually all oxidised, CO_2 production falls and O_2 starts to saturate the surface, poisoning the reaction.

An O_2/CO mixed beam experiment of ratio 4:1 with starting temperature 383K (see Figure 3.9) yielded interesting differences. The initial sticking probabilities of O_2 and CO are 0.35 and 0.42 respectively. CO_2 evolution was observed immediately after the reactant molecules interacted with the surface due to greater CO_2 desorption at this temperature. O_2 and CO uptake can be seen to become steady-state in nature after ~25s at a sticking probability of 0.02 and 0.38 respectively due to the continual production and desorption of CO_2. Between time 128s-166s, the beam flag was closed, displaying a drop in O_2 and CO S(t) to zero. However, the evolution of CO_2 did not stop immediately due to surface CO and O species still reacting. When the flag was opened again, O_2 and CO sticking once again resumed at 0.2 and 0.4 respectively and CO_2 evolution increased. Heating caused an immediate increase in

CO_2 production due to greater desorption and increased O_2 sticking. O_2 sticking probability peaked at 446K at 0.32. At this same temperature, CO_2 evolution also reached a maximum. CO desorption was also seen to peak at this temperature. Subsequent heating resulted in a rapid decrease in CO_2 production due to the absence of surface CO molecules. CO desorption peaked at ~440K, 15° higher than at lower temperature dosing possibly due to a lack of β_1 binding site formation at this higher temperature. In figure 3.9.A, the movements of the beam flag are indicated by the up and down arrows. The downward arrow indicates the lowering of the flag, alowing the beam of molecules to interact with the surface. An upward arrow represents the blocking of the beam.

A

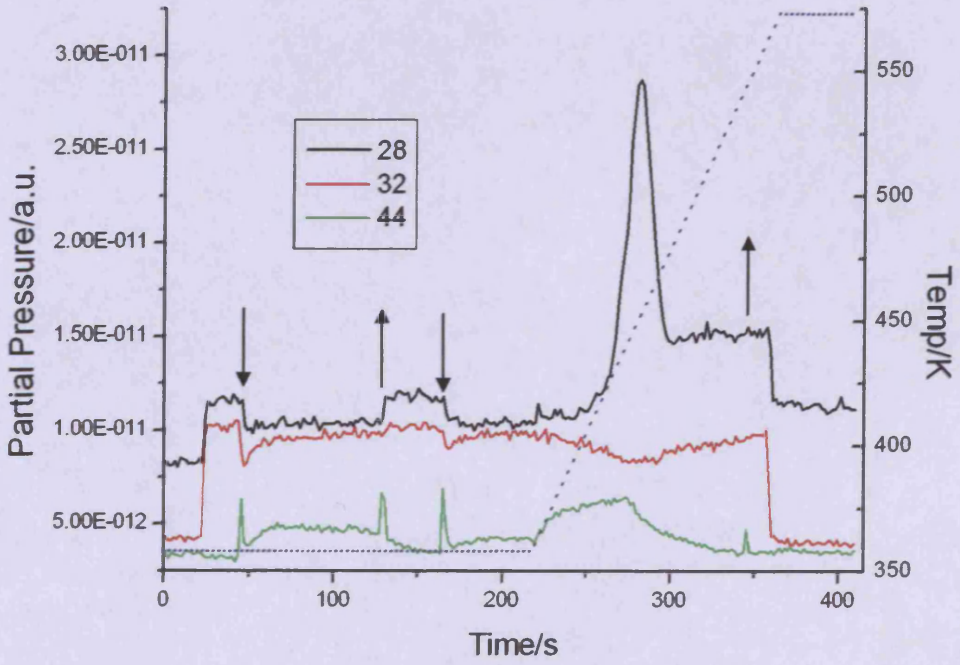

B

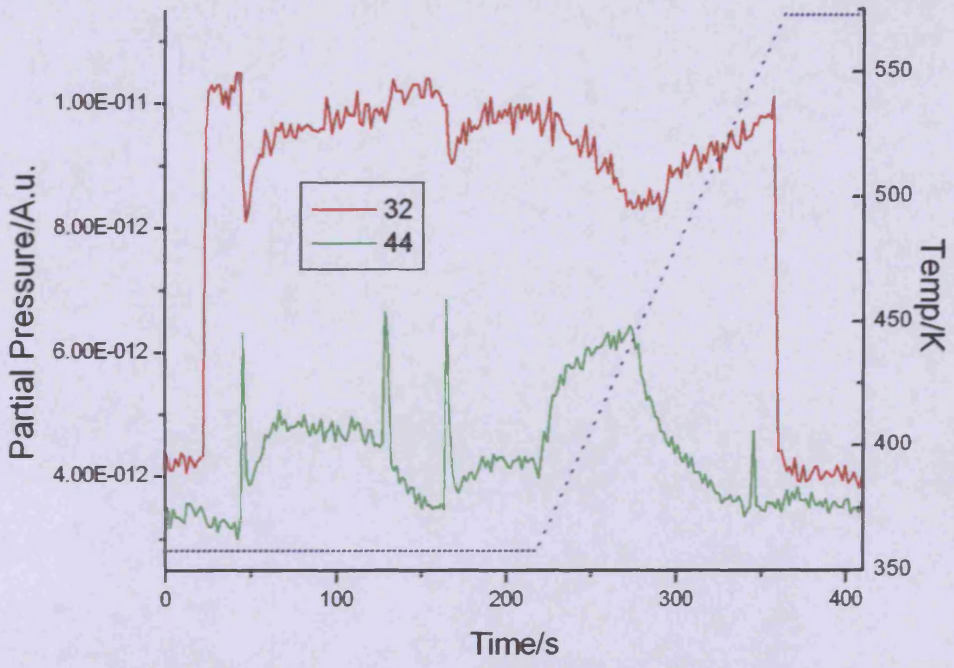

Figure 3.9.A Mixed beam experiment, initial temperature 383K; O_2 : CO ratio 4:1 showing masses 28,32 and 44. ***B.*** Enlarged mass 32 and 44 signal plot. The temperature can be obtained from the dotted line.

Similar mixed beam experiments were carried out with different ratios of O_2:CO. Figure 3.10 below is a mixed beam profile for O_2 and CO of ratio 1:1. The mass 32 and 44 signals have been magnified by a factor of x10. CO has an initial S(t) of 0.5 and the desorption peaks at 440K. The O_2 initial S(t) is 0.43, which drops to zero after 95s. Upon heating, O_2 sticking once again increases to a maximum of 0.52 as CO desorption frees up available surface sites. An interesting feature of the mixed beam experiment of O_2:CO in a ratio of 1:1 is the manner in which the CO_2 and O_2 are similar in nature. This highlights direct relationship between the ability of oxygen to stick to the surface and for the formation and desorption of CO_2.

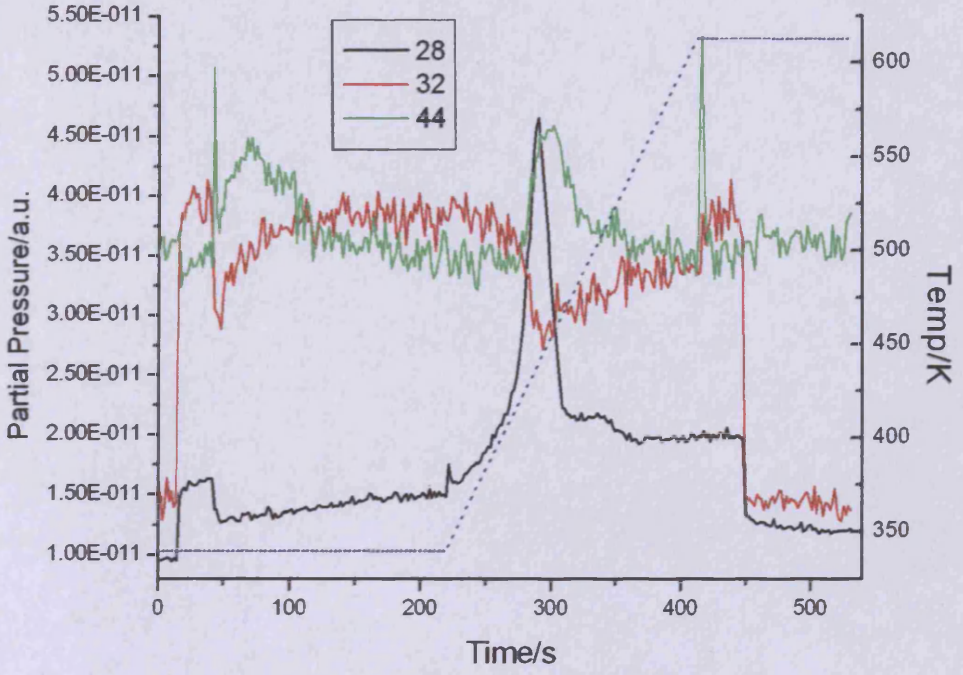

Figure 3.10 Mixed beam experiment, initial temperature 340K; O_2 : CO ratio 1:1 showing masses 28,32 and 44. Masses 28 and 44 magnified x10.

The temperature is represented by the dotted line.

CO and O_2 have been shown to readily react to form CO_2 at ambient temperatures. The adsorption of CO however can passivate the reaction by saturating the surface, inhibiting the adsorption of O_2. Heating the surface however causes CO desorption resulting in free adsorption sites for O_2. As more adsorption sites become available, O_2 $S_{(t)}$ increases and CO_2 production resumes. This may be relevant to the VAM synthesis since CO is a major by-product of the industrial process.

3.2.3 Ethylene on Pd (111)

3.2.3.1 Background

Ethylene is produced industrially via the steam cracking of saturated hydrocarbons such as naphtha. It is used widely in selective oxidation reactions to produce acetaldehyde and acetic acid[55-58]. Palladium supported catalysts are commonly employed in these processes. Ethylene is also one of the three main components in the production of vinyl acetate and is responsible for the 'vinyl' part of its name.

Ethylene has been studied previously on a range of different noble metal surfaces. Many studies have attempted to elucidate the nature of the surface species and its bonding properties on various Pd crystal surfaces. On the (100) plane, ethylene has been shown to bind to the surface as either a di-σ- or π-bonded species at 80K[59]. TPD results indicated that upon heating, the π-bonded species desorbs molecularly in a broad peak from 100K to 300K. The di-σ- bonded form however decomposes upon heating forming ethylidene species ($HCCH_3$) and eventually methylidyne species (CH) at 300K.

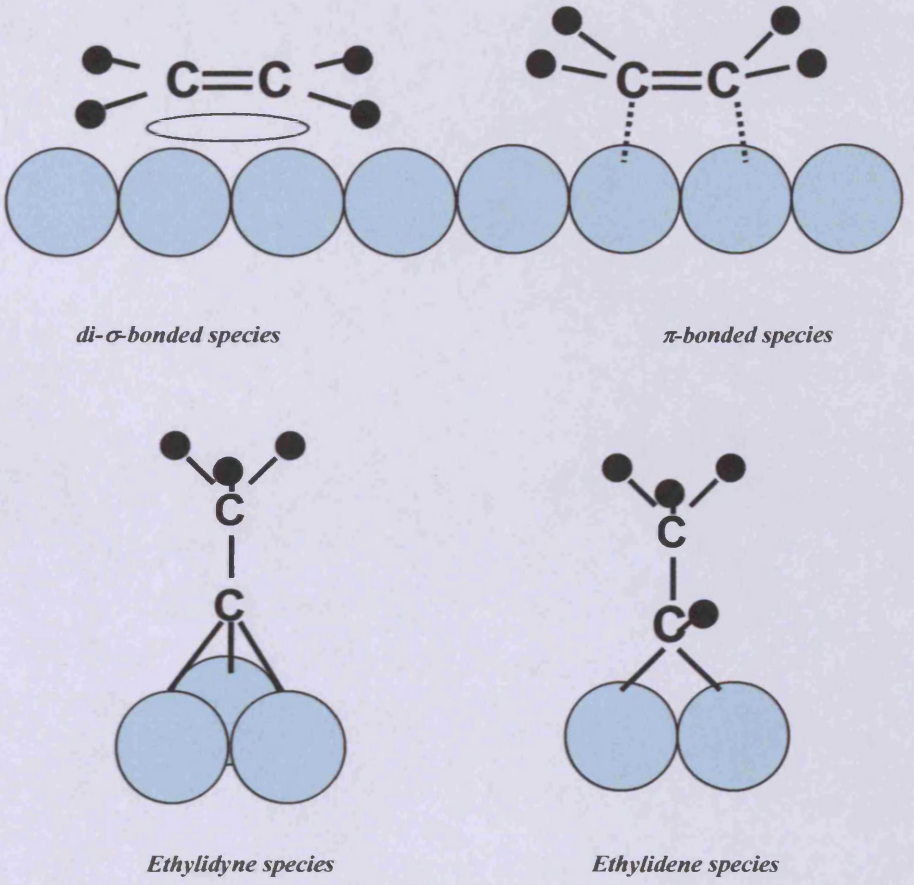

Figure 3.11 Different bonding configurations of ethylene on the Pd (111) surface

Ethylene adsorption on the Pd (111) has been investigated previously using infrared spectroscopy[60] electron energy loss spectroscopy[61] and high resolution XPS[62]. It has been observed from these various techniques that below 200K, ethylene adsorbs molecularly as a di-σ- or π-bonded species. The bonding of ethylene with the Pd (111) surface changes at ambient temperatures where dissociation occurs. There is much evidence that up to 350K, an ethylidyne species is the predominant adsorbate formed on Pd (111)[61-63]. Figure 3.11 displays the different bonding systems which have been observed. DFT studies have indicated a possible ethylidene intermediate as

a possible route of ethylene decomposition to ethylidyne[64]. there has been much interest in the ethylene to ethylidyne mechanistic pathway in recent times because it has been thought that the alkylidyne species may interfere with the catalytic hydrogenation and dehydrogenation reactions of hydrocarbons[65,66]. At more elevated temperatures greater than 350K decomposition of the molecule occurs and the situation is less clear[67]. Evidence of a partially dehydrogenated adlayer was observed up to 400K with the existence of CH and CCH species[68,69].

Recently, the formation of carbide has been shown to be an important factor with regards to VAM synthesis on Pd catalysts. The presence of PdC bulk resulted in a decrease in performance and deactivation of the catalyst[70]. On Pd (110), the interaction of ethene with the Pd (110) surface has been investigated. Ethylene has been shown to adsorb with a high probability over the temperature range 130 to 800 K with the low-coverage sticking probability dropping from 0.8 at 130 K to 0.35 at 800K[71,72]. Dehydrogenation was shown to occur at ~300 K and is fast above 350 K. Above 450K, adsorption continues at a high rate with continuous hydrogen evolution and C deposition onto the surface[72]. It has been proposed that in the intermediate temperature range, the carbonaceous species formed are located in the top layer and therefore interfere with adsorption, whereas when C goes subsurface above 450 K, the adsorption is unaffected. The deposited carbon was easily removed again by reaction with oxygen, thus implying that the carbon remains in the near surface region, probably consisting of a few atomic layers. LEED TPD and AES studies have shown similar results on the Pd (111) surface[73]. Between 350K and 440K, ever greater dehydrogenation of the molecule was observed as the ethylidyne adlayer decomposed depositing carbon onto the surface. At this temperature, the bulk was still shown to

have pure palladium properties. Above this temperature, the concentration of surface carbon was seen to decrease, forming a Pd_xC_y surface. Above 540K, the surface-bulk diffusion rate became fast, limited only by the ethylene gas supply. An activation energy of 107 $kJmol^{-1}$ for carbon diffusion from surface adsorption sites was derived in the temperature range 400-650K. Oxidation of ethylene has also been studied using XPS in an oxygen rich atmosphere. Carbon was seen to start to dissolve into the bulk at 480K leading to an altered C1s binding energy of 284.45eV at 500K[74]. Carbon segregation from the bulk has been shown to promote the oxidative reaction by suppressing the formation of a dense chemisorbed adlayer of oxygen[75].

The formation and distortion of graphite structures after ethylene adsorption has been studied using XPS on the Pt (111) surface[76]. Elemental carbon was observed after annealing the surface at 700-800K[77]. In order to form graphite on the surface, temperatures >800K were employed. Migration of carbon into the bulk of the crystal was seen to occur in this temperature range and segregation was observed after cooling the sample. It was proposed that by simply changing the temperature of the surface it is possible to either diffuse carbon into or out of the bulk. At a lower temperature of 250-320K on platinum surfaces, ethylene decomposition was seen after adsorption to occur via carbon-carbon bond breaking yielding methane[78]. The purpose of the following studies is to shine further light on the decomposition reaction pathways and to determine the nature of carbon dissolution.

3.2.3.2 Ethylene sticking measurements on Pd (111);

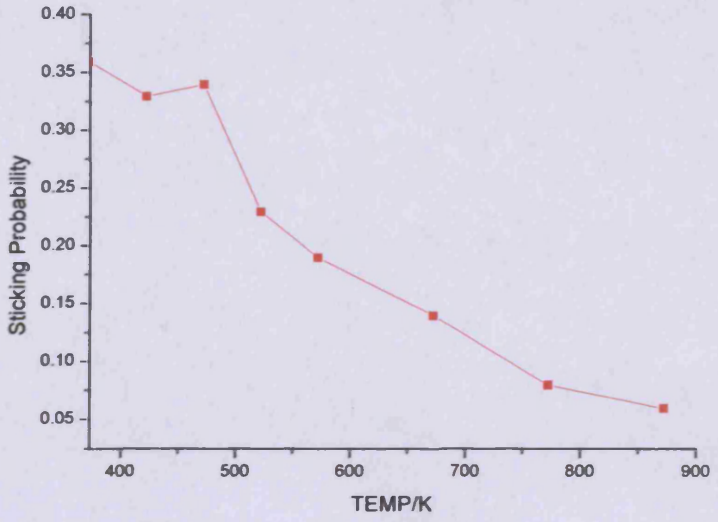

Figure 3.12 Initial sticking probability of ethylene on Pd (111) at different temperatures

Figure 3.12 displays the initial sticking probability of ethylene on a clean Pd (111) surface with respect to substrate temperature. As the temperature of the surface is increased, $S_{(0)}$ decreases. A decrease in S_0 as temperature increases can be attributed to a decrease in the residence time for the molecule. The less time a molecule resides in a precursor state, the less probable it is to undergo an energy exchange (thermalization) process with the surface needed for chemisorption to occur. By 873K, the reactivity of the surface towards ethylene had decreased to the extent that $S_{(0)}$ was not accurately measurable. Below 373K, $S_{(0)}$ was seen to decrease probably due to surface contamination from residual gases, such as CO, present in the system.

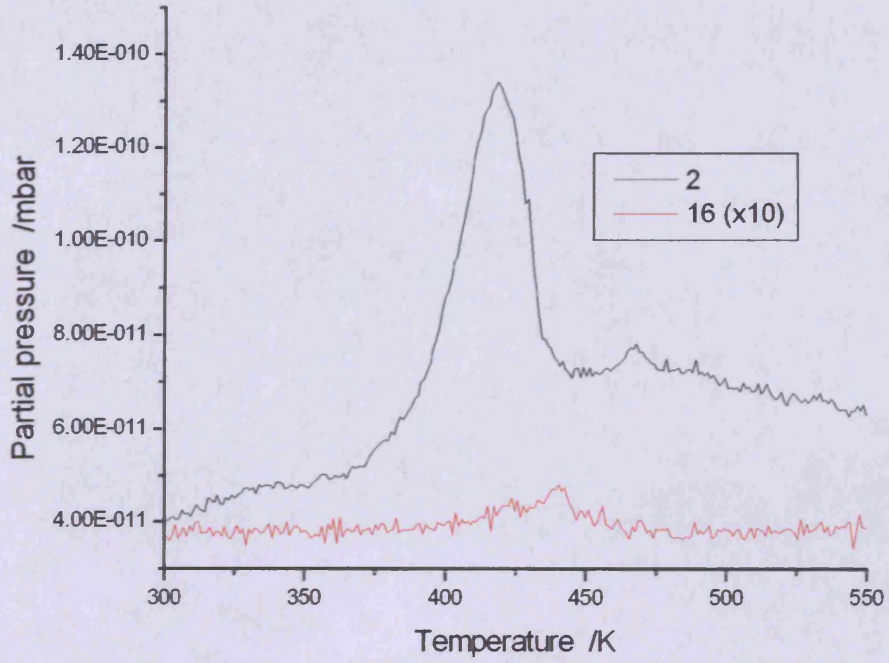

Figure 3.13 TPD of Ethylene background dosed 50L at $1x10^{-7}$mbar at 300K

To investigate the possible products formed from heating an ethylene dosed surface, a temperature programmed reaction was carried out with a heating ramp of ~$1Ks^{-1}$. Figure 3.13 shows the TPD profile after 50L of ethylene was background dosed into the chamber to a pressure of 1 $x10^{-7}$mbar at a sample temperature of 300K. A large desorption peak for H_2, mass 2, is seen peaking at ~420K. The H_2 evolution occurring at this temperature must be from the decomposition of the surface ethylidyne species (CCH_3). Another small H_2 desorption peak can also be seen at 468K as further H_2 evolution is occurring Mass 16 was also monitored to see any possible methane formation occurring. A small peak can be seen at 433K indicating a possible pathway for methane production

Molecular beam sticking measurements for ethylene on clean Pd (111) are given in figure 3.14. Sticking probability is shown in relation to the substrate temperature and the coverage of the beamed gas.

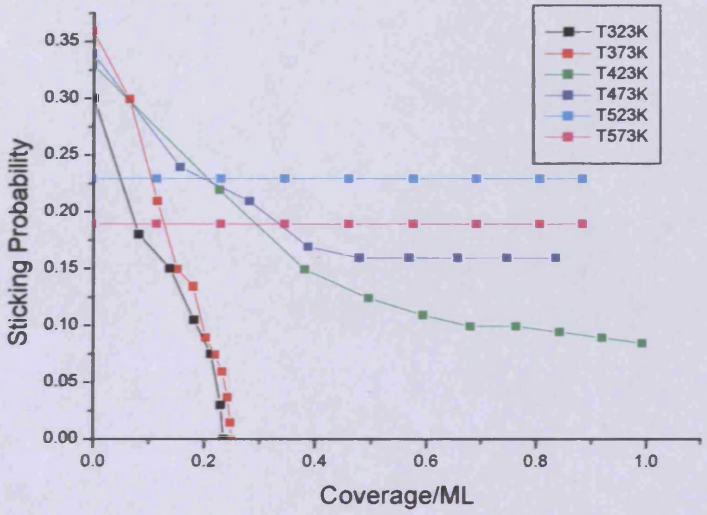

Figure 3.14 Sticking probability (S) for ethylene adsorption as a function of amount adsorbed on the surface at several different temperatures.

Ethylene initially sticks to the surface with a relatively low S_o at all temperatures between 323K and 573K, ranging from 0.36 at 373K to 0.19 at 573K. Saturation occurs at a coverage of ~0.25ML at room temperature. Ethylene has previously been shown to undergo dehydrogenation at elevated temperatures on the (110) surface[80]. This in turn deposits carbon onto the surface, evolving $H_{2(g)}$. The reaction was also observed as becoming 'steady-state' in nature by 473K. The Pd (111) surface however only exhibited continuous reactivity at temperatures above 523K. At ambient temperatures, ethylene binds to the surface forming a molecular a coverage of 0.25ML. As temperatures increase, ethylene decomposes depositing carbon onto the surface. At high temperatures there is continual decomposition of

carbon and uptake on the surface. Sticking experiments were performed for half an hour at 573K, depositing >10 monolayers of carbon, however no drop in activity was observed. XPS scans of the C1s peak (not shown) did not imply that the surface was carbonised. From this it has been logical to assume that a great deal of the surface carbon deposited via the dehydrogenation reaction had been lost to the bulk of the substrate.

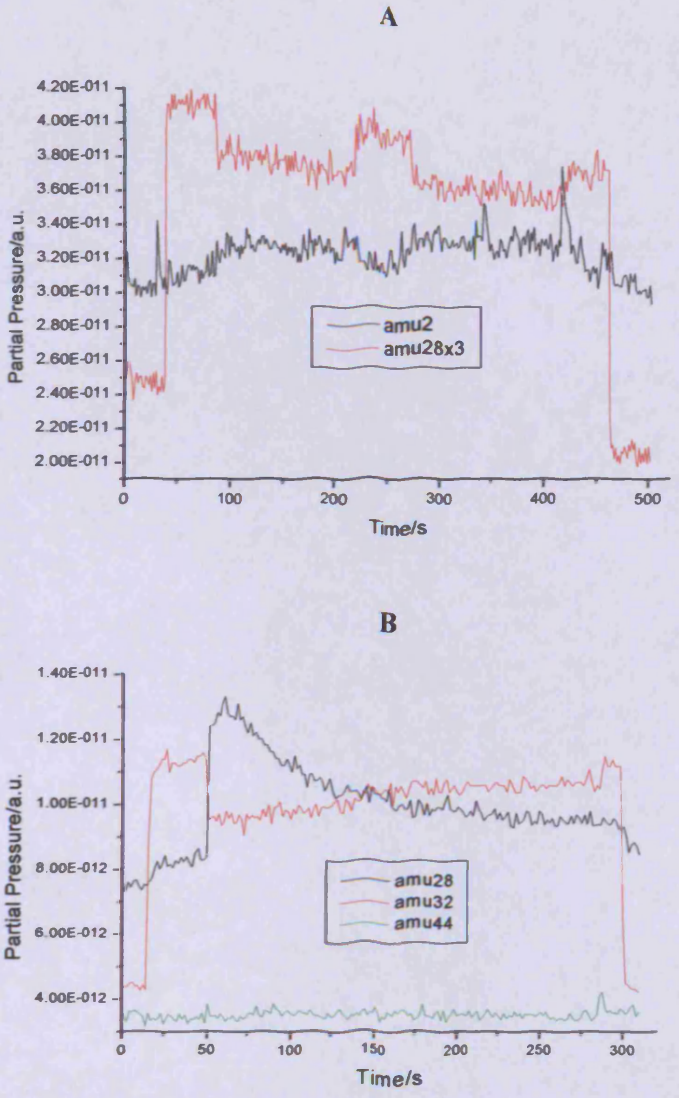

Figure 3.15.A. Beam experiment for ethylene sticking on clean Pd (111) at 573K. ***B.*** Oxygen sticking at same temperature directly after A. CO production observed but no CO_2

Figure 3.15A shows a typical beam profile for ethylene at 573K. Initially ethylene at this temperature has a S_0 of 0.18. Steady-state reactivity is also seen at this temperature since there is a continual sticking of ethylene. It is also possible to observe the increase and decrease in H_2 production from this dehydrogenation as the beam flag is opened and closed. Oxygen sticking experiments were performed directly after each ethylene reaction. Figure 3.15B shows oxygen S_0 of 0.27 at 573K followed by a gradual clean-off of the surface of deposited carbon. The immediate formation of CO indicates that the deposited carbon from ethylene dehydrogenation is being oxidised. Oxygen sticking becomes steady-state in nature after 175s indicating possible migration of carbon from the sub-surface region. CO evolution was not seen to drop immediately after the beam flag was closed due to the further oxidation of surface carbon by the remaining oxygen atoms.

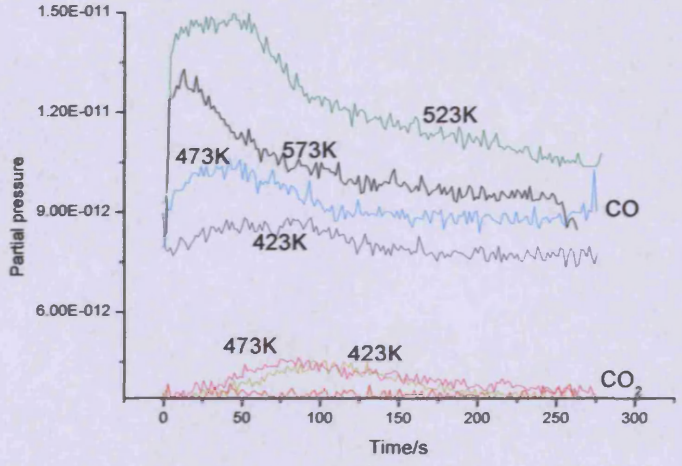

Figure 3.16 Oxygen beamed directly after Ethylene beamed on Pd (111) at allocated temperature for 5min

Figure 3.16 shows the evolution of desorbing products whilst beaming O_2. At high temperatures, 573K and 523K, CO production was observed as soon as oxygen

interacted with the surface, possibly due to immediate CO desorption after formation. Little CO evolution was observed at 423K indicating the presence of a low coverage of deposited carbon from ethene dehydrogenation. The CO evolution at 423K peaks at approximately 75s. This slow evolution can be attributed to the low concentration of surface carbon and the gradual build-up of oxygen. As the CO surface concentration increases, surface repulsions between molecules increase causing increasing desorption to occur. At 423K CO_2 evolution is also observed. CO_2 production can be attributed to a high concentration of surface oxygen atoms and a relatively low concentration of carbon. At 423K, after much of the carbon has been oxidised to CO and desorbed, the concentration of oxygen atoms increases allowing further the complete oxidation of surface carbon to occur. A similar situation can also be observed at 473K. At this higher temperature the affinity for CO desorption is much greater. The CO desorption peaks after 40s, much sooner than at 423K. This is due to an increased rate of desorption at higher temperatures. As could be expected, CO_2 production also occurs much sooner due to a greater tendency for desorption. An equation demonstration the carbon clean-off reaction is shown below.

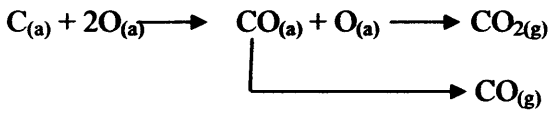

There was significantly more CO evolution at 523K. CO evolution peaked almost immediately after oxygen was beamed onto the surface and remained relatively constant for the first 50s. At this elevated temperature the lifetime of CO on the surface is extremely short, therefore and carbon oxidation that occurs will yield CO immediately. For this reason it might be expected that the CO evolution would

peak very rapidly and would then gradually 'tail-off'. However, at 523K, the CO production does peak but plateaus for the initial 50s. This can be attributed to migration of near-surface carbon to the surface, replacing the oxidised carbon. For the first 50s, equilibrium exists between the rate of CO desorption and the rate of carbon migration from the sub-surface to the surface. As the carbon concentration in the near-surface region decreases, the rate of surface migration decreases and therefore CO production drops. At this elevated temperature, no CO_2 is observed due to the short lifetime of the molecule on the surface after formation.

At 573K, CO evolution reaches a peak almost immediately after exposure to the oxygen beam. The amount of CO produced was significantly less than that evolved at 523K. This can be attributed to a decrease in uptake of ethylene since the sticking probability at this temperature is ~75% of that at 523K. This decrease means that less ethylene would undergo adsorption and dehydrogenation and therefore fewer carbon atoms would be deposited onto the surface. However if this were the case, one would expect the total amount of CO produced to be less than observed at 473K which is not the case. At 573K a greater evolution of CO occurs than at 473K. This is surprising since the sticking probability at this elevated temperature is 50% of that seen at 473K, therefore there should be less carbon deposited. This can once again be attributed to the migration of near-surface carbon. However, the decrease in CO evolution with respect to 523K can also be attributed to the possibility that at this temperature the rate of carbon dissolution is high enough that much of it is lost before oxidation can occur. Once again, the total oxidation of surface carbon to CO_2 is not observed due to the rapid desorption of CO when produced.

Due to the observations and conclusions gained from figure 3.16, it was thought relevant to attempt to probe the effect of time on the amount of carbon on the surface after ethene dehydrogenation. Figure 3.17 shows results from a series of experiments performed in order to probe this observation. The Pd (111) crystal was initially beamed with ethene for 5min at a sample temperature of 573K. Subsequently, oxygen was beamed at surface at the same initial temperature. The variable was the time in-between stopping dosing ethene and starting the oxygen beam. As was seen previously in figure 3.15, upon exposing the carbon dosed surface to oxygen, immediate production of CO was observed. However the amount of CO produced in this carbon clean-off reaction varies greatly. There is significantly more CO production when the sample was left unexposed for 5min than for 10min. This would indicate that in this dormant period, migration of surface carbon inwards is occurring. As would be expected, the amount of CO produced also decreases when left for 15min. However there is no observable difference in CO evolution between 15min and 30min periods between beaming.

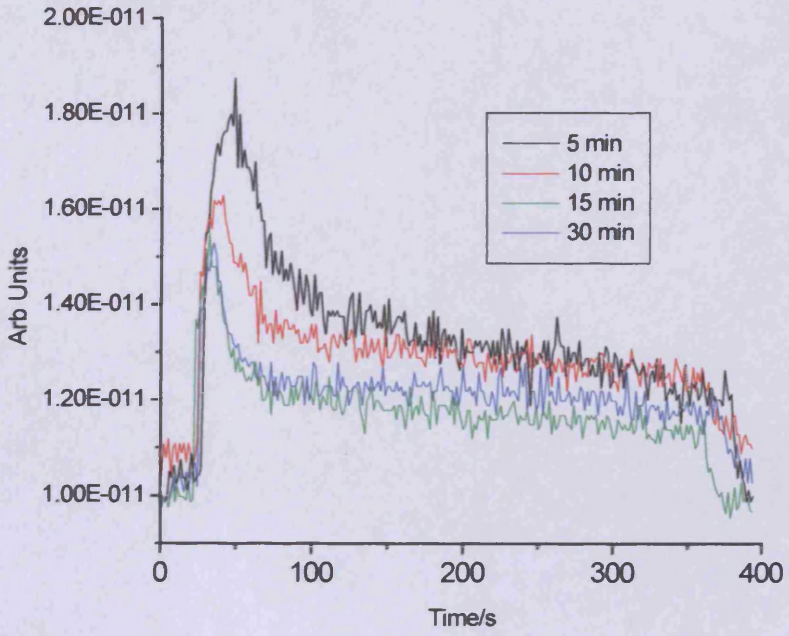

Figure 3.17 CO evolution after ethylene dosing at 573K. Different dormant periods shown

Interestingly, CO evolution doesn't decrease to zero, indicating the presence of surface carbon even after this time period. This would indicate that equilibrium has been reached between the rate of CO desorption and the rate of sub-surface carbon migrating to the surface. Since carbon is removed from the surface in oxygen clean-off, the concentration of surface carbon decreases. This decrease changes the dynamics of the system such that the net flow of carbon changes direction during oxygen treatment. Carbon is no longer dissolving into the bulk of the crystal but is instead migrating to the surface to maintain equilibrium.

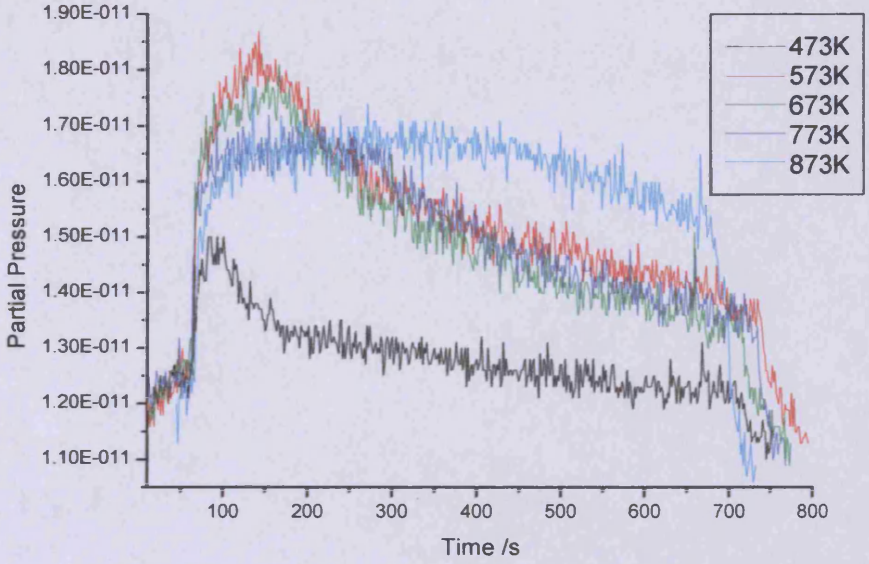

Figure 3.18 CO evolution from carbon clean-off after 15min ethene dosing

Ethylene was beamed onto the Pd (111) surface for a specific period of time. At elevated temperatures >473K constant sticking of the molecule was observed indicating dehydrogenation and subsequent bulk migration of carbon. After Ethylene had been dosed, the surface was then subjected to oxygen treatment. The resulting CO evolution profiles can be seen in figure 3.18. At 473K, immediate CO evolution was observed, peaking 29s after the initial exposure. The production rapidly drops off due to the clean-off of surface carbon. CO_2 production was also observed at this temperature, its production peaking after 44s once again due to the low concentration of surface carbon. At higher temperatures, a much more interesting phenomenon was observed. The carbon deposited from the dehydrogenation reaction which had previously gone into the bulk, returns to the surface. At 573K and above, much greater CO production occurs because of this bulk migration to the surface. At 573K, 673K and 773K CO evolution peaks at 80s, 95s, and 117s after initial exposure of oxygen respectfully. This difference in maximum CO evolution can be attributed to

the rate at which carbon migrate back to the surface. At the highest temperature, 873K, a relatively constant steady-state production of CO occurs. Carbon must be migrating from the bulk at the same rate as it is being oxidised implying great freedom of movement of bulk species at this temperature. This affinity for surface migration at high temperature means it must be thermodynamically favourable and therefore endothermic in nature.

The process of ethene adsorption and dehydrogenation are summarised. Deposition of carbon, and the subsequent bulk dissolution and oxidation are detailed in the equations below. At ambient temperatures <373K, Ethylene binds to the surface forming an ethylidyne species as shown in the first part of eqn1. As the temperature increases, dehydrogenation occurs yielding H_2 and forming CCH_x. This partial decomposition occurs below 423K. By 473K, total dehydrogenation happens (eqn2). At higher temperatures >423K, migration of surface carbon into the crystal bulk is favourable (represented by the forward direction in eqn3). However, as was seen at 873K, carbon can migrate from the bulk to the surface meaning this reaction is reversible and can reach equilibrium.

1. $C_2H_{4(g)} \rightarrow CCH_{3(a)} \rightarrow CCH_{x(a)} + H_{2(g)}$

2. $C_2H_{4(g)} \rightarrow 2C_{(s)} + 2H_{(g)}$

3. $C_{(s)} \leftrightarrow C_{(b)}$

4. $O_{2(g)} \rightarrow 2O_{(s)}$

5. $C_{(s)} + O_{(s)} \rightarrow CO_{(s)}$

6. $CO_{(s)} \rightarrow CO_{(g)}$

Carbon clean-off experiments were also carried out after longer periods of deposition. Figure 3.19 below shows the CO evolution curves after the sample was exposed to the ethene beam for 30min. The effect of temperature was once again investigated to see its affects on carbon migration. At 573K, the highest initial evolution of CO was observed. This would imply that at this 'low' temperature, there is the highest concentration of surface carbon available for oxidation. As the temperature is increased to 673K, the amount of initial CO evolution has decreased. It could be concluded that this happens because less carbon is deposited on the surface at this temperature due to a decrease in steady state sticking probability of the ethene molecule. However, after initial CO evolution has occurred, a more steady-state production of CO is reached which is significantly higher than at the lower temperature. This can be attributed to the build up of carbon in the near-surface region and its surface migration to once again restore equilibrium.

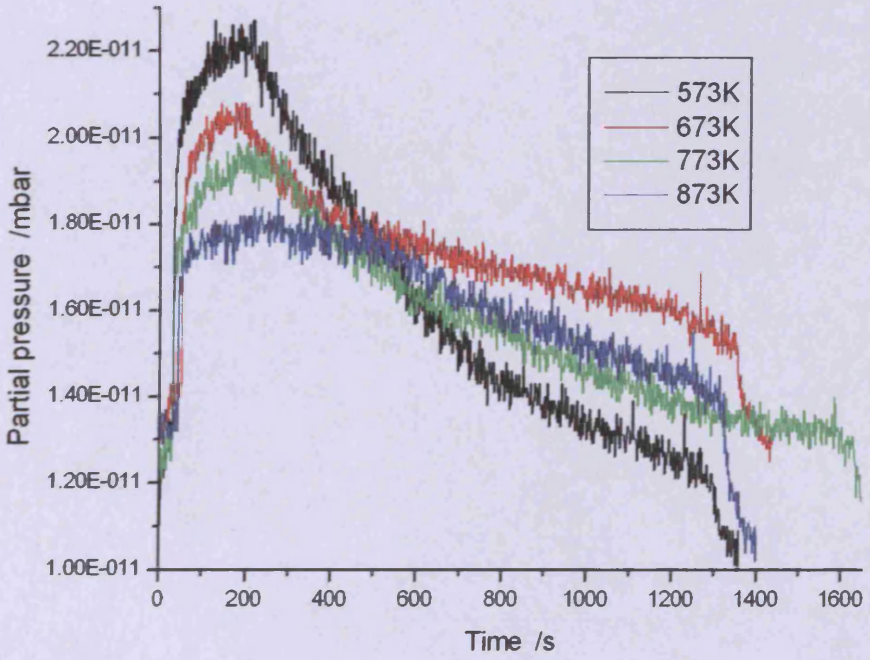

Figure 3.19 CO evolution from carbon clean-off after 30min ethene dosing

3.2.4 Acetic Acid on Pd111

3.2.4.1 Background

Studying the reactivity of acetic acid with the Pd (111) surface is of fundamental importance simply due to its role as a feedstock chemical in the production of VAM. The chemistry of acetic acid and its interactions with various transition metals has been widely studied on various transition metal surfaces due to its relevance in heterogeneous catalysis. Studies on Pd (110) have shown acetic acid to form acetate species at 325K which binds to the surface through both oxygen atoms in a bidentate fashion[79]. Similar bonding has also been proposed for the (111) surface. Three stable adsorption sites for acetate have been identified using DFT and LEED[80]. The most stable configuration of the OCO group was the atop-bridge-atop position where the two oxygen atoms sit directly above two adjacent palladium atoms.

The reactivity of acetate species on different surface has also been studied. On Pd (110), the acetate species was seen to decompose between 320 and 440K yielding CO_2, hydrogen and surface carbon[81]. This has also been observed on the Rh (110) surface[82]. Studies have also revealed that on the (111) surface, co-adsorbed oxygen stabilises the acetate species in this range resulting in autocatalytic decomposition at higher temperatures[83]. Similar findings have been shown on the (100) surface where the acetate species was stabilised by oxygen atoms up to 380K[84]. Lambert et al identified two different types of adsorbed dissociated acetic acid molecules observed using XPS, HREELS and TPR[85]. Both were acetate species either bonded in a mono-dentate or bi-dentate fashion. The mono-dentate species was seen to form at high

coverages due to the reduction in surface coordination and decomposition was observed between 200 and 275K. The scheme illustrated below shows the processes observed after adsorption of acetic acid on the Pd (111) surface at room temperature and the effect of temperature[85].

275-375K	$CH_3COOH_{(g)}$	⟶	$CH_3COO_{(a)} + H_{(a)}$
	$CH_3COO_{(a)}$	⟶	$CO_{2(g)} + CH_{3(a)}$
		⟶	$CO_{(a)} + CH_{3(a)} + O_{(a)}$
	$CO_{(a)} + O_{(a)}$	⟶	$CO_{2(g)}$
	$2CH_{3(a)} + 3O_{(a)}$	⟶	$2C_{(a)} + 3H_2O_{(g)}$
325-425K	$H_{(a)} + H_{(a)}$	⟶	$H_{2(g)}$
470-525K	$CO_{(a)}$	⟶	$CO_{(g)}$

3.2.4.2 Reactivity sticking profiles and TPD

An acetic acid molecular beam was introduced to the Pd (111) single crystal at different surface temperatures. To calculate the sticking probability of acetic acid, either the molecular ion's mass or that of a cracking fragment would have to be monitored. No such masses were observed when acetic acid was introduced because of the affinity of the molecule to stick to the chamber walls. Previous TPR studies have monitored acetic acid reactivity by placing the sample directly facing the mass spectrometer ioniser[85]. This allowed direct desorption form the surface to be monitored without interference from the chamber walls Different masses were observed to see if any products were formed during this exposure.

Figure 3.20 show partial pressure trace for two different masses observed when the surface was subjected to the acetic acid beam. As described earlier, CO_2 and H_2 (masses 44 and 2) have been the principal products observed from the decomposition process. At 323K, no H_2 or CO_2 was evolved from the surface. Acetic acid has been shown previously to bind with the surface at this temperature possibly forming stable acetate species or adsorbed decomposition products. At 373K however, CO_2 evolution was observed immediately after surface exposure to the beam. CO_2 desorption at this temperature would free up surface sites allowing further adsorption of acetic acid. The acetate species at this elevated temperature therefore undergoes decomposition via the following reaction;

$$CH_3COOH_{(g)} \rightarrow CH_3COO_{(a)}$$

$$CH_3COO_{(a)} \rightarrow CO_{2(g)} + CH_{3(a)}$$

323K

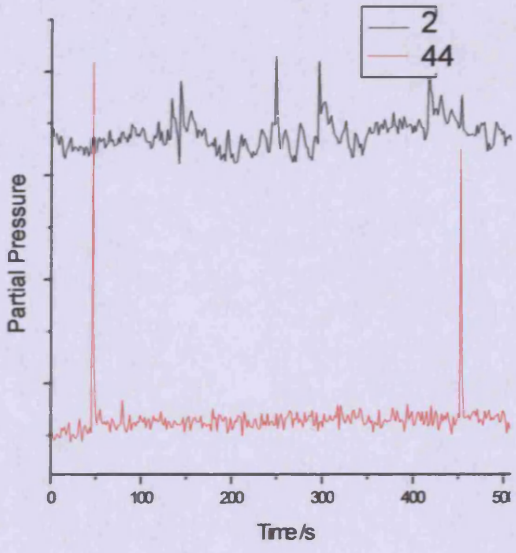

373K

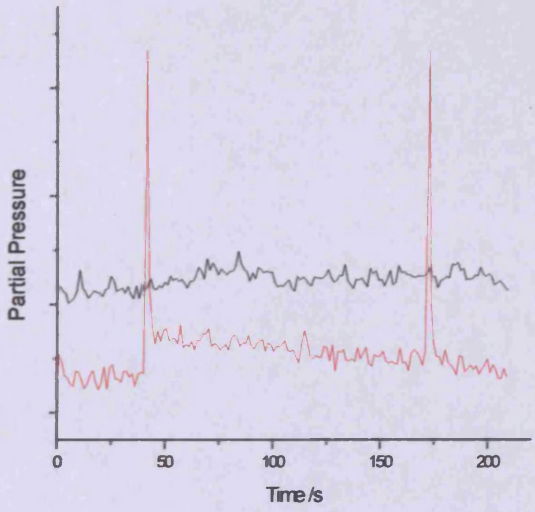

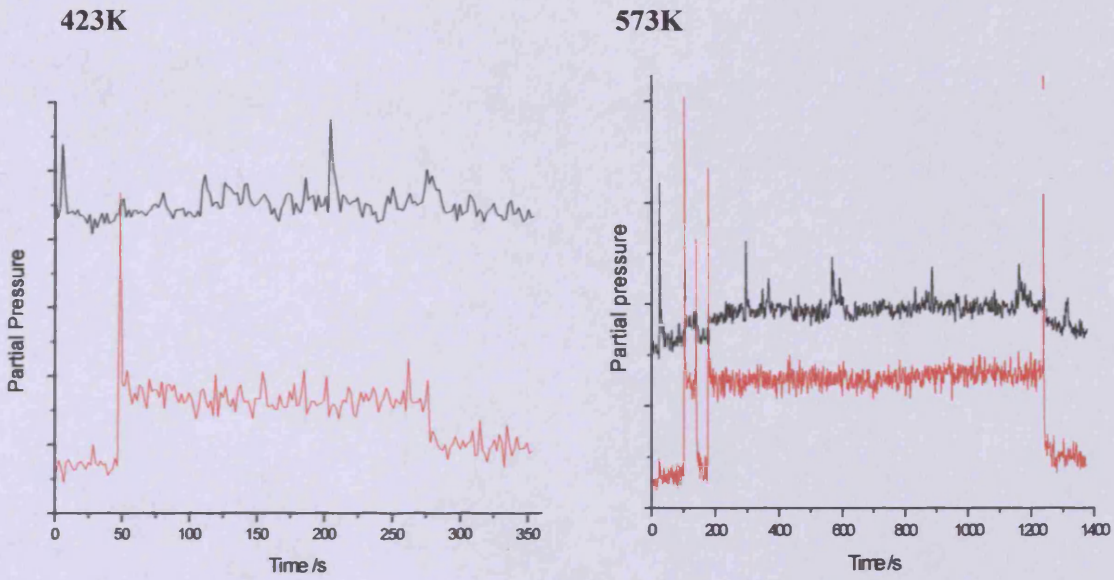

Figure 3.20 Two different masses were observed to elucidate product formation from acetic acid interaction with the Pd111 surface at 323K, 373K, 423K and 573K respectfully. (RED = amu 44; BLACK = amu 2)

After ~100s, the evolution of CO_2 ceases due to a termination in this decomposition reaction. This decrease in reactivity can be attributed to the build-up of surface CH_3 species or atomic carbon which would inhibit the binding of further acetic acid molecules. At this temperature no H_2 evolution was observed, discounting the possibility of further dehydrogenation of CH_3 groups. CO_2 forms from the cleavage of the C-C bond in the acetate species formed upon adsorption. Increasing the temperature of the surface changes its reactivity to adsorbed acetate species. At 423K, CO_2 evolution was observed immediately after exposure to the incident beam. The amount of CO_2 produced however is much greater than at 373K with CO_2 evolution still occurring strongly after 200s of exposure. This increase in surface

reactivity must be due to the absence of poisoning from CH_x species on the surface. By 573K reactive decomposition of acetic acid is continuous. CO_2 was produced constantly over a long period of time. It was also possible to see the H_2 signal increase and decrease when the beam was broken by the flag. Similar to ethylene, total dehydrogenation occurs at this temperature leaving surface carbon atoms. These atoms once again diffuse into the bulk freeing up sites allowing further adsorption onto the surface.

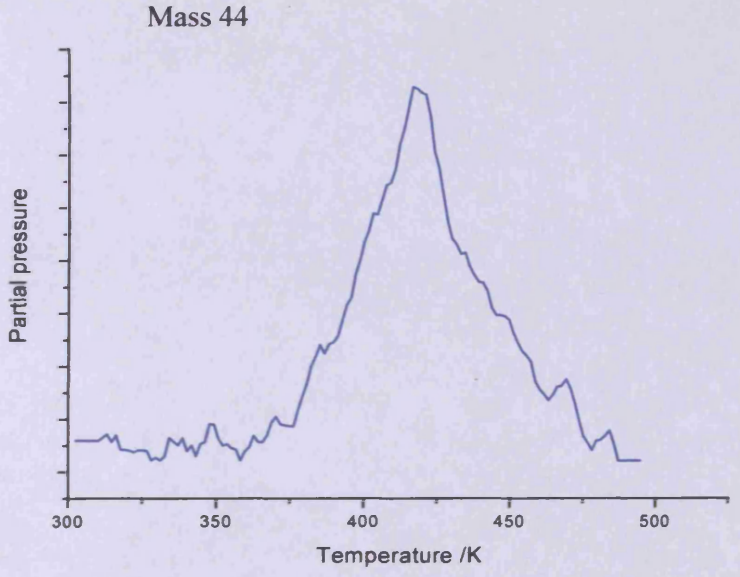

Figure 3.21 TPR of acetic acid dosed on Pd (111), (300L at $1x10^{-7}$mbar)

TPD was also performed to investigate the desorption products shown here in figure 3.21. Acetic acid was dosed at 300K for 300L and the sample was heated at a rate of ~1K/s. H_2 was seen to evolve across this temperature range, most notably between 300K and 375K. CO_2 production started at 375K and was seen to peak at 418K. By 473K CO_2 production ceased implying all of the acetate groups had

decomposed. This is consistent with the molecular beam experiments shown in figure 3.20 where no CO_2 evolution occurred at 323K but was present at 373K. TPR studies of acetic acid dosed at 170K showed CO_2 formation in two regimes 200-275K and 275-375K form the mono-dentate and bi-dentate species respectively[85]. Since acetic acid was dosed at 300K, decomposition of the molecule may have occurred initially whilst dosing, stabilising further adsorption of the molecule. Surface carbon has been shown previously to stabilise acetate groups on the Pd (110) surface resulting in increasingly higher decomposition temperatures with greater surface carbon[81].

Tysoe et al have previously used RAIRS and MS to study the reaction of ethylene with acetate species on O_2 covered Pd (111)[86]. VAM production was observed, removing surface acetate species. As the surface became more depleted, ethylidyne species were observed, implying that they are not involved in the formation of VAM. Numerous experiments were carried out to try to produce VAM Mr(43) from the direct reaction of ethylene and acetic acid. Acetic acid was predosed onto the surface at different coverages and ethylene was subsequently beamed on. At ambient temperatures, no ethylene sticking was observed indicating surface site saturation with acetate species. At temperatures >473K ethylene sticking and dehydrogenation was observed similar to results seen on clean Pd indicating decomposition of acetate species and bulk migration of surface carbon. Predosing ethylene before beaming acetic acid was also carried out at different surface temperatures with similar negative results. Since no VAM production was observed it can be concluded that the preadsorption of an O_2 layer is critical in VAM formation.

3.2.5 Acetaldehyde on Pd (111)

3.2.5.1 Background

Acetaldehyde is a significant molecule in numerous catalytic systems. Palladium (II) catalysts have been used industrially to produce acetaldehyde in the homogeneous Wacker process via the oxidation of ethylene[87]. It has also been shown to play an important role as a by-product of the heterogeneous alkoxylation of ethylene to vinyl acetate[88].

TPD and HEELS analysis of low temperature acetaldehyde adsorption on Pd surfaces has revealed two different bonding configurations[89,90]. Below 200K both a weakly bound species bonded in a mono-dentate fashion via the oxygen atom (η^1) and a more strongly π-bonded moiety (η^2) were observed. The η^1 desorbs above 200K leaving the η^2 species which dehydrogenates to produce stable acetyls ($CH_3C{=}O$). The acetyls underwent decarbonylation at 280K releasing CO and surface methyl groups (CH_3) on Pd (110). Isotopic labelling suggested that scission of C-C bonds preceded C-H scission for acetyl intermediates on the (110) surface. On Pd (111), the reverse was observed, producing methylene (CH_2) species[91]. Molecular beam results for the (110) surface have shown initial dehydrogenation followed by decarbonylation at room temperature producing methane and surface CO[92]. Similar results were observed on Rh (111) where methane production was observed at 267K and was determined to be dependant on the coverage[93]. At low coverages <0.05ML, no methane evolution was seen. Co-adsorption of deuterium enhanced methane production implying selectivity was partially controlled by the availability of hydrogen. Above 423K on Pd (110), total dehydrogenation of the molecule was

reported with steady-state sticking and CO production. This implies once again bulk diffusion of carbon into the surface of the sample.

RAIRS and TPD studies have been carried out by Tysoe et al to investigate the decomposition pathways of vinyl acetate on Pd (111). Upon heating a vinyl acetate dosed surface from 237K to 290K, the acetyl-O bond cleavage was observed. This produces surface acetyl and vinyloxy (CH_2CHO-) groups. Further heating resulted in desorption of acetaldehyde at 310K via the hydrogenation of these two groups. Total decomposition to CO, CO_2 and methane was observed at higher temperatures[94]. The production of acetaldehyde as a decomposition product of VAM highlights its relevance in the industrial process.

3.6.2 TPD and beam results of acetaldehyde

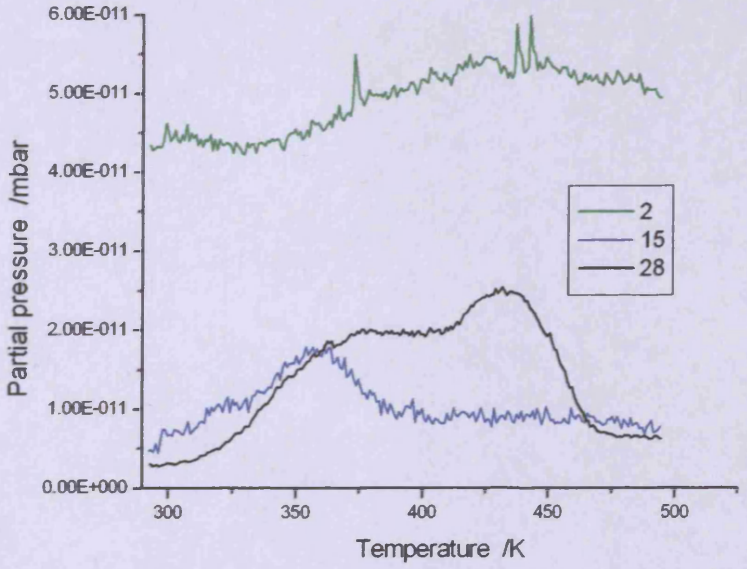

Figure 3.22 3L background dose of acetaldehyde on Pd111 at 295K

Figure 3.22 shows the TPR profile for an acetaldehyde background dose of 3L at 1 x10^{-8}mbar. By 323K, CO has started to desorb from the surface, peaking at 373K. The CO produced here can be identified as a decomposition product of the acetaldehyde dosed onto the surface since background dosed CO does not start desorbing until 375K. The initial production of CO coincides with an increase in mass 15, indicating methane evolution and evidence for the decarbonylation mechanism cited previously on Pd (110). Methane production peaks at 357K and has ceased by 389K. Above this temperature H_2 evolution can be seen to occur as the partial pressure of mass 2 increases. This is due to the heating of the surrounding sample support and not from surface desorption

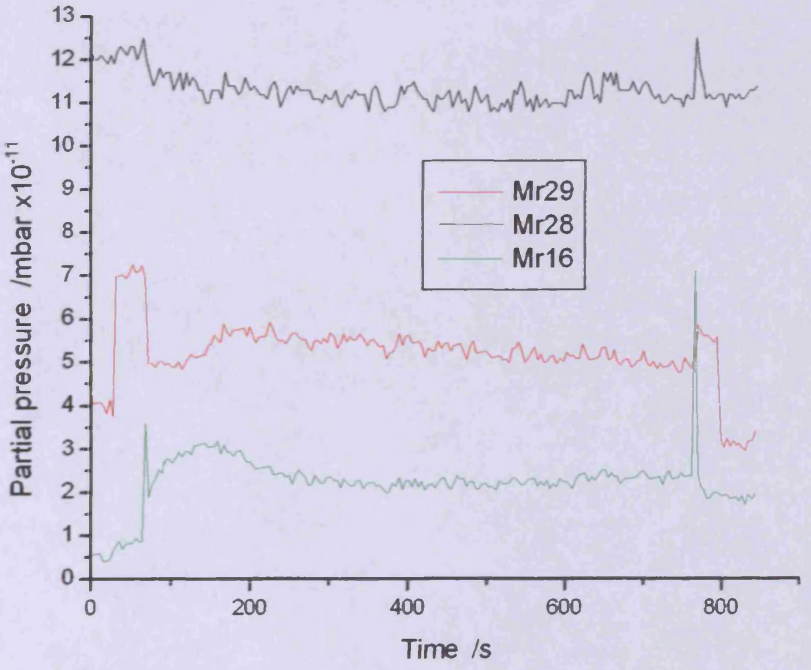

Figure 3.23 Acetaldehyde beamed onto Pd (111) surface at 318K

Figure 3.23 shows the profiles of various important masses observed when acetaldehyde was beamed directly onto the clean Pd (111) surface. The mass 29

cracking fragment was found to be the most suitable for measuring this molecule as it didn't overlap with the masses of other relevant molecules. The initial S_0 of 0.69 indicates that the molecule is very reactive towards the Pd (111) surface, significantly more than ethylene and oxygen. For the first 45s, constant sticking is seen in tandem with an increase in mass 16. This increase can be attributed to the formation of methane on the surface. This methane formation and desorption in-turn frees up more surface sites for acetaldehyde to bond to maintaining the high $S_{(t)}$. Surprisingly no increase in CO was observed at this temperature despite CO evolution occurring on Pd (110) at this temperature. TPD data shows CO evolution only occurring above 323K because CO does not seem to desorb. After this initial period of activity, the $S_{(t)}$ decreases to ~0.32 as CO molecules block adsorption sites on the surface. This decrease in reactivity in turn causes the methane production to decrease. However, even after 700s, acetaldehyde was still reacting with the surface and methane evolution was still occurring. For this to be the case, CO desorption must occur since otherwise it would block surface binding sites, inhibiting acetaldehyde adsorption. Since no visible CO evolution can be seen, the mass 28 signal must therefore be a product of both CO and a cracking fragment of acetaldehyde. The lack of increase in mass 28 from the production of CO is offset by the sticking of acetaldehyde. Acetaldehyde was also beamed onto the surface at elevated temperatures (423K) and the beam profile can be seen below in figure 3.24. CO evolution was seen to evolve immediately after the beam flag was dropped indicated by an increase in the Mr28 signal. However no methane formation occurred.

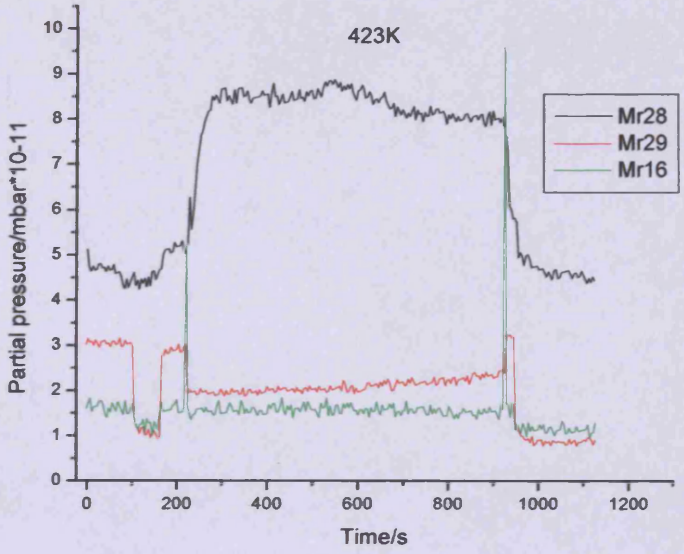

Figure 3.24 Acetaldehyde beamed onto the Pd (111) surface at 423K

This result of beaming acetaldehyde at a higher temperature indicates a different decomposition pathway occurring. Instead of decarbonylation, total dehydrogenation of the molecule would explain the absence of methane. This more destructive decomposition pathway at higher temperatures agrees with previous TPD studies proposed by Barteau et al[89,90]. The overall reactivity of is also markedly different than at low temperatures. Instead of an initial period of high activity and then a decrease due to CO poisoning, reactivity remains relatively constant. This is due to the readiness of CO to desorb at this temperature freeing up surface adsorption sites. The $S_{(0)}$ is lower (0.53) than at ambient temperatures however after depositing ~5ML of acetaldehyde, it has only decreased to 0.42. This small decrease in sticking probability (~21%) would imply that the surface is still reactive. However, upon dehydrogenation of the molecule, carbon is deposited onto the surface which should in-turn decrease reactivity. Surface carbon must therefore undergo surface migration

as seen with both ethylene and acetate decomposition previously. Indeed, at temperatures >523K, the sticking probability showed no decrease at all over a long dosing period implying facile bulk migration.

3.6.3 XP spectra of acetaldehyde

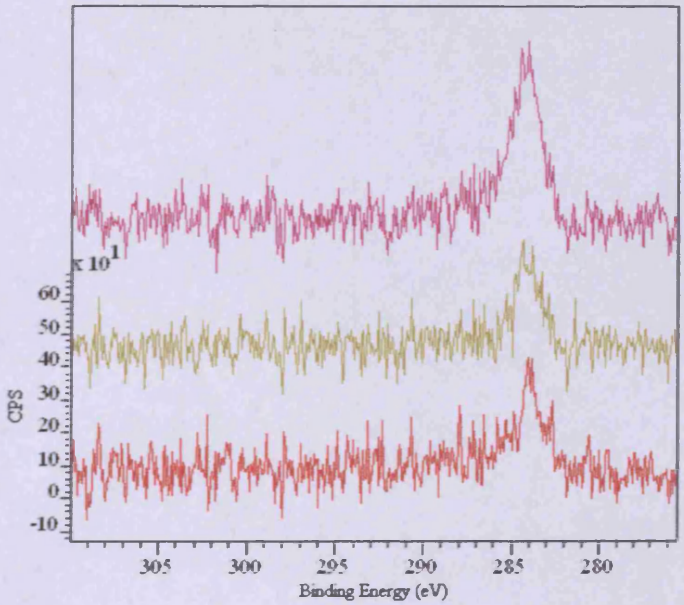

Figure 3.25 XP spectra of the C1s region after dosing 12L of acetaldehyde at temperatures 298K (RED), 473K (GREEN) and 393K (MAGENTA)

In order to investigate the presence of surface carbon the surface was dosed with 12L of acetaldehyde at different temperatures. After dosing, the surface was cooled back to room temperature and XP spectra of the Pd 3d and C 1s region were obtained. The XPS spectrum of the C1s region for the clean Pd has been subtracted from both sets of data due to the overlap of the Mgβ satellites positioned at 291 and 286eV due to the Pd 3d peaks. Figure 3.26 shows the C 1s region after dosing

acetaldehyde. Quantification of the peaks at 298K and 473K showed carbon to have saturated the surface to a coverage of 0.5ML and 0.45ML respectively. However at 393K, a much larger build-up of ~1.5ML was seen. At 298K, carbon saturation is probably due to surface CO molecules deposited after decarbonylation and possibly some CH_x species. Since steady-state dehydrogenation has been seen previously to occur above 473K, it can be assumed that any deposited carbon must have dissolved into the bulk of the crystal leaving a stable surface layer. This agrees with carbon incorporation studies carried out by Gabasch et al using similar methods[94]. Studies on Pd (110) have also shown a decrease in carbon peak intensity at higher temperatures due to dissolution[91]. At the interim temperature of 393K, carbon is dissolving into the bulk but at a much slower rate than at 473K. Because of this, a build-up of carbon occurs in the near surface region. The rate of acetaldehyde decomposition is limited by the ability of carbon to migrate into the bulk.

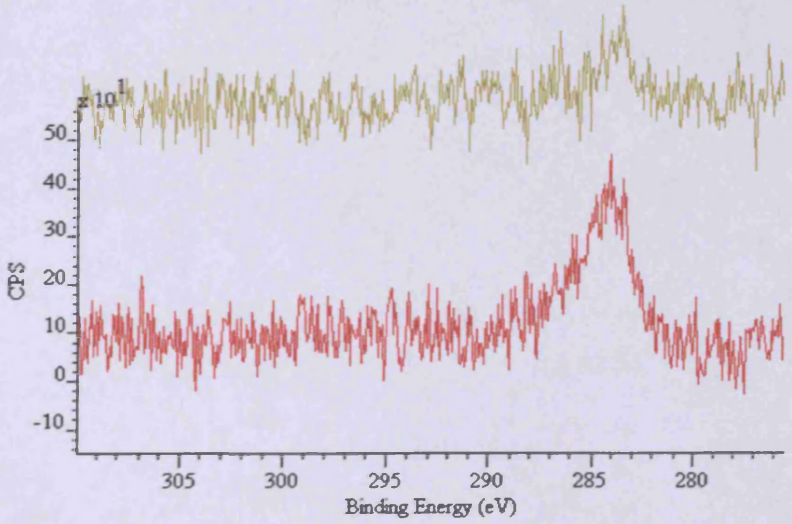

Figure 3.26 XPS spectra of C1s after dosing acetaldehyde at 393K (RED) and subsequently heating the surface to 523K (GREEN)

Experiments were performed in which the surface was background dosed with acetaldehyde at 1 $x10^{-7}$mbar and the effect of heating the surface was investigated. XPS spectra obtained after dosing at 393K and subsequent heating to 523K can be seen above in figure 3.26. The concentration of surface carbon was calculated to be $3.29x10^{15}$atoms/cm^2, approximately ~2.5ML. A significant decrease in carbon can clearly be seen after heating the sample to 523K. The surface concentration of carbon decreased to ~0.4ML, a 84% drop in composition. This is due to surface carbon migrating into the bulk of the sample. At 393K, most of the peak is made up of atomic carbon (284eV) however there is a distinct shoulder at higher binding energy 286.5eV. This can be attributed to the presence of CO. After heating this shoulder is no longer seen due to the desorption of CO. A small shift to a lower binding energy (0.5eV) can also be seen in the carbon peak after heating. This could be due to the formation of palladium carbide in the near surface region. The Pd3d doublet also exhibited a shift to lower binding energy (0.3eV) indicating a change in its electronic interactions.

The reactivity of acetaldehyde on Pd111 can be summarised in the following scheme[90];

1. $CH_3CHO_{(g)} \rightarrow CH_3CHO_{(a)}$
2. $CH_3CHO_{(a)} \rightarrow CH_{3(a)} + H_{(a)} + CO_{(a)}$
3. $CH_{3(a)} + H_{(a)} \rightarrow CH_{4(a)}$
4. $CH_{4(a)} \rightarrow CH_{4(g)}$
5. $CO_{(a)} \rightarrow CO_{(g)}$
6. $2H_{2(a)} \rightarrow 2H_{2(g)}$

7. $CH_3CHO_{(a)} \rightarrow C_{(a)} + 2H_{2(a)} + CO_{(a)}$

8. $C_{(a)} \rightarrow C_{(b)}$

Across the temperature range studied, acetaldehyde adsorbed with a relatively high $S_{(0)}$. Acetaldehyde's propensity for reacting with the Pd (111) surface indicates a favourable rate for step 1 shown by the high sticking probability. Steps 2-4 summarise the decomposition pathway observed at ambient temperature. Decomposition of the molecule occurs resulting in CO, CH_3 groups and atomic hydrogen. This stable CH_3 species readily reacts with the free surface hydrogen atoms yielding CH_4. Methane desorption becomes more favourable as the concentration of adsorbed molecules increases due to greater surface repulsions. At elevated temperatures, step 3 does not occur due to the instability of CH_3 group. C-H bond cleavage instead occurs resulting in carbon deposition and hydrogen evolution. Both CO and H_2 desorption takes place (steps 6+7) at this elevated temperature allowing further adsorption of incident molecules. Carbon migration into the bulk (step 8) starts to occur at a significant rate at temperatures >423K allowing steady-state dehydrogenation to occur ad infinitum.

The Pd (111) surface studied here appears to be very similar in nature to the Pd (110) surface previously[92]. Acetaldehyde was shown to adsorb onto the (111) surface with a high initial sticking probability (0.69) at ambient temperatures and underwent decarbonylation. Acetaldehyde exhibited a slightly higher initial sticking probability (0.8) on the (110) surface at ambient temperatures and decarbonylation was also observed[91]. The slightly higher $S_{(0)}$ can be attributed to the greater openness of the (110) surface allowing increased adsorption. Similar chemistry has also been

observed on the Rh (111) surface with methane evolution occurring at 267K[92]. On the Pd (111) surface, dehydrogenation of the molecule also occurred in a similar manner to the (110) surface. This similarity in reactivity is surprising since normally the (111) surface displays much less reactive qualities than the (110) surface.

3.3 Conclusions

The interaction of the Pd (111) surface with oxygen, ethylene and acetic acid, the three feedstock compounds used in the production of VAM, was studied under UHV conditions. All three molecules exhibited reactivity with the surface. Oxygen underwent adsorption across a broad temperature range from 300K to >800K. Increased uptake of O_2 was observed at higher temperatures due to the migration of surface O atoms into the sub-surface region. Both ethylene and acetic acid exhibited similar chemistry to that seen previously on the Pd (110) surface[81,91]. Decomposition of the molecules at elevated temperatures resulted in the deposition of surface carbon. Steady-state reactivity was also observed above 473K due to dissolution of carbon into the bulk. Acetaldehyde has also been studied since it has been shown to be a decomposition product of VAM[94]. Acetaldehyde would also be a product of the C-O single bond cleavage in VAM. Decomposition of the compound was also seen to occur on the (111) surface in a similar fashion to (110). Decarbonylation was observed at ambient temperatures with dehydrogenation occurring at higher temperatures. All of the organic molecules have shown a propensity towards decomposition either partial or total at different temperatures. The destructive nature of the surface is of course an undesirable feature with regards to the industrial

process. Carbon dissolution was observed for all organic molecules and O_2 after decomposition with steady-state reactivity occurring >473K showing Pd to act like a sponge. The formation of PdC has been reported previously to be a factor in the deactivation of the catalyst in VAM synthesis[70]. The effect of Au on surface reactivity is explored in the following chapters with regards to decomposition and carbon uptake.

3.4 References

1. H. Conrad, J. Kuppers, F. Nitschke, A. Plagge, *Surf. Sci.*, **69** (1977) 668
2. T. Matsushima, *Surf. Sci.*, **157** (1985) 297
3. P. Brix, G. Herzberg, *J. Chem. Phys.* **21** (1953) 2240
4. J. W. He, U. Memmert, P. R. Norton, *J. Chem. Phys.*,**90** (1989) 5088.
5. J. Goschnick, M. Wolf, M. Grunze, W. N. Unertl, J. H. Block, J. Loboda-Cackovic, *Surf. Sci.*,**178** (1986) 831.
6. M. Milun, P. Pervan, M. Vajic, *Surf. Sci.*, **211** (1989) 887.
7. J. W. He,, P. R. Norton, *Surf. Sci.*,**204** (1988) 26.
8. M. Bowker, Chapter 4., '*Cohesion & Structure of Surfaces*', D. G. Pettifor (Ed.), Elsevier Science (1995), 285.
9. V. A. Bondzie, P. Kleban, D. J. Dwyer, *Surf. Sci.*,**347** (1996) 319.
10. S. Ladas,R. Imbhil,G. Ertl, *Surf. Sci.*, **219** (1989) 88.
11. M. Bowker, I. Z. Jones, R. A. Bennett, S. Poulston, *Studies in Surf. Sci. & Catal.*,**116** (1998) 431.
12. K. Yagi, D. Sekiba, H. Fukutani, *Surf. Sci.*, **442** (1999) 307.

13. H. Conrad, G. Ertl, J. Kuppers, E. E. Latte, *Surf. Sci.*,**65** (1977) 245

14. X. Guo, A. Hoffman, J. T. Yates Jr, *J. Chem. Phys.*, **9** (1989) 5200.

15. X. Guo, A. Hoffman, J. T. Yates Jr, *J. Chem. Phys.*, **10** (1989) 5787.

16. M. K. Rose, A. Borg, J. C. Dunphy, T. Mitsui, D. F. Ogletree, M. Salmeron, *Surf. Sci.*, **561** (2004)69

17. T. Engel, J. Phys. Chem., **69** (1978) 373

18. P. Sjovall, P. Uvdal, *Chem. Phys. Lett.*,**282** (1998) 355.

19. G. Zheng, E. I. Altman, *Surf. Sci.*, **462** (2000) 151

20. G. Zeng, E. I. Altman, *J. Phys. Chem. B.*, **106** (2002) 1048

21. D. Zemlyanov, H. Gabasch, W. Unterberger, K. Hayek, B. Klotzer, E. Kleimenov, D. Teschner, S. Zafeiratos, M. Havecker, A. Knop-Gericke, R. Schlogl, J. Han, F. H. Ribeiro, B. Aszalos-Kiss, T. Curtin, *Surf. Sci.*, **600** (2000) 983

21. E. H. Voogt, A. J. M. Mens, O. L. J. Gijzeman, J. W. Geus, *Surf. Sci.*, **373** (1997) 210

22. S. Nagarajan, K. Thirunavukkarasu C. S. Gopinath, J. Counsell, L. Gilbert, M. Bowker, *J. Phys. Chem. C.*, **113** (2009) 9814

23. J. T. Yates, P. A. Thiel, W. H. Weinberg, *Surf. Sci.*, **82** (1979) 22

24. E. A. Crathorn, D. MacGowan, S. R. Morris, A. P. Rawlinson, *J. Catal.*, **149** (1994) 254.

25. L. H. Little, N. Sheppard, P. J. C. Yates, *Proc. Roy. Soc.*, **242** (1960) 259.

26. J. M. Davidson, P. M. Mitchell, N. S. Raghavan, *Front. Chem. React. Eng.*, **1** (1984) 300.

27. E. Drent and H.M. Brudzelaar. *Chem. Rev.* **96** (1996), pp. 663–681.

28. A. Sen., *Acc. Chem. Res.*, **26** (1993), 303.

29. G. Filardo, A. Galia, F. Rivetti, O. Scialdone and G. Silvestri. *Electrochim. Acta.*, **42** (1997), p. 1961

30. I. Yamanaka, A. Funakawa, K. Otsuka, *J. Catal.*, **221,** (2004), 110-118.

31. I. Tomiya, K. Yasuhiko, I. Akira, I. Kenji, *Eur. Pat. Appl.* (1981), 37 pp

32. D. Gavril, V. Loukopoulos, G. Karaiskakis, *Chromatographia.*, **59** (2004) (11/12), 721-728.

33. H. H. Madden, G. Ertl, *Surf Sci.*, **35** (1973) 211

34. J. Tracey, *J. Chem. Phys.*, **56** (1972) 2736

35. R. W. McCabe, L. D. Schmidt, *Surf. Sci.*, **66** (1977) 101

36. H. P. Bonzel, J. J. Burton, *Surf Sci.*, **52** (1975) 223

37. J. M. Gottfried, K. J. Schmidt, S. L. M. Schoeder, K. Christmann, *Surf Sci.*, **536** (2003) 206

38. P. H. McBreen, S. Moore, A. Adnot, D. Roy, *Surf. Sci.*, **194** (1988) L112

39. G. Ertl, H. Conrad, J. Kuppers, *Surf. Sci.*, **76** (1978) 323

40. Wesner, D. A. Weber, W. Hartmann, D. Guentherodt, G. Effner, *Phys. Rev. B.*, **48(3)** (1993) 1806-19

41. X. Guo, J. T. Yates Jr, *J. Chem . Phys.*, **90** (1989) 11

42. E. E. Latte, J. Koch, G. Ertl, H. Conrad, *Surf. Sci.*, **43** (1974) 462

43. N. V. Hieu, J. H. Craigh Jr, *Surf. Sci. Lett.*, **145 2/3** (1984) L493

44. M. P. Kriskinova, G. M. Bliznakov, *Surf. Sci.*, **123** (1982) 61

45. M. Bowker, Q. Guo, R. W. Joyner, *Surf. Sci.*, **259(1-2)** (1991) 45

46. G. Ertl, T. Engel, *Chem. Phys. Lett.*, **54** (1978) 95

47. T. Engel, *J. Phys. Chem.*, **69(1)** (1978) 1

48. K. Thirunavukkarasu, C. S. Gopinath, *Catal. Lett.*, **119** (2007) 50

49. U. Burghaus, I. Z. Jones, M .Bowker, *Surf. Sci.* **454/456** (2000) 326

50. Y. T. Wong, R. Hoffman, *J. Phys. Chem.*, **95** (1991) 859

51. H. Ohtani, M. A. Van Hove, G. A. Somorjai, *Surf. Sci.*, **187** (1987) 372

52. K. W. Kuhn, J. Szanyi, D. W. Goodman, *Surf. Sci. Lett.*, **274** (1992) L611

53. M. Bowker, Q. Guo, R. Joyner, *Surf. Sci.*, **33** (1991) 253

54. T. Engel, G. Ertl, *J. Chem. Phys.*, **69(3)** (1978) 1

55. J. Xie, Q. Zhang, K. T. Chuang, *Catal. Lett.* **93** (2004) 181

56. Sano, K.; Uchida, H.; Wakabayashi, S. *Catal. Surv. Jpn.* **3** (1999) 55

57. Seoane, J. L.; Boutry, P.; Montarnal, R. *J. Catal.* **63** (1980) 191

58. A. B. Evnin, J. A. Rabo, P. H. Kasai, *J. Catal.* **30** (1973) 109

59. E. M. Stuve, R. J. Madix, *Surf. Sci.* **152/153** (1985) *532*

60. M. Kaltchev, A. W. Thompson, W. T. Tysoe, *Surf. Sci.*, **391** (1997) 145

61. L. L. Kesmodel, J. A. Gates, *Surf. Sci.* **111** (1981) L747

62. M. Sock, A. Eichler, S. Surnev, J. N. Anderson, B. Klötzer, K. Hayek, M. G. Ramsey, F. P. Netzer, *Surf. Sci.*, **545** (2003) 122.

63. J. A. Gates, L. L. Kesmodel, *Surf. Sci.*, **124** (1983) 68

64. V. Pallassana, M. Neurock, V.S. Lusvardi, J.J. Lerou, D.D. Kragten and R.A. Van Santen. *J. Phys. Chem. B* **106** (2002) 1656.

65. F. Zaera and G.A. Somorjai. *J. Am. Chem. Soc.* **106** (1984) 2288

66. F. Zaera. *Langmuir* **12** (1996) 88

67. N. Sheppard, *Annu. Rev. Phys. Chem.* **39** (1988) 589

68. L. L. Kesmodel, *J. Electron Spectrosc. Relat. Phenom.*, **29** (1983) 307

69. I. Jungwirthova, L. L. Kesmodel, *J. Phys. Chem. B*, **105** (2001) 674

70. Y. F. Han, D. Kumar, C. Sivadinarayana, A. Clearfield, D. W. Goodman, *Catal. Lett.* **94** (2004) 131

71. M. Bowker, C. Morgan, N. Perkins, R. Holroyd, E. Fourre, F. Grillo, A. MacDowall, *J. Phys. Chem. B*, **109** (2005) 2377

72. M. Bowker, C. Morgan, *Catal. Lett.* **98** (2004) 67

73. H. Gabasch, K. Hayek, B. Klotzer, A. Knop-Gericke, , R. Schlogl, *J. Phys. Chem. B.* **110** (2006) 4947

74. H. Gabasch, E. Kleimenov, D. Teschner, S. Zafeiratos, M. Havecker, A. Knop-Gericke, R. Schlogl, D. Zemlyanov, B. Aszalos-Kiss, K. Hayek, B. Klotzer, *J. Catal.* **242** (2006) 340

75. H. Gabasch, A. Knop-Gericke, R. Schlogl, W. Unterberger, K. Hayek, B. Klotzer, *Catal. Lett.* **119** (2007) 191

76. E. M. Pazhetnov, S. V. Koshcheev, A. I. Boronin, *Kinet. Catal.* **44** (2003) 414

77. R. I. Kvon, S. V. Koscheev, A. I. Boronin, *Mol. Catal.A.* **158** (2000) 297

78. E. Yagasaki, R. I. Masel, *J. Am. Chem.* **112** (1990) 8746

79. J. Davis, M. Barteau, *Surf. Sci.* **256** (1991) 50

80. J. James, D. K. Saldin, T. Zheng, W. T. Tysoe, D. S. Sholl, *Catal. Today.* **105** (2005) 74

81. M. Bowker, C. Morgan, J. Couves, *Surf. Sci.* **555** (2004) 145

82. Y. Li, M. Bowker, *J. Catal.* **142** (1993) 630

83. J. Davis, M. Barteau, *Surf. Sci* **260** (1996) 215

84. Z. Li, F. Gao, W. T. Tysoe, *Surf. Sci,* **602** (2008) 416

85. R. D. Haley, M. S. Tikhov, R. M. Lambert, *Catal. Lett.* **76** (2001) 125

86. D. Stacchiola, F. Calaza, L. Burkholder, W. T. Tysoe, *J. Am. Chem. Soc.* **126** (2004) 15385

87. D. E. James, J. K. Stille, *J. Organomet. Chem.***108** (1976) 401.

88. E. Crathorne, D. Macgowan, S. Morris, A. Rawlinson, *J. Catal.* **149** (1994) 254

89. J. Davis, M. A. Barteau, *J. Am. Chem. Soc.* **111** (1989) 1782.

90. M. Mavrikakis, M. A. Barteau, *J. Mol. Catal. A.* **131** (1998) 135

91. M. A. Barteau, R. Shekhar, R. V. Plank, J. M. Vohs, *J. Phys. Chem. B.* **101** (1997) 7939

92. M. Bowker, R. Holroyd, N. Perkins, J. Bhantoo, J. Counsell, A. Carley, C. Morgan, *Surf. Sci.* **601** (2007) 3651

93. C. J. Houtman, M. A. Barteau, *J. Catal.* **130** (1991) 528

94. W. T. Tysoe, F. Calaza, D. Stacchiola, M. Neurock. *Surf. Sci.* **598** (2005) 263

95. H. Gabasch, K. Hayek, B. Klotzer, A. Knop-Gericke, R. Schlogl, *J. Phys. Chem. B.* **110** (2006) 4947

4. *The interaction of Au with the Pd (111) surface*

4.1 Introduction

It has been shown previously that Au is of great importance regarding the formation of effective catalysts in a variety of industrial processes[1]. There have been many studies regarding the role Au has in the catalytic production of VAM. It has been proposed that Au enhances the selectivity of the acetoxylation of ethylene by suppressing the formation of CO from the combustion of acetic acid[2]. The formation of carbide has also been observed in used Pd and Pd-Au catalysts[3,4]. Pd-Au/SiO_2 mixed metal catalysts have been investigated with XPS and XRD, and the alloying of Au with Pd was found to be very effective in preventing carbide formation on the Pd catalysts for VAM synthesis[5]. Activity has also been shown to improve due to the addition of Au to the catalyst[6].

Since Au has been shown to play such an important role in VAM production it is important to try to understand what exactly its role is on the atomic level. A simple way of probing this relationship is to deposit Au onto the Pd (111) surface and study the adlayer and substrate using surface science techniques,. The nature of the interactions between substrate and overlayer needs to be fully understood before any experiments involving VAM related molecules can be carried out. One of the fundamental questions asked regarding any deposition is "how does the thin film grow on the surface?" The growth mode of one metal on another is affected by a number of factors such as surface free energies, growth rate, substrate temperature and strain energies. Since there is only a 4.9% lattice mismatch between Au (111) and Pd (111)[7] surfaces, the strain energy is not likely to be a crucial factor in determining the growth mode. Generally the surface free energies of adsorbate (γ_A), substrate

(γ_S) and the interface (γ_I) play more important roles than other factors. Three simple models of metallic overlayer growth mode exist. The first is the Frank–Van der Merwe growth mode or layer by layer growth, in which a new layer starts to grow only after finishing the growth of the previous one. This is due to γ_S being greater than $\gamma_A + \gamma_I$ resulting in a tendency for the adsorbate to spread over the surface in order to reduce the free energy of the substrate. When deposited, the atoms are bound more strongly to the substrate than they are to each other. They aggregate to form monolayer islands of deposit which enlarge as deposition continues until a complete monolayer has formed. The second is the Volmer-Weber (or 3D) growth mode. This involves the congregation of deposited atoms into islands leaving uncovered areas of the substrate. This is caused by $\gamma_A + \gamma_I$ being greater than γ_S. The 3D islands form to reduce the surface free energy of the adsorbate, leaving the substrate exposed. The third mode is Stranski-Krastanov which incorporates characteristics of both of the previous models. Initially deposition occurs via the Frank–Van der Merwe growth mode, however after the first full metallic layer has formed, growth carries on as an island (Volmer-Weber). Figure 4.1 below shows the nature of these three growth modes. Previous research has shown the surface free energy of palladium and gold to be 2.05J/m^2 and 1.63J/m^2 respectively[8,9]. Because palladium has a greater surface free energy, it has been postulated that the growth mode is Frank- Van der Merwe.

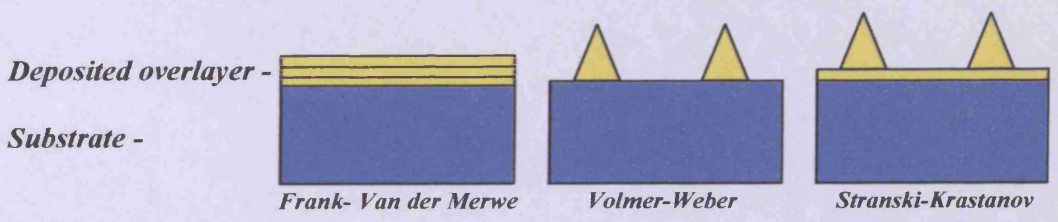

Figure 4.1 Three basic growth modes of thin film growth from vapour deposition

When investigating the nature of adsorbed layers on a sample, XPS has proved itself to be a powerful technique. The changes in binding energy of core electrons can yield information on changes in bonding states. Also, whilst depositing a metal, the growth of the adsorbate peaks and the attenuation of the support metal can indicate which growth mode is present.

A variety of techniques have been used previously to investigate the interaction of gold with palladium surfaces. Photoemission spectroscopy of sub-monolayer amounts of Au on Pd (111) have shown different spectral structures compared to multi-layer coverages[7,10]. The splitting of the valence band peaks increases smoothly as coverage increases, which indicates that Au is more atomic like at low coverages but approaches a metallic state as the Au-Au distance decreases. This smooth change implies these atoms are well dispersed rather than in islands. The epitaxial growth of Au has also been studied using ion scattering and low energy electron diffraction[11]. The growth of Au, up to a coverage of a monolayer, was seen to adopt the same surface structure and spacing as the Pd (111) surface. Above this coverage the Au lattice spacing was seen to increase to resemble that of bulk Au (111) by a coverage of 8ML. Interestingly, the lattice spacing for the Pd substrate was also seen to increase as a result of the deposition. By contrast, recent STM studies of the growth of Au on Pd (111) at 300K showed the formation of a rough surface morphology with Pd exposed even after a deposition of several monolayers[12,13]. Upon annealing up to 600K, the surface was shown to still consist of Au islands separated by Pd cracks. Above this temperature, intermixing was observed producing a more homogeneous surface. Above 900K, all of the Au diffused into the bulk of the

crystal once again exposing the Pd surface. It was also proposed that the presence of Au in the Pd greatly enhances the reactivity of the surface towards certain reactions, by lowering the temperature of desorption of the product formed[13]. Tysoe et al have also studied the growth of the Au on Pd (111) system and the effects of annealing the surface[14,15], Using XPS and AES a layer-by-layer growth mode was observed. Au was shown to intermix quickly above 600K at high coverages and that by varying the amount of Au deposited it is possible to achieve a full range of surface compositions. Au was also shown to stabilise VAM on the surface when coupled to two Pd atoms, inhibiting decomposition pathways.

LEED and Auger studies of Au deposition on the Pd (110) surface at 130K have indicated a Stranski-Krastinov growth mode where the critical thickness of Au is 2ML[16,17]. In contrast, using MEIS after deposition at 300 K the growth mode was determined to be to be layer-by-layer only, and suggested misfit dislocations at higher coverage[18,19]. This difference has been attributed to the differences in MVD dosing temperature and coverages.

Shen et al carried out studies of the growth of Pd overlayers on Au (111) at room temperature and concluded that it grew in a layer by layer mode[20,21]. It was later confirmed using STM that the Pd assumes a hexagonal structure with a lattice spacing equal to the that of the substrate[22]. Pd was also shown to migrate into the bulk after annealing the surface to 400K[23,24]. This is a significantly lower than the Au/Pd (111) system and distinctly highlights the affinity for Au to segregate at the surface. Segregation of Au has been observed in a Au_3Pd (110) alloyed single crystal resulting in a near pure Au composition in the top two atomic layers[25]. Pd-Au alloy surfaces

have also been widely investigated by Goodman *et al* using molybdenum as a support metal[26-28]. Preferential surface segregation of Au was observed after annealing Pd-Au mixtures on Mo with different surface compositions observed at different temperatures[26]. The most prevalent surface ensemble observed using LEISS and XPS was that of a single isolated Pd atom surrounded by Au. It was also shown using IRAS that by varying the concentration of the initial Pd-Au it was possible to control the concentration of single Pd atoms on the surface[27]. With regards to VAM, enhanced rates of production at low coverages of Pd on Au, demonstrates the crucial role of two non-contiguous, suitably spaced Pd atoms. It was proposed that the role of the Au is to isolate these atoms in such a way that the desired reactive mechanism is still possible but by-product reactions are inhibited[28].

4.2 Deposition and growth of Au

In order to form gold films on the Pd (111) surface, an MVD evaporator was constructed as described in Chapter 2. The end of the evaporator was about 15 cm from the crystal surface during dosing. The cylindrical case reflects heat back onto the filament, thus insulating the doser contents from the main chamber and reducing heat dissipation. In addition, it contains and controls the gold vapour which leaves the aperture as a localised beam. It can be assumed that a constant supply of power to the filament produces a constant flux of Au atoms. This allows the amount of Au dosed to be regulated by the length of time of the dose. Deposition was performed at a crystal temperature of ~300K.

Au was deposited onto the surface for consecutive 40s doses. XPS spectra of the Pd3d and Au4f regions were taken after each consecutive dosing in order to monitor the growth of the Au layer. XPS spectra were also obtained for the C1s and O1s regions in figure 1A, a small peak can be seen for clean Pd in the Au4f region before dosing any Au. This can be attributed to the presence of a weak Pd 4s (86eV) feature which overlaps the Au4f signal. A similar observation can be seen with the Pd3d region in figure 4.2B where the Pd $3d_{5/2}$ (335eV) region is overlapped by the Au $4d_{5/2}$ (334eV) orbital. Because of this superposition of the two orbitals, only the Pd $3d_{3/2}$ (340eV) peak is used for quantitative analysis of the surface film. In figure 4.2B it is also possible to see the growth of Au on the surface from the Au $4d_{3/2}$ signal at a binding energy of 352eV.

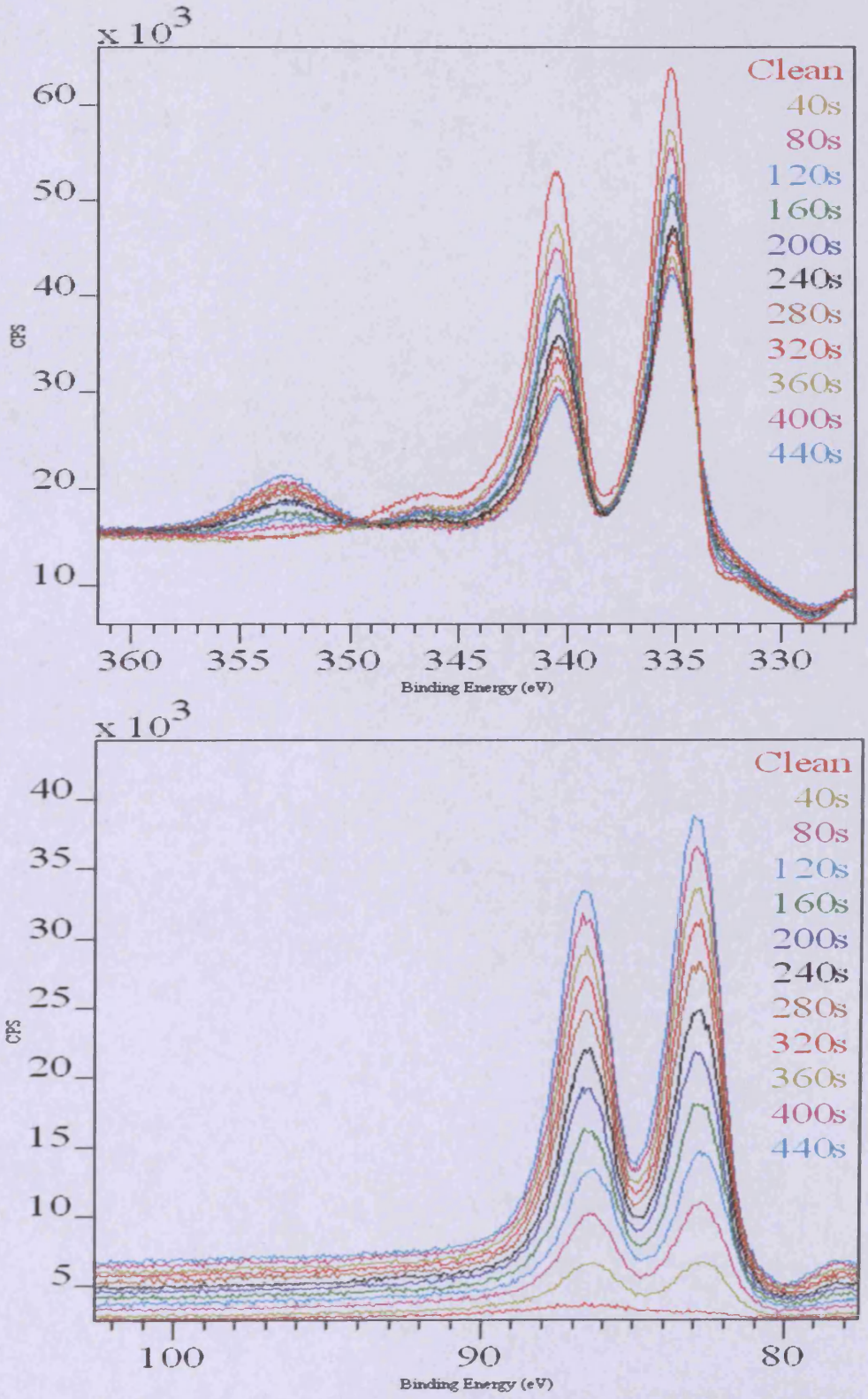

Figure 4.2 ***A***: Au4f peak as a function of Au deposition time
B: Pd3d peak as a function of Au deposition time

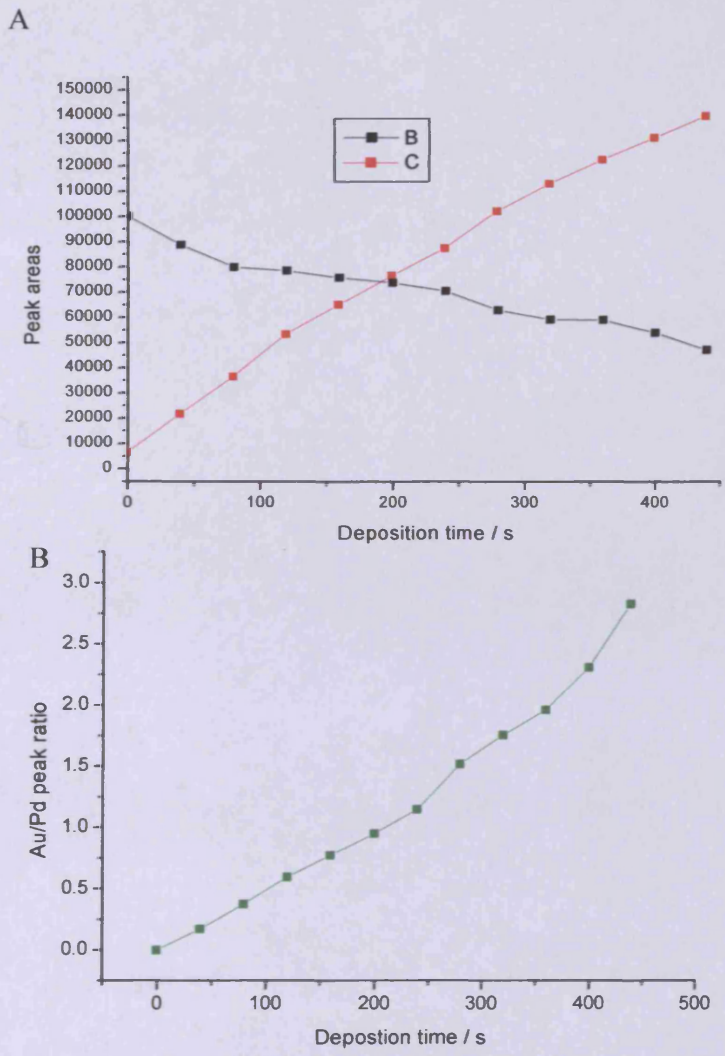

Figure 4.3 **A:** Integrated areas of Au4f and Pd3d(3/2) peaks vs duration of deposition
B: Au4f/Pd3d(3/2) peak ratio vs deposition time

The integrated areas of both the Au 4f and Pd $3d_{3/2}$ peaks were obtained for quantitative analysis. Figure 4.3A shows the integrated area of the Pd $3d_{3/2}$ and Au 4f peaks as Au was deposited on the surface. Figure 4.3B displays the ratio of these two values as a function of deposition time. As expected, as the length of time of deposition increases, the Au 4f signal peak increases. The Pd $3d_{3/2}$ intensity also decreases due to attenuation of the electron flux by the deposited Au atoms. In figure 4.3B, the gradient of the plot would seem to become steeper as deposition occurs due

to the shielding of Pd by the Au overlayer. This agrees with previous work carried out which concluded a layer-by-layer growth mode[14]. Unfortunately, it is not feasible to observe when a complete monolayer of Au has been deposited, because no clear change in gradient can be distinguished due to sampling depth of XPS.

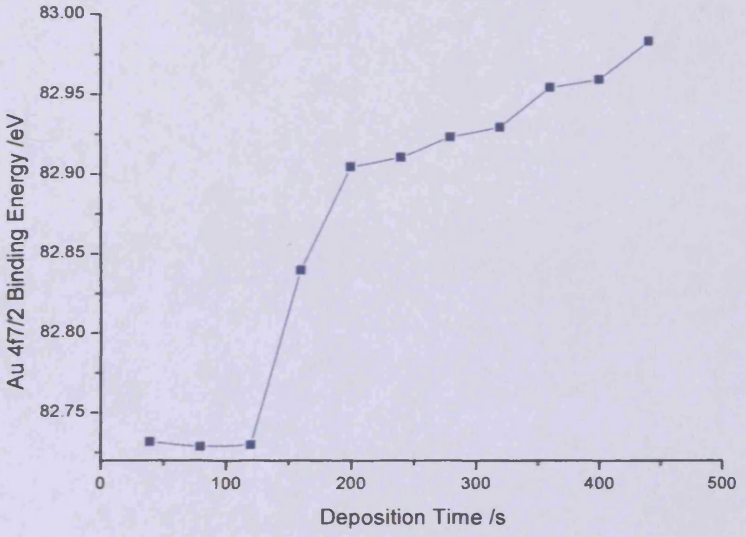

Figure 4.4 Au $4f_{7/2}$ binding energy as a function of deposition time

Figure 4.4 shows the shift in binding energy of the Au $4f_{7/2}$ peak as the amount of Au deposited increases. After 40s, 80s, and 120s of Au deposition, the Au $4f_{7/2}$ electron binding energy is lower than that of bulk Au metal (83eV) by ~0.3eV. This can be attributed to the effect of surface Pd atoms on the electronic configuration. Pauling electronegativities of Pd (2.20) and Au (2.54) would suggest slight electron transfer from Pd to Au, consistent with these chemical shifts. The lower coordination of Au atoms may also explain the decrease in binding energy at low coverages - reduced coordination leads to a lower valence bandwidth which can result in surface core-level shifts. This phenomenon has been seen previously, with the binding energy of the surface adlayer only becoming bulk-like after 3ML[14]. The low binding energy

of 4f electrons due to their atomic-like environments agrees with previous research using PES[7,10]. The splitting of the valence band has been shown to increase as deposition occurs, indicating a dispersion of atomic gold not island formation.

4.3 Quantification of XP spectra

Since it is was not possible to accurately determine the point at which 1ML of Au had been deposited, further quantification of the spectra was needed. The equations 4.1 and 4.2 below, described previously in chapter 2, can be used to quantify the thickness d and atom concentration σ of the Au adlayer. By comparing the results yielded from both methods, it was possible to estimate the amount of Au after different deposition times.

4.1. $$d = \frac{\lambda(\ln I - \ln I_0)}{-\cos\phi}$$ **4.2.** $$\sigma = \frac{I_A KE_A \mu_S \rho_S N_A \lambda_S \cos\phi}{I_S KE_S \mu_A M_S}$$

Using equation 4.1, it was possible to obtain values for the depth (d) of Au as a function of deposition time. By assuming the atomic radius of a neutral Au atom, 0.135nm, is equal to the depth of a single atomic layer, it was possible to calculate the coverage in monolayers. Due to the assumptions described previously regarding equation 4.1, it was thought wise to compare the results with those generated from equation 4.2. The concentration of surface atoms for Pd (111) is ~$1.33 \times 10^{15} cm^{-2}$. Assuming that the surface concentration of deposited Au is the same, it is possible to work out the coverage (σ) using eqn 4.2. Both sets of results are shown below in

Figure 4.5 The two calculations yield different results regarding the time needed to deposit a single atomic layer of Au. Equations 4.1 and 4.2 predict the formation of 1ML of Au to occur after 23s and 78s respectively.

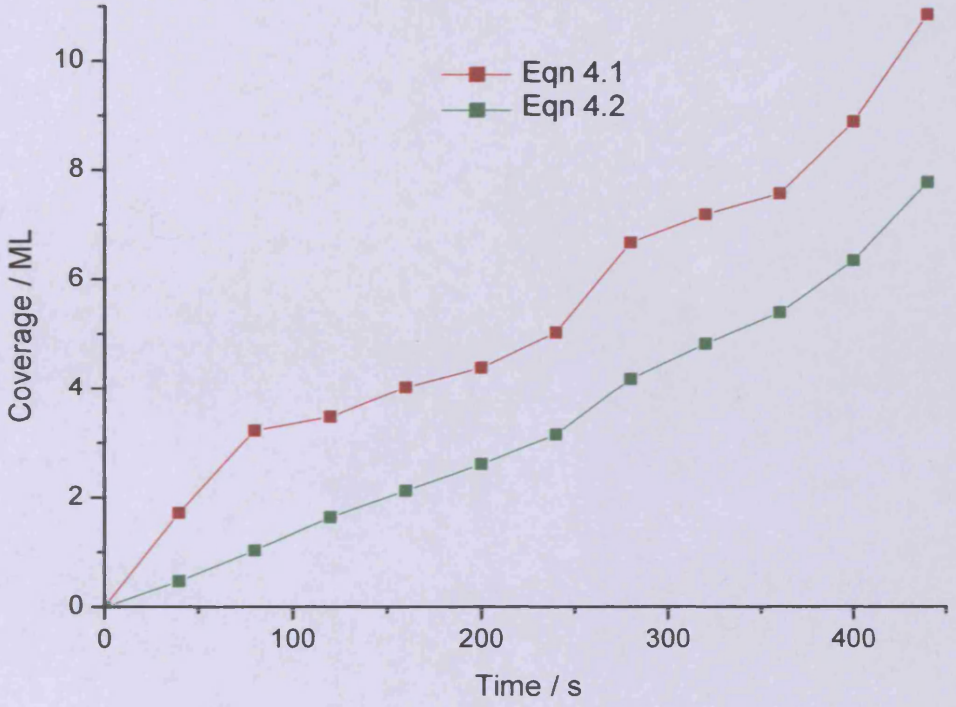

Figure 4.5 Au coverages as a function of deposition time calculated from equations 4.1 and 4.2

4.4 Effect of Annealing

Both Au and Pd are fcc metals with a lattice mismatch of 4.8%. It has been shown previously that Au has an affinity to form a miscible alloy with Pd[24]. This can be attributed to the negative heat of formation across the composition range, indicating favourable atomic interactions. The most favoured composition is Pd 40%

Au 60%. Because of the possibility of a thermodynamically favourable alloy, it can be assumed that any Au dosed onto the surface would be drawn into the bulk at equilibrium. However, Au dosed onto the surface was not seen to migrate inwards at room temperature. This can be attributed to the lack of surface energy needed to initially overcome the repulsive surface forces and to penetrate and break Pd-Pd lattice bonds.

In order to investigate the migration of Au atoms into the bulk, Au was dosed onto the Pd (111) surface and the sample was heated to increasing temperatures for 300s and then cooled back down for analysis. XPS data was obtained before and after Au deposition to ensure cleanliness of sample and after each heating cycle. Figure 4.6A shows the effect of heating the Au dosed surface on the intensity of the Au 4f region. Up to 550K, no significant change in the intensity of the Au signal was observed. Previous studies have shown little change in the concentration of surface Au up to 600K[13,15]. Above this temperature, up to 673K, a steady decrease in the Au intensity can be seen. After heating to 723K, the Au intensity had decreased significantly. This would imply a significant migration of surface Au into the bulk of the crystal. Similarly, in the Pd 3d region, a decrease in the Au $4d_{3/2}$ peak begins at 598K with a significant loss of the signal by 723K. Since the Au has diffused into the bulk of the crystal, it would be logical to expect the surface concentration of Pd to increase. Indeed the Pd $3d_{3/2}$ peak intensity increases steadily across this range as an effect of heating with significant increases in Pd observed above 648K.

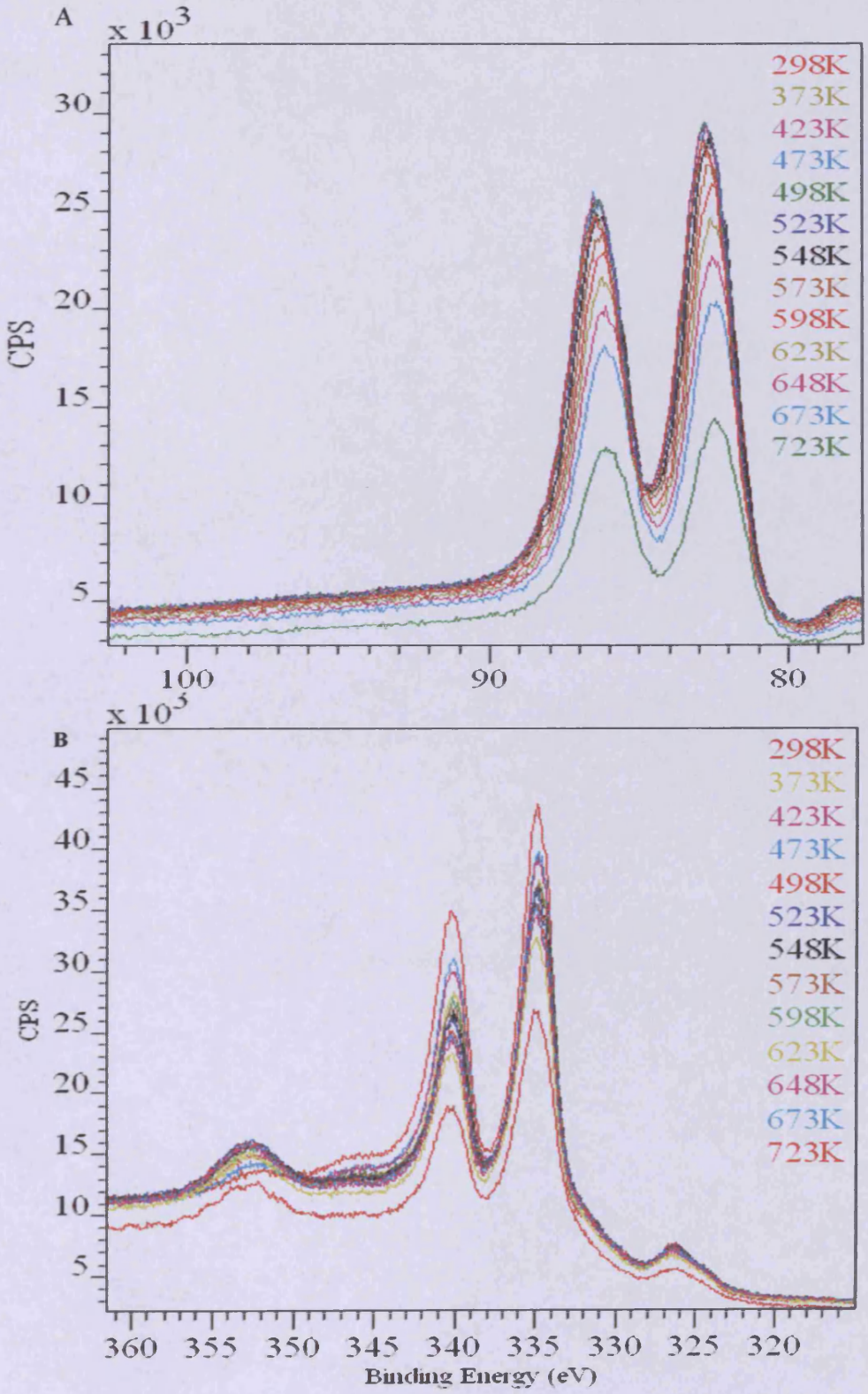

Figure 4.6 A: Au 4f region after annealing to increasing temperatures **B:** Pd 3d region after annealing

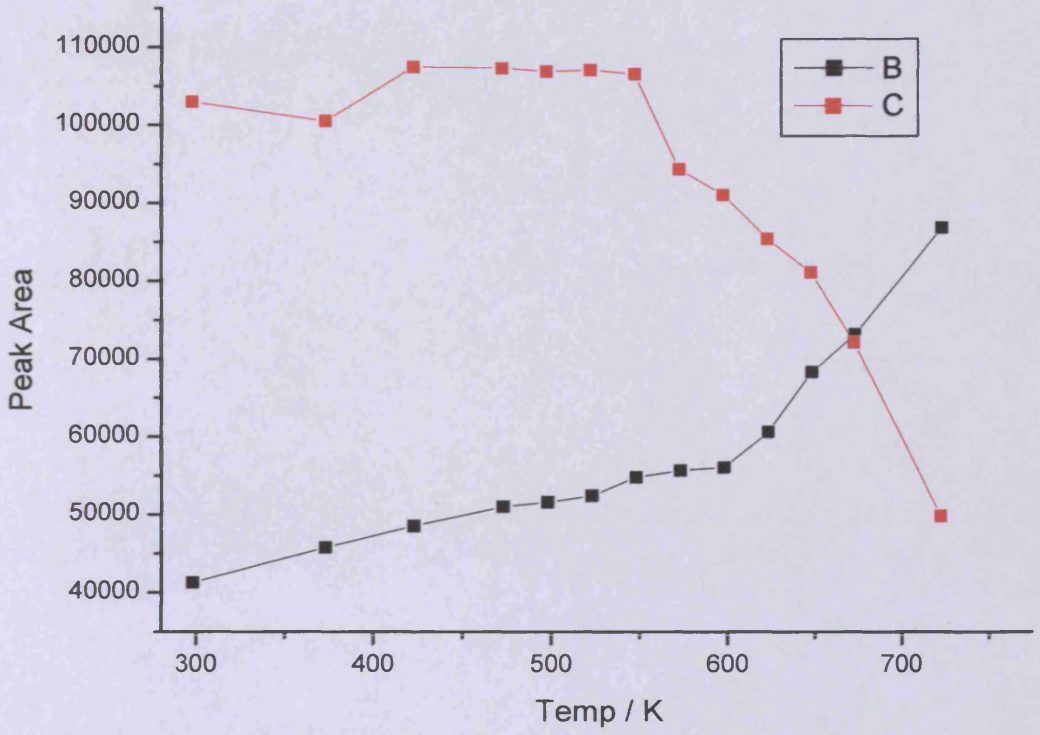

Figure 4.7 Au 4f (red) and Pd 3d3/2 (black) peak areas vs annealing temperatures

Figure 4.7 shows the change in peak intensity of both Au and Pd peaks after heating. No significant decrease in the Au signal can be seen until heating to 573K. Above this temperature, the amount of surface Au decreases with every subsequent heating cycle.

A different observation can be seen regarding the effect of heating on the Pd signal. With each annealing cycle, the Pd signal increases such that by 548K, the intensity of the Pd $3d_{3/2}$ peak has increased by a factor of 33% of its initial intensity. Above this temperature a marked increase in the Pd intensity is seen. Above 578K, this increase in Pd signal can simply be attributed to the migration of Au into the bulk. However the increase at more ambient temperatures must be due to the restructuring

of surface species since there is no decrease in the intensity of the Au signal. Figure 4.8 below shows the ratio of Au 4f:Pd $3d_{3/2}$ as a function of surface annealing temperature. The ratio of Au:Pd decreases gradually up to 548K and more significantly at higher temperatures.

Figure 4.9 shows the change in binding energy of the Au $4f_{7/2}$ peak as the surface is undergoes annealing cycles to increasing temperatures. Before annealing, the deposited Au peak position was typical of atomic Au. However, after annealing the surface above 500K, a shift to a lower binding energy can be seen. This decrease in binding energy of 0.35eV is an indication of a change in the electronic state. It can be attributed to an alloying of the Au with the bulk Pd metal as the Au migrates subsurface. As alloying occurs, electron transfer would occur from the Pd atoms in the lattice to the more electronegative Au atoms. A chemical shift of 0.2eV has been reported previously in the $Au4f_{7/2}$ feature for a $Au_{45}Pd_{55}$ alloy and a shift of 0.7eV shift in an alloy of $Au_{10}Pd_{90}$[29,30]. This would indicate that the shift in the $Au4f_{7/2}$ binding energy correlates with the degree of alloying of Au. No observable shift in the Pd 3d3/2 peak was observed after each annealing cycle probably due to the large signal for bulk Pd not affected by the Au

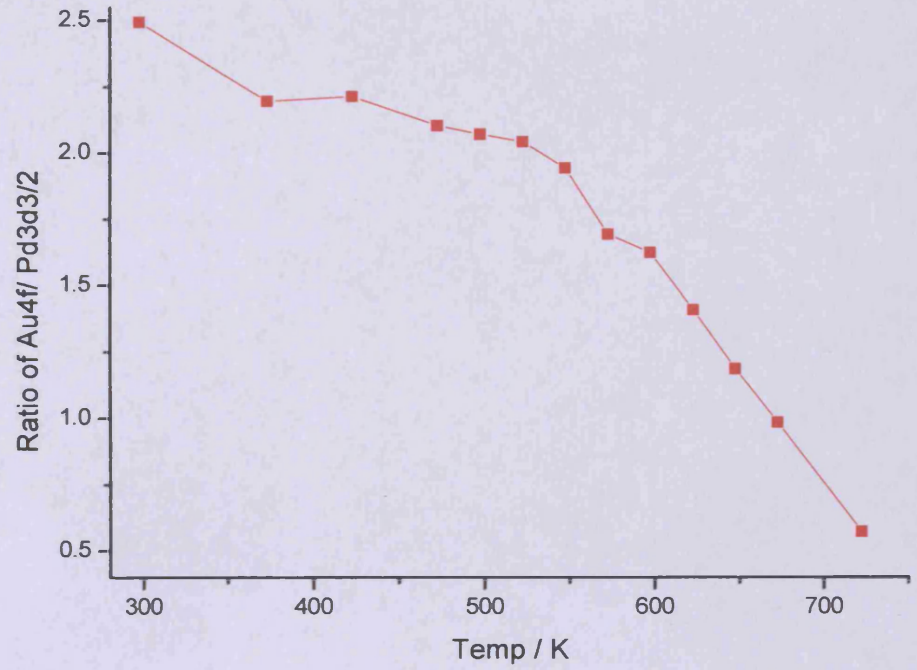

Figure 4.8 Au4f : Pd3d3/2 ratio vs Annealing temperature

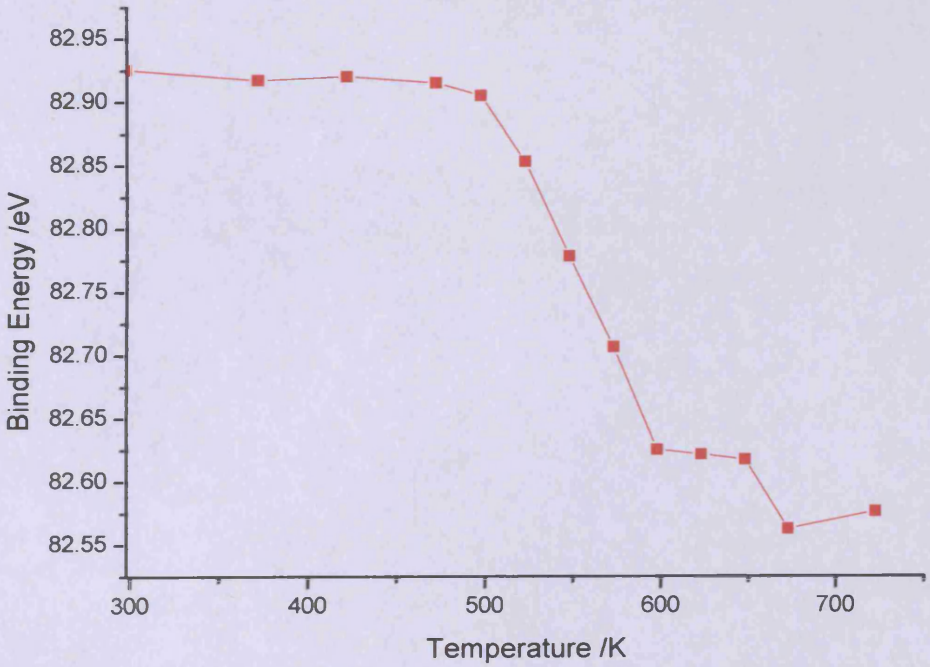

Figure 4.9 Binding energy of Au 4f 7/2 peak as a function of annealing temperature

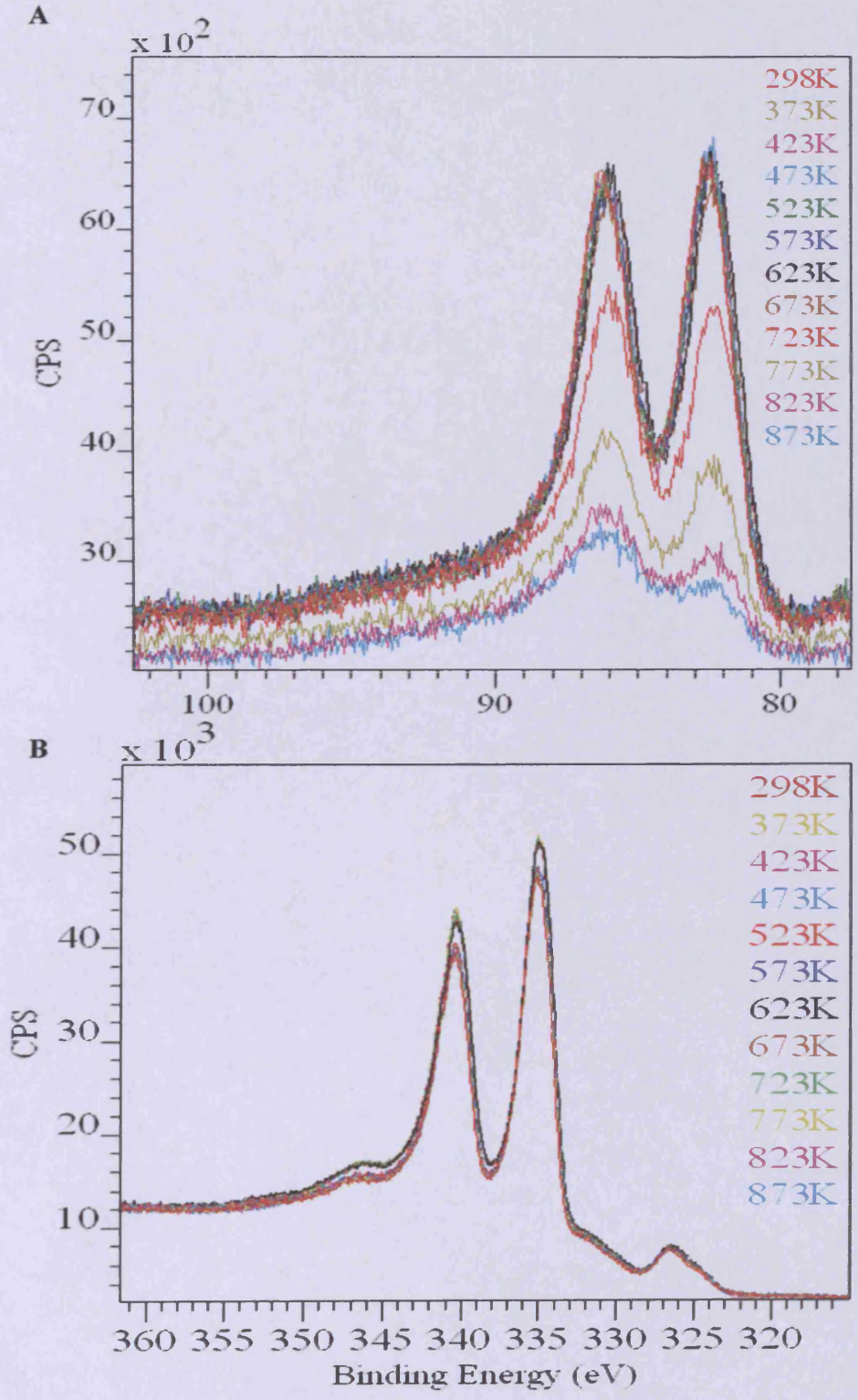

Figure 4.10 A. Au 4f region after annealing to increasing temperatures **B.** Pd 3d region after annealing after deposition of Au

Since bulk Au is unreactive, it can be assumed that the reactivity of multilayer Au on Pd also exhibits this inert quality. It should also be considered that in the catalytic system Au and Pd have an intertwined role. Because of this relationship between the two metals, it was considered important to investigate whether the amount of Au on the surface affects its affinity for bulk migration and alloying. Au was dosed for a much smaller length of time (50s) in order to probe this relationship. Figures 4.10A and B show the XPS data for the Au 4f and Pd $3d_{3/2}$ regions at this smaller coverage, and the effect different temperature heating cycles have on the surface concentration. As observed at the higher coverage, the concentration of surface Au decreased with consecutive heating cycles. However, at this lower coverage, there is no decrease in Au concentration until above 600K. After annealing for 300s at this temperature, a significant decrease in the Au signal was observed; above this temperature the amount of surface Au decreased greatly. By 873K almost all of the Au had gone into the bulk. Due to the large signal for Pd $3d_{3/2}$ peak relative to the amount of Au deposited, there is not such a stark change in the intensity with the heating cycles. Figure 4.11A below shows the change in peak areas of both sets of peaks as a function of annealing temperature. At such a low coverage of Au, the overlapping of the Pd 4s orbital interferes with the quantification of the Au 4f area. One solution employed here involved the subtraction of the value of the Pd 4s peak area for the clean metal surface. Figure 4.11B shows the change in binding energy of deposited Au as the surface is annealed. As seen previously, the binding energy for the $Au4f_{7/2}$ electrons at low coverages is lower than that of metallic Au. As the sample is heated above 450K, the binding energy once again starts to shift to lower values. This large shift away from the value of bulk Au would indicate alloy formation with a high Pd content.

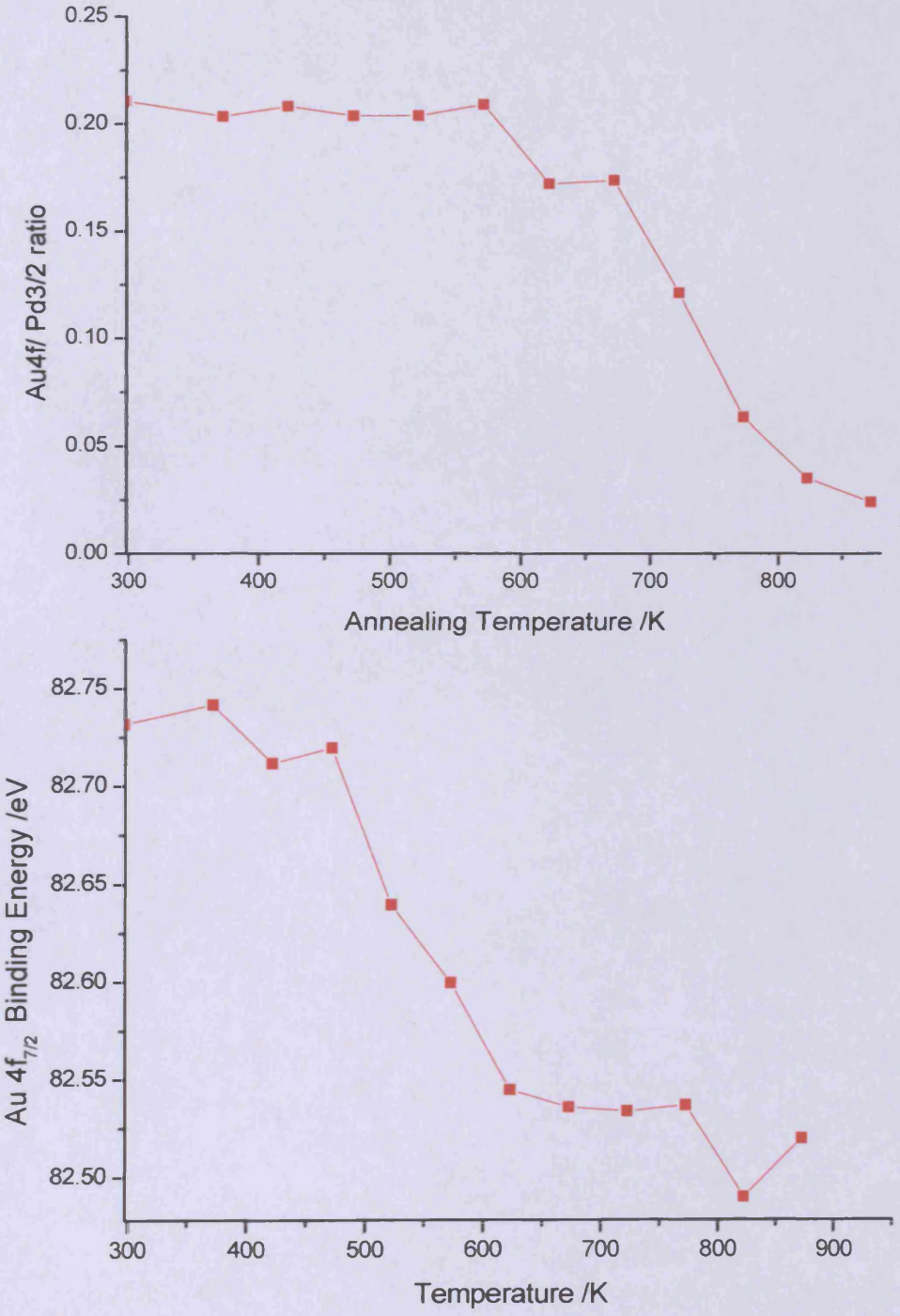

Figure 4.11 **A:** Au 4f / Pd 3d3/2 peak ratio vs annealing temperature

B: Au $4f_{7/2}$ Binding energy vs annealing temperture

4.5 Conclusions

Au was successfully deposited onto the Pd (111) substrate at room temperature for successive periods and the growth of the adlayer was observed using XPS. At low coverages, a decrease in the binding energy of the Au 4f was observed with respect to atomic Au. This was attributed to deposition and growth occurring not via islands but via single atoms. This layer-by-layer growth agrees with previous studies in the literature[14,15]. As more Au was deposited, the $Au4f_{7/2}$ binding energy shifted closer to that of metallic Au. It has been concluded that after this time period, at least one monolayer of Au has been deposited. As more Au was deposited, the binding energy became close to bulk Au (83eV).

Calculations regarding the concentration of Au yielded distinctly different values for the deposition time needed to form a single monolayer. The sudden change in binding energy of the Au electrons may also be a good indicator of monolayer formation. Further studies regarding the reactivity of the surface at different Au coverages will be discussed in chapter 5. It has been thought that by probing the reactivity of the surface it would be possible to accurately determine the monolayer. This could be carried out by examining the change in sticking probability of surface sensitive molecules for different Au coverages.

The effect of heating gold dosed surfaces of different coverages has also been carried out. Au was seen to dissolve into the bulk of the crystal above 550K. This is similar to what has been seen previously using AES[12,13]. This affinity for alloying agrees with studies showing the relative heats of formation to be exothermic over the

entire composition range with a maximum value at a composition of 40% Pd[31]. The binding energy of Au was also seen to decrease as bulk migration occurred. This was attributed to charge transfer of electrons from the Pd lattice to migrating Au atoms.

4.6 References

1. M. Haruta, T. Kobayashi, H. Sano, *Chem. Lett.*, **16** 405-408 (1987)
2. M. Neurock, W. D. Provine, D. A. Dixon, G. W. Coulston, J. J. Lerou, R. A. van Santen, *Chem. Eng. Sci.*, **51** (1996) 1691.
3. M. Bonarowska, J. Pielaszek, V. A. Semikolenov, Z. Karpinski, *J. Catal.*, **209** (2002) 528.
4. M. Bonarowska, A. Malinowksi, W. Jusczy, Z. Karpinski, *Appl. Catal. B.* : *Environ.*, **30** (2001) 187.
5. Y. F. Han, D. Kumar, C. Sivadinarayana, A. Clearfield, D. W. Goodman, *Catal. Lett.*, **94 (3-4)** (2004) 131.
6. W. D. Provine, P. L. Mills, J. J. Lerou, *Stud. Surf. Catal.*, **101** (1996) 191.
7. D. L. Weissman-Wenocur, P. M. Stefan, B. B. Pate, M. L. Shek, I. Lindau. W. E. Spicer, *Phys. Rev. B* 27 (1983) 3308.
8. L. Z. Mezey, J. Giber, *Jpn. J. Appt. Phys.* **11** (1982) 1569
9. W. R. Tyson, W. A. Miller, *Surf. Sci.* **62** (1977) 267
10. R. Fischer, T. Fauster, *Phys. Rev. B* **51**, (1995) 7112
11. Y. Kuk, L. C. Feldman, P. J. Silverman, *Phys. Rev. Lett.* **50**, (1983) 51112.
12. T. G. Owens, T. E. Jones, T. C. Q. Noakes, P. Bailey, C J. Baddeley, *J. Phys. Chem. B.* **110** (2006) 21152

13. C. J. Baddeley, M. Tikhov, C. Hardacre, J. R. Lomas, R. M. Lambert. *J. Phys. Chem.* **100** (1996) 2189

14. F. Calaza, Z. Li, J. Boscoboinik, W. T. Tysoe. *Surf. Sci.* **602** (2008) 3523

15. Z. Li, F. Gao, Y. Wang, F. Calaza, L. Burkholder, W. T. Tysoe. *Surf. Sci*, **601** (2007) 1898

16. P. J. Schmitz, H. C. Kang, W. Y. Leung, P. A. Thiel, *Surf. Sci.*, **248** (1991) 287.

17. P. J. Schmitz, W. Y. Leung, H. C. Kang, P. A. Thiel, *Phys. Rev. B*, **43 (11),** (1991), 8834.

18. M. Vos, I. V. Mitchell, *Nucl. Instr. & Meth. In Phys. Res.*, B**72** (1992) 447.

19. M. Vos, I. V. Mitchell, *Phys. Rev. B*, **45 (16),** (1992) 9398.

20. Shen, X. Y.; Frankel, D. J.; Hermanson, J. C.; Lapeyre, G. J.; Smith, R. J. *Phys. Rev. B* **1985**, *32*, 2120.

21. Shen, X. Y.; Frankel, D. J.; Lapeyre, G. J.; Smith, R. J. *Phys. Rev. B* **1986**, *33*, 5372.

22. Maroun, F.; Ozanam, F.; Magnussen, O. M.; Behm, R. J. *Science* **2001**, *293*, 1811.

23. Y. Kuk, L. C. Feldman, P. J. Sliverman. *J. Phys. Rev. Lett.* **50** 1983 511

24. H. H. Shih, E. Bauer, H. Poppa, *Surf. Thin. Solid. Films.* **88** (1982) L21

25. J. Kuntze, S. Speller, W. Heiland, *Phys. Rev. B.* **60** (1999) 9010

26. C. W. Yi, K. Luo, T. Wei and D. W. Goodman, *J. Phys. Chem. B.* **109,** (2005) 18535

27. T. Wei, J. Wang and D. W. Goodman, *J. Phys. Chem. C,* **111**, (2007) 8781

28. M. S. Chen, D. Kumar, C.W. Yi, D. W. Goodman, *Science*, **310**, (2005) 291

29. J. Hedman, M. Klasson, R. Nilsson, C. Nordling, M.F. Sorokina, O.I. Kljushnikov, S.A. Nemnonov, V.A. Trapeznikov, V.G. Zyranov, *Phys. Scripta* **4** (1971) 195.

30. S. Hufner, G. K. Wertheim, J. H. Wernick, *Solid. State. Commun.* **17** (1975) 417

31. J. B. Darby, *Acta Mat.* **14** (1966) 265.

5. *The effect of Au on the reactivity of the Pd (111) surface*

5.1 General overview of the Au/Pd system

In recent times, the promotional effect Au has on Pd catalysts has been of great interest. The role of Au in the production of VAM has been discussed in chapter 1 and highlights the importance of understanding the fundamental nature of Au as a component in bimetallic systems. The synergistic effect between Au and Pd is a phenomenon of considerable interest and has been given much attention in the scientific community.

The oxidation of primary alkyl alcohols using O_2 instead of stoichiometric oxygen donors has been of interest. Au/Pd-TiO_2 catalysts have yielded very high turnover frequencies with improved selectivity after the addition of Au nanocrystals[1]. Scanning transmission electron microscopy (STEM) and XPS showed the nanocrystals to be made up of an Au-rich core with a Pd-rich shell. It has been proposed that the role of the Au is as an electronic promoter for Pd. Alumina supported Au/Pd catalysts have also been found to be efficient catalysts for the direct synthesis of H_2O_2 from H_2 oxidation by O_2 at low temperatures[2-5]. This bimetallic catalyst produced more H_2O_2 than either of the pure Au or Pd catalysts. STEM and high resolution electron microscopy studies of iron oxide and alumina supported catalysts for this reaction have also shown nanoparticles with Pd-rich shells[3]. Carbon supported Au/Pd catalysts which had been pretreated with acid gave high yields of H_2O_2 with a much higher selectivity[6]. This treatment was shown to decrease the size of the alloy nanoparticles. By decreasing the size of the nanoparticles, the sites for the decomposition reaction of H_2O_2 were blocked. It has been assumed that Au alters the physical or electronic structure of Pd sufficiently to inhibit its hydrogenation

ability. Pd supported on Au nanoparticles have also been shown to be considerably more active for the hydrochlorination of trichloroethene than either Pd-black, Pd on alumina or Pd nanoparticles[7]. The selectivity of the hydrodechlorination of dichlorofluoromethane by carbon supported Pd/Au catalysts has also been shown to be closely related to the extent of the alloying between the two metals[8]. During these studies, a substantial amount of carbon was incorporated into the Pd bulk, not from the support but from the CFC molecule. The importance of the alloying of the two metals on the catalyst activity was observed for the hydrogenation of aromatics[9]. This was also true for the catalytic oxidation of glycerol[10]. It was determined that both geometric and electronic effects participated in producing a strong enhancement in activity.

Structural changes of a commercial supported $PdAu/SiO_2$ catalyst for VAM production were investigated using XRD, TEM/EDXS, XPS and FTIR spectroscopy[11]. The deactivation was shown to be caused by the enrichment of the exposed surface with Pd. An industrially aged $Pd\text{-}Au\text{-}K/SiO_2$ was shown to have undergone extensive sintering and to have formed palladium acetate. However, the alloying composition hadn't significantly changed after use indicating palladium acetate had no role in the sintering mechanism[12].

Goodman et al have studied VAM synthesis over Pd-Au catalysts extensively and have concluded that the reaction is structure sensitive[13-16]. The proposed role of Au is to isolate Pd atoms into Pd monomeric sites which enhance the rate of VAM production and increase selectivity. The formation of these monomers was investigated on Pd/Au (100) and Pd/Au (111) surfaces by the adsorption of CO and by

the use of IRAS[14]. Annealing the surface resulted in the loss of Pd ensembles leaving exclusively isolated Pd atoms. VAM synthesis was also carried out on the two surfaces for different Pd coverages by reacting together acetic acid, ethylene and oxygen. The turn-over frequency peaked on the (100) surface at a Pd coverage of 0.07ML (1ML defined as 1Pd atom per substrate Au atom). At this coverage only isolated monomeric Pd atoms were present. The high activity in VAM formation was attributed to be from an ensemble effect. The rate-limiting step for VAM formation has been previously assumed to be the coupling of surface ethylenic species and acetate[17,18]. The optimum distance between the two active sites of an acetate species and a π-bonded ethylenic species was estimated to be 0.33nm. This is similar in distance between two neighbouring Pd monomers (0.403nm). The formation of Pd monomers may also inhibit the formation of undesirable by-products such as CO, CO_2 and surface carbon. STM images of these monomers have been obtained on both surfaces[19,20]. The addition of Au was also shown to greatly reduce the amount of carbon formed on the surface[13, 21]. On continuous Pd sites, the formation of di-σ bonded ethylene and ethylidyne species were observed resulting in decomposition and carbidisation of the surface[22,23].

Similar geometric and electronic effects were also observed in the conversion of acetylene to benzene on Pd/Au (111) surfaces[24,25]. The surface was shown to be catalytically active until 0.6ML after which a roughened surface was observed, suppressing cyclisation activity. Alloying the two via heating was shown to have a major effect on the desorption temperature of benzene which consequently resulted in it being a more effective catalyst. The coupling of acetylene to benzene has been studied on annealed Au films on Pd[26]. The presence of Au was shown to enhance the

activity of the surface. A Pd composition of ~82% was shown to give highest activity equating to a $AuPd_6$ ensemble. Au was once again shown to decrease the temperature for desorption of benzene, the rate-limiting step, minimizing adsorbate decomposition.

The following studies discussed here regard the effect Au has on the reactivity of the Pd (111) surface. Various molecules present in the overall synthesis of VAM have been investigated and comparisons have been made regarding the differences between the clean Pd (111) surface discussed in chapter 3 and the effect of Au.

5.2 CO on Au/Pd (111)

In order to probe the effect on the reactivity of the Pd (111) surface, the sample was dosed with Au via metal vapour deposition. Using a molecular beam reactor, it was possible to observe the change in reactivity of the surface with different gases at different surface coverages. After cleaning the surface, Au deposition was carried out at room temperature. Before any experiments were carried out, the surface was then flashed to 523K in order to desorb any contaminating CO adsorbed from the background gases. The reactivity of CO on the clean Pd (111) surface was studied extensively in chapter 3. CO has also been shown to bond to the surface in a variety of configurations on the (111) surface; 3-fold-hollow, bridging and atop. TPD and RAIRS studies of CO adsorption on Au/Pd (111) surfaces have shown CO to bind to Au atop sites at low temperatures for multilayer Au coverages[26,27]. Annealing the surface caused Au dissolution and subsequent adsorption of CO onto Pd atop sites. Further annealing resulted in larger ensembles of Pd atoms allowing bridging and 3-fold-hollow CO binding to occur. Since CO was shown to display interesting chemistry on this surface, it was considered important to see the affect of Au. Au was dosed for different time periods followed by CO molecular beam experiments.

CO molecular beam experiments were performed on the Pd (111) surface dosed with Au for different time periods. The initial sticking probability of CO was seen to decrease in a near linear fashion as the dosing time increased. After dosing Au for 180s, no adsorption of CO was observed. This would indicate that after this deposition, no Pd atoms were available CO molecules to interact with. This also agrees with previous studies showing no reactivity between bulk Au and CO at this

temperature[28]. Since Au has been shown previously to grow in a layer-by-layer fashion, it can be assumed that the amount of Au on the top surface layer is proportional to the deposition time period[27]. Figure 5.1 below shows the change in composition of the top surface layer as a function of deposition time. Figure 4.4 in the previous chapter showed the change in Au $4f_{7/2}$ binding energy as a function of deposition time. A large shift in the binding energy to bulk like Au was seen to occur between depositions of 120 and 200s. This agrees with the suppression of CO uptake after 180s indicating the surface to be completely Au in nature. However, since the deposition time required to complete 1ML is significantly longer than that calculated in the previous chapter it may be possible that Au is forming multi layers whilst still leaving a small portion of the Pd surface exposed. This would agree with STM studies by Baddeley et al who found Pd atoms were still visible after 3ML of Au deposition[29].

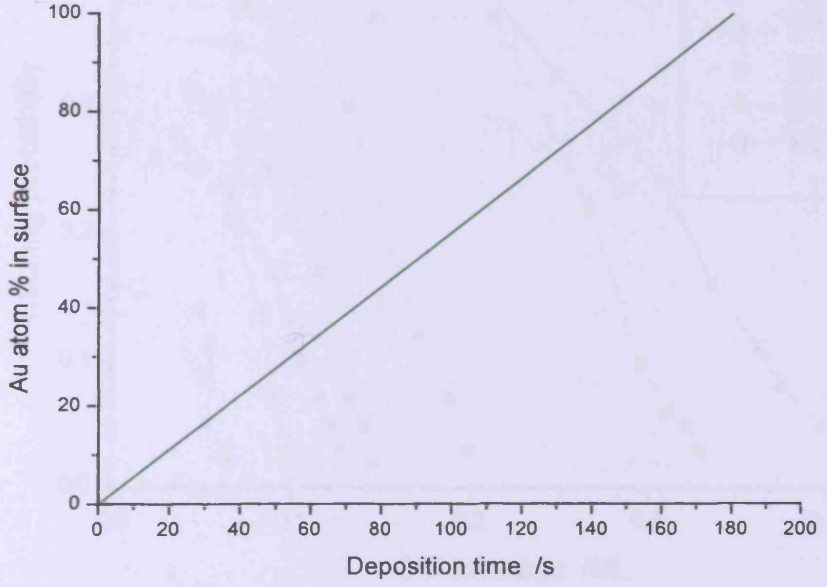

Figure 5.1 Percentage of Au surface atoms vs deposition time

Figure 5.2 below shows the change in sticking probability of CO molecules on the Pd (111) surface as a function of CO uptake for different coverages of Au. Uptake of CO at 373K on clean Pd was found to be ~0.4ML by comparison to the saturation coverages at other temperatures. After depositing Au for one sixteenth of a monolayer, the total CO uptake decreased by 17.6%. After an eighth of a monolayer deposition, a 50% decrease in uptake was observed. There is a much more significant decrease in the total uptake possibly due to the blocking of the 3-fold hollow binding sites. Subsequent depositions of higher Au coverage resulted in less CO reactivity and less total uptake confirming the blockage by Au of Pd adsorption sites. CO sticking was attempted at a coverage of 2/3ML, however due to low adsorption, it was not possible to plot the uptake curve accurately.

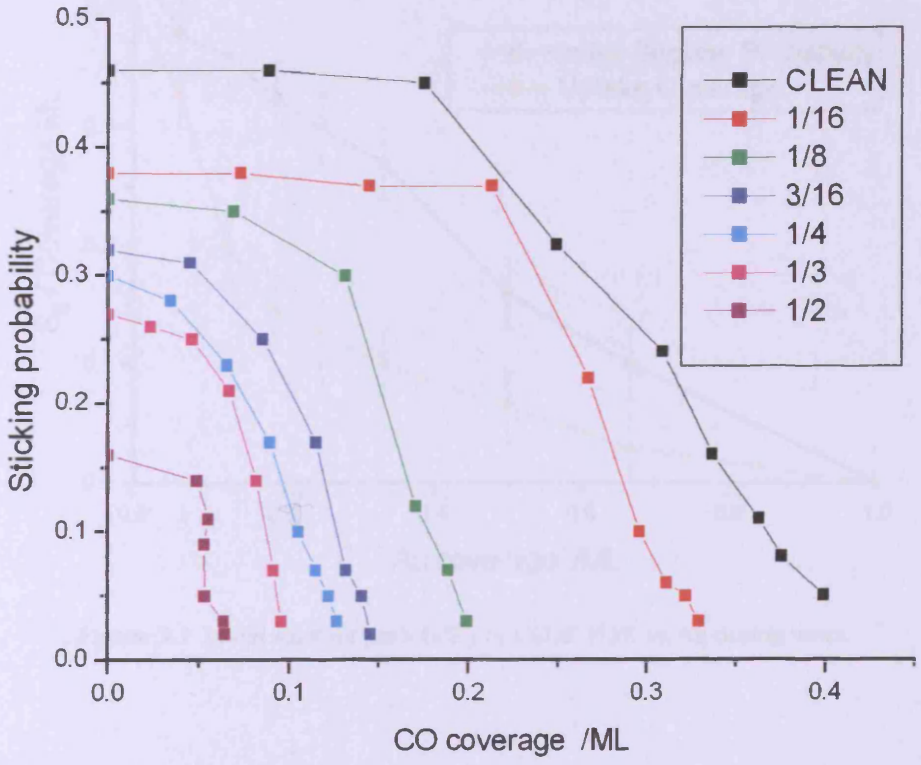

Figure 5.2 CO uptake curves at different Au coverages at 373K

Figure 5.3 shows the change in initial sticking probability and uptake coverage as the coverage of Au increases. On clean Pd, S_0 was found to be ~0.45 at 373K. As increasing amounts of Au were deposited, S_0 can be seen to decrease in a near linear fashion. Uptake coverage of CO however decreases more significantly as Au is deposited to higher coverages. This can be attributed to the blockage of the preferred 3-fold-hollow binding sites. At higher Au coverage, CO is restricted to binding to Pd atop and bridging sites. This agrees with previous studies where CO adsorption on atop and bridging Pd sites was observed for 4ML Au adlayers annealed to 620K and 740K respectively[26].

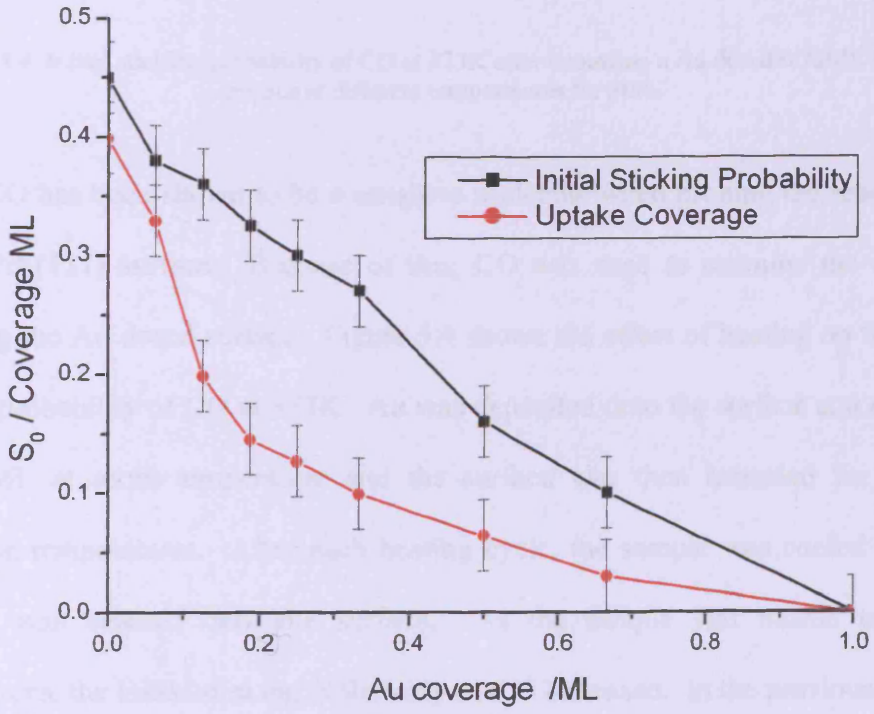

Figure 5.3 Initial sticking probability of CO at 373K vs Au dosing times

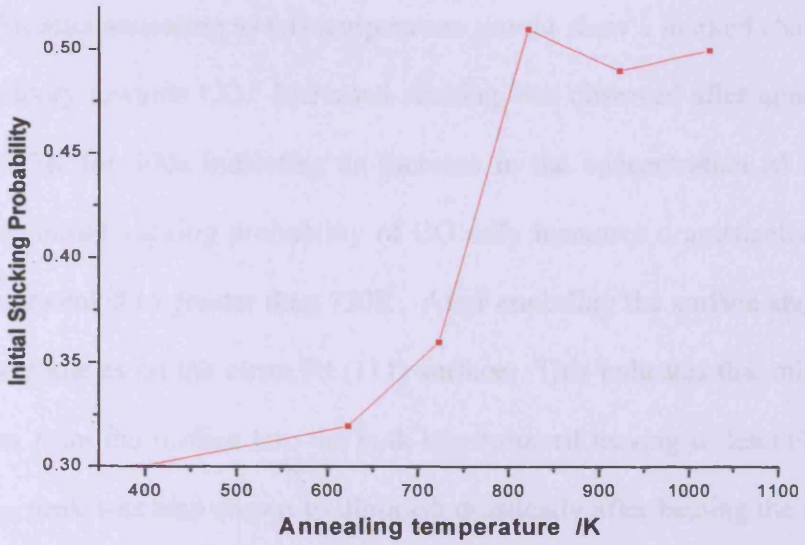

Figure 5.4 Initial sticking probability of CO at 373K after annealing a Au dosed 0.25ML Pd(111) surface at different temperatures for 300s

CO has been shown to be a sensitive molecule when probing the reactivity of the Au/Pd (111) surface. Because of this, CO was used to examine the effect of annealing the Au dosed surface. Figure 5.4 shows the effect of heating on the initial sticking probability of CO at 373K. Au was deposited onto the surface at a coverage of 0.25ML at room temperature and the surface was then annealed for 300s at increasing temperatures. After each heating cycle, the sample was cooled to 393K and CO was beamed onto the surface. As the sample was heated to higher temperatures, the initial sticking probability of CO increased. In the previous chapter, figure 4.10 showed XP spectra of Au dosed surfaces heated to increasing temperatures. The amount of surface Au decreases due to migration into the bulk. This was attributed to its affinity to alloy with the bulk Pd metal. Increased CO adsorption after annealing the surface to increasing temperatures can be attributed to a loss of surface Au to the bulk of the sample. Results discussed previously also

indicated that Au at this coverage starts to migrate into the bulk at ~650K. A decrease in surface Au after annealing to this temperature should show a marked change in the surface reactivity towards CO. Increased sticking was observed after annealing the sample to 623K for 300s indicating an increase in the concentration of Pd atoms. However the initial sticking probability of CO only increases dramatically after the surface was annealed to greater than 720K. After annealing the surface above 820K, CO S_0 is the same as on the clean Pd (111) surface. This indicates that migration of all Au atoms from the surface into the bulk has occurred leaving a clean Pd surface. The Au $4f_{7/2}$ peak was also shown to diminish drastically after heating the surface to ~750K agreeing with the CO sticking data presented here.

5.3 Oxygen on Au/Pd(111)

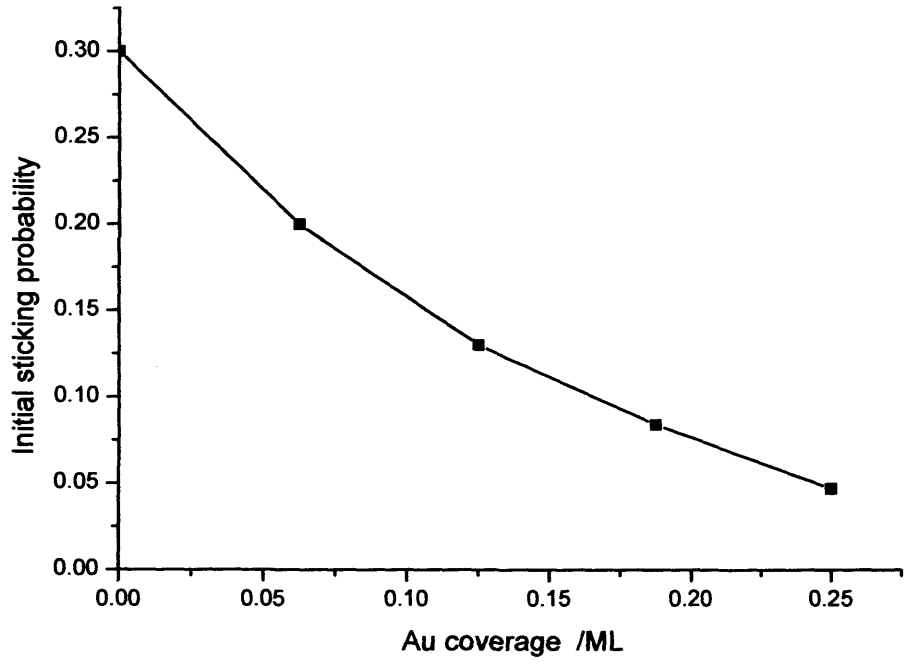

Figure 5.5 O_2 initial sticking probabilities at 373K vs Au coverage

Another important molecule regarding the Au/Pd system and VAM production is O_2. The reactivity of this molecule was studied for different Au coverages at 373K. The sample was cleaned, Au deposition was carried out at room temperature and the sample was then flashed to 523K to desorb any CO which may have adsorbed from the background. Figure 5.5 shows the change in initial sticking probability of oxygen on Pd (111) as the surface coverage of Au increases. A significant 33% decrease in the initial sticking probability of O_2 was observed after 1/16ML Au deposition. This is much greater decrease in reactivity than for CO. By 1/3ML, no sticking of O_2 was observed. All available adsorption sites for O_2 were blocked by this coverage.

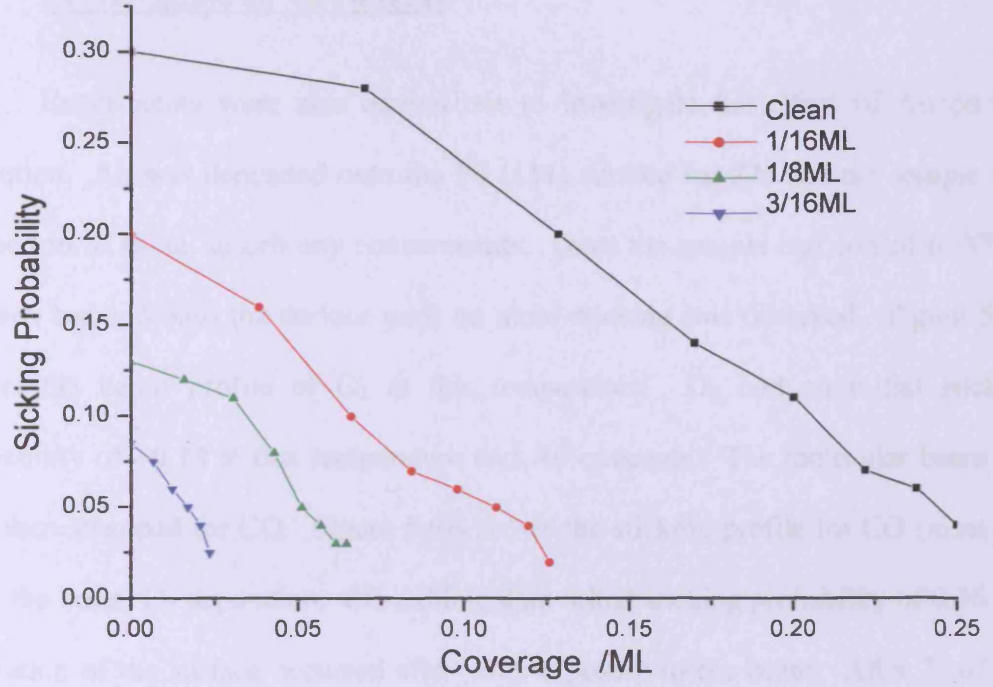

Figure 5.6 Sticking probability vs coverage of oxygen at 373K for different Au deposition coverages

Figure 5.6 shows the effect of Au deposition on the sticking probability and uptake of O_2. On clean Pd at this temperature, O_2 saturates to a coverage of 0.25 ML. By dosing Au to a coverage of one sixteenth of a monolayer, the uptake of oxygen was halved. By dosing Au for an eighth of a monolayer, the total uptake of O_2 was halved again. This shows that even a relatively small amount of Au has a huge impact on the reactivity of Pd towards O_2. The deactivation of the surface with respect to O_2 is even more pronounced than for CO. This would indicate that the adsorption of O_2 is much more surface sensitive than CO and is greatly affected by surface Au.

5.4 CO Oxidation on Au/Pd (111)

Experiments were also carried out to investigate the effect of Au on CO oxidation. Au was deposited onto the Pd (111) surface for 22s and the sample was flashed to 523K to desorb any contaminants. Once the sample had cooled to 373K, O_2 was beamed onto the surface until no more sticking was observed. Figure 5.6A shows the beam profile of O_2 at this temperature. O_2 had an initial sticking probability of ~0.13 at this temperature and Au coverage. The molecular beam gas was then swapped for CO. Figure 5.6B shows the sticking profile for CO (mass 28) after the initial O_2 deposition. CO exhibited an initial sticking probability of 0.36 and saturation of the surface occurred after ~30s exposure to the beam. After 7s of CO beaming, CO_2 evolution was observed. This is due to dissociated O adatoms on the surface reacting with adsorbed CO species. Evolution of CO_2 peaks 13s after initial exposure and appears to have an induction time until reaction (sharp CO_2 peaks at 25s and 120s are caused by the mechanical movement of the flag). On the clean Pd (111) surface at this temperature, CO_2 evolution was observed immediately upon exposure of CO and production peaked after only 10s. However it is evident from the O_2 beam profile that significantly less O_2 was adsorbed resulting in a much lower coverage of O_2 atoms. Since less O atoms were present on the surface and CO sticking was reduced by surface Au, build-up of CO took much longer. As the surface became more concentrated in CO, the oxidation reaction and desorption pathway became more favourable due to increased surface repulsions. On clean Pd, this occurs more quickly whereas on Au dosed Pd, the reaction proceeds more slowly.

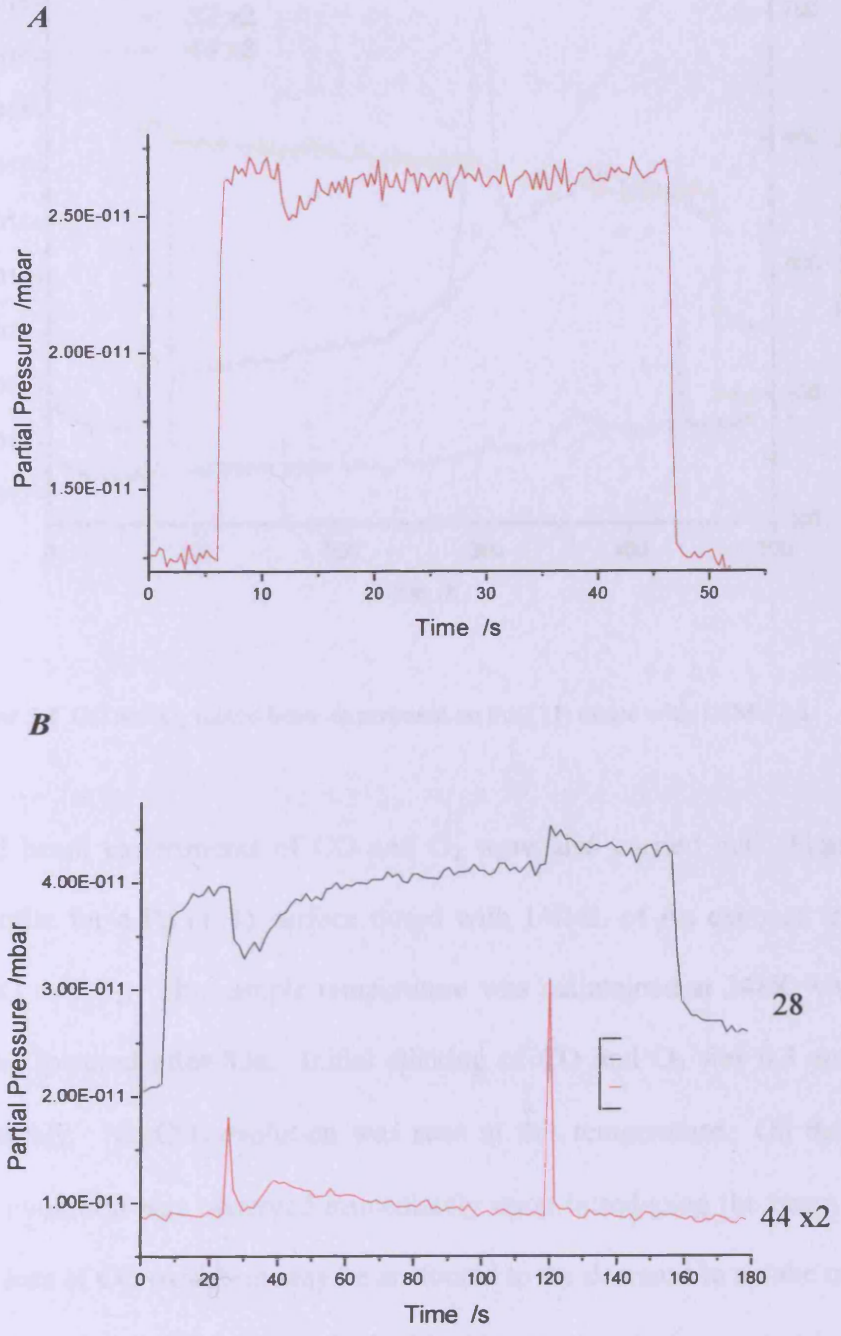

Figure 5.7 A. O_2 sticking on 22sAu dosed surface at 373K.

B. CO beam profile on 22s Au dosed surface after O_2

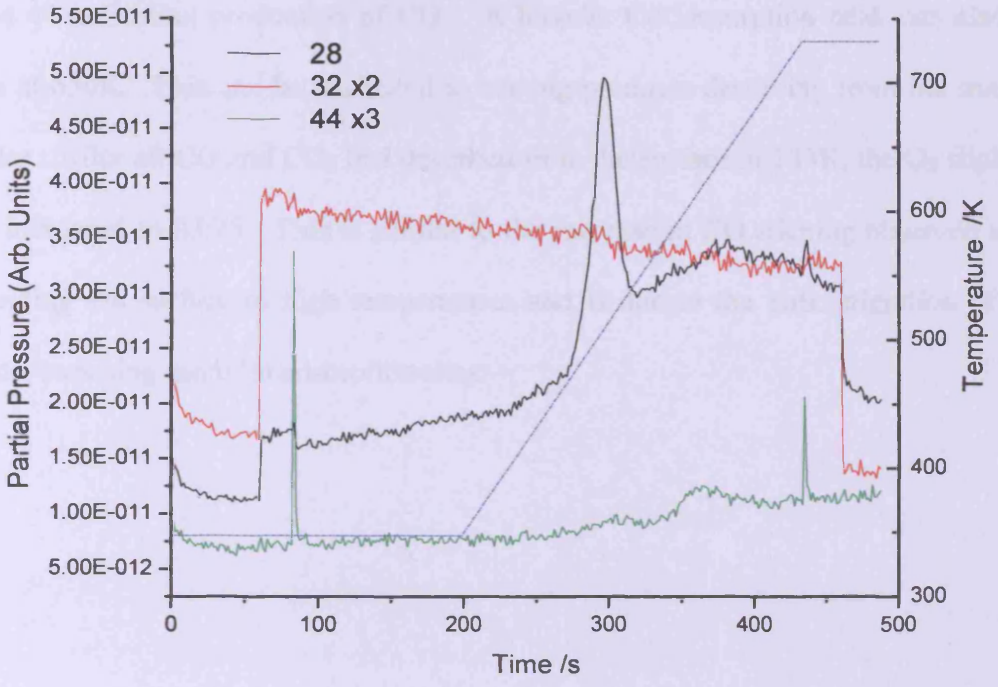

Figure 5.8 CO and O_2 mixed beam experiment on Pd(111) dosed with 1/4ML Au

Mixed beam experiments of CO and O_2 were also carried out. Figure 5.8 shows the profile for a Pd (111) surface dosed with 1/4ML of Au exposed to a 1:1 mixture of CO and O_2. The sample temperature was maintained at 348K when the beam flag was lowered after 83s. Initial sticking of CO and O_2 was 0.3 and 0.05 ±0.03 respectively. No CO_2 evolution was seen at this temperature. On the clean surface, CO_2 evolution was observed immediately upon introducing the beam to the surface. The loss of CO oxidation may be attributed to the decrease in uptake of O_2 at this Au coverage. Once adsorption of the incident beam gases had ceased, the sample was heated. Upon heating the sample CO desorption was observed which peaked at 473K. O_2 sticking was can be seen immediately after the CO desorption peak. This increase in uptake can be attributed to the vacation of adsorption sites by CO molecules. As O_2 adsorption occurs, a small desorption peak at 483K can be seen for

mass 44 indicating production of CO_2. A broader CO desorption peak can also be seen at 650K. This can be attributed to heating products desorbing from the sample holder. After all CO and CO_2 had desorbed from the surface at 733K, the O_2 sticking had increased to 0.075. This is similar to the increase in CO sticking observed after annealing the surface to high temperatures and is due to the bulk migration of Au atoms, exposing more Pd adsorption sites.

5.5 Ethylene on Au/Pd (111)

At ambient temperatures, ethylene has been shown to form ethylidyne species on the Pd (111) surface[30,31]. This conversion has been studied recently using DFT and is thought to occur via a three-step mechanism, ethylene → vinyl → ethylidene → ethylidyne[32]. Coverages of 1/3, 1/4 and 1/9ML of ethylene were used in these model calculations and the dehydrogenation of ethylene was found to be the rate-determining step for all coverages. The rate of formation of ethylidyne was found to decrease as coverage increased due to the desorption pathway becoming more favourable at higher coverage. At 1/9ML coverage, more neighbouring sites were available for dehydrogenation and hydrogen diffusion, also favouring this conversion process. Experimental results also agree with the mechanism for the formation of ethylidyne, and show an activation barrier for its formation with respect to gas-phase ethylene to be 49 ±5 kJ/mol[33]. Coverage of ethylidyne has also been found to saturate to 0.25ML on the Pd (111) surface[34]. Figure 5.8 shows the change in initial sticking

probability of ethylene on Pd (111) for different coverages of Au. After depositing Au to a coverage of only 0.065ML, the initial sticking probability had decreased by 57% to 0.1. After depositing Au to a coverage of 0.13ML, no reactivity was observed. This low coverage is all that is necessary for the Au to completely passivate the Pd (111) surface towards ethylene. No hydrogen evolution or any other decomposition products were observable for the two different Au coverages. This is due to the high background pressure of hydrogen in UHV and the low sticking of ethylene, any evolution which could have occurred would be unobservable. This decrease in reactivity indicates that the adsorption of ethylene on Pd (111) is very surface sensitive. Only a small amount of Au was needed to stop ethylene binding and forming ethylidyne.

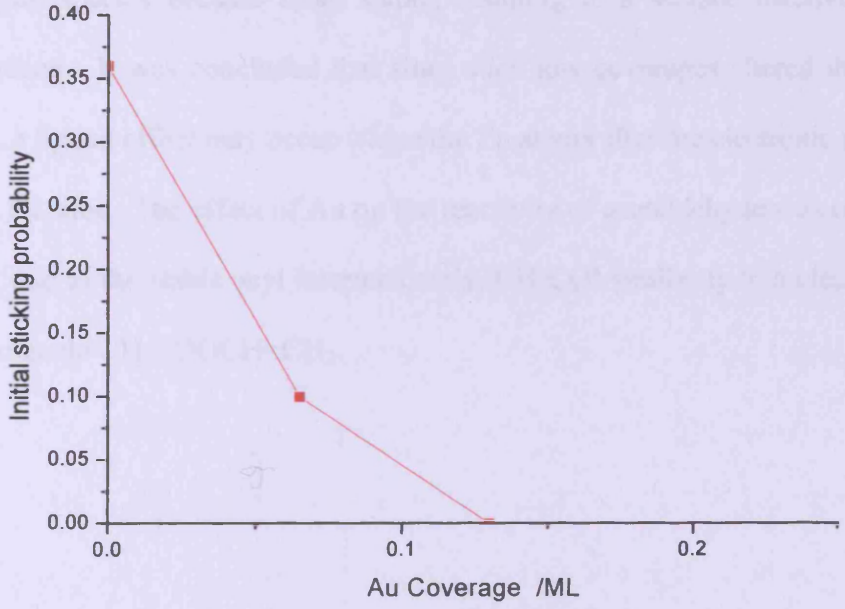

Figure 5.9 Initial sticking probability of ethylene at 373K vs Au coverage

5.6 Acetaldehyde on Au/Pd (111)

Previous studies of aldehydes on various different surfaces have shown bonding to occur via the overlap of π-orbitals in the carbonyl group with surface metal's d orbital electrons[35-37]. This mode is known as η_2 bonding and occurs above 170K. Acetaldehyde was shown to decarbonylate at ambient temperatures through a stable acyl intermediate, resulting in the formation of methane and CO. At elevated temperatures, further decomposition was shown to occur via a ketene intermediate. TPD and HREELS studies of Zn dosed Pd (111) surfaces have been carried out previously[38]. Low coverages of Zn (0.03ML) were shown to inhibit the decarbonylation of acetaldehyde and to decrease the desorption temperature of CO formed from dehydrogenation. As the concentration of Zn was increased, surface acetaldehyde species became more stable, resulting in a surface inactive towards decomposition. It was concluded that since such low coverages altered the surface reactivity, a ligand effect may occur where the Zn atoms alter the electronic properties of nearby Pd sites. The effect of Au on the reactivity of acetaldehyde was considered important due to the stable acyl intermediate's (CH_3CO) similarity to a cleaved vinyl acetate molecule $CH_3COOCH{=}CH_2$.

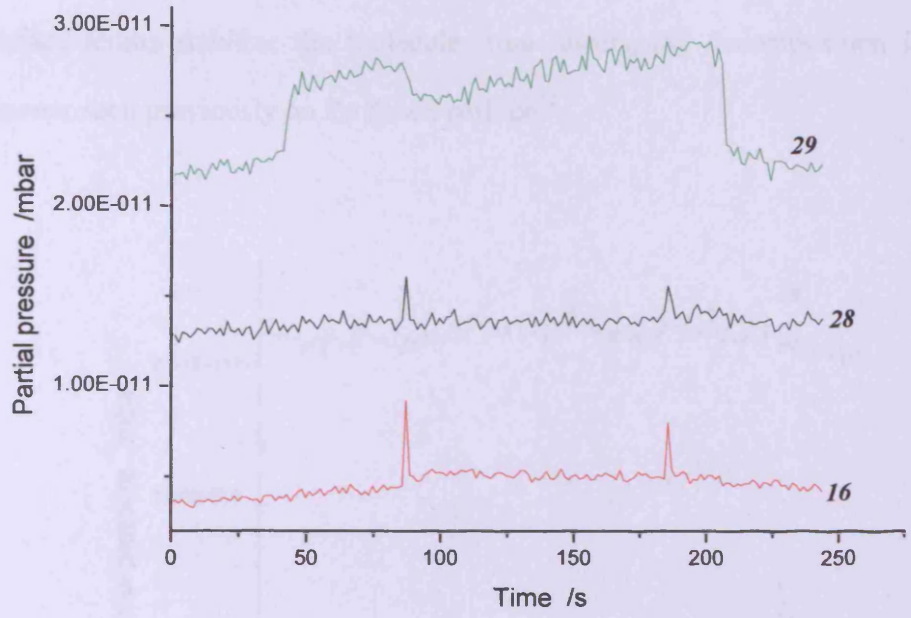

Figure 5.10 Molecular beam experiment of acetaldehyde on Pd(111) at 309K after 1/6ML Au deposition

Acetaldehyde is of considerable interest to the Au/Pd system and VAM production due to the molecule's similarity to cracked vinyl acetate molecule. On clean Pd (111) acetaldehyde was shown in chapter 3 to undergo two different decomposition reactions in different temperature regimes. At ambient temperatures, decarbonylation was seen to be the favoured pathway, evolving methane and poisoning the surface with CO. At higher temperatures (473K), a more destructive dehydrogenation reaction was observed producing CO and H_2 leaving carbon on the surface. Figure 5.9 shows a molecular beam profile for acetaldehyde beamed onto the Pd (111) surface at 309K after a 1/6ML Au dosing. At this temperature on clean Pd, an initial sticking probability of 0.68 would have been observed. However due to the passivating effect of the Au, the $S_{(0)}$ decreased to 0.3, a 56% drop in reactivity. Despite acetaldehyde adsorption occurring at this temperature and Au coverage, very

little methane evolution (mass 16) was observed. This would imply that the Au surface atoms stabilize the molecule from undergoing decomposition in a similar manner seen previously on Zn dosed surface[38].

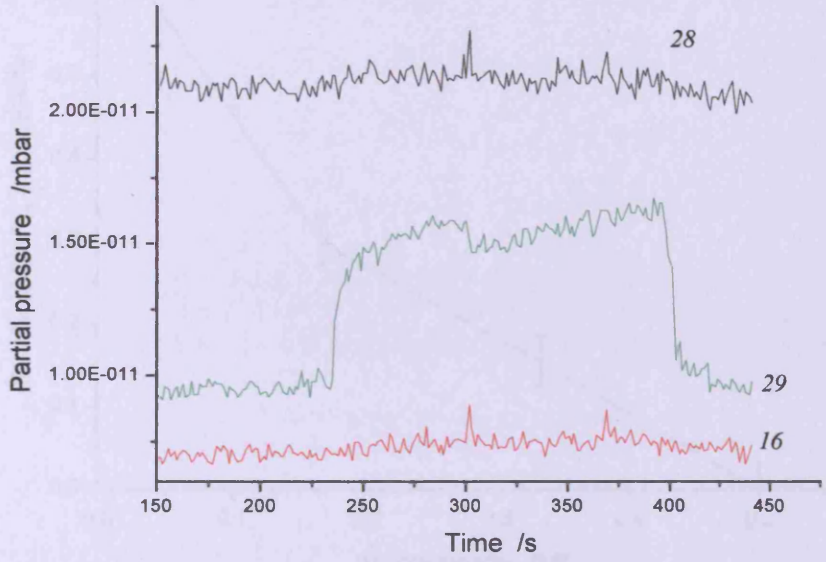

Figure 5.11 Molecular beam experiment of acetaldehyde on Pd(111) at 309K after 1/3ML Au deposition

Acetaldehyde beam experiments were also carried out at higher Au coverages of 1/3ML. At this coverage, reactivity of the molecule with the surface was observed to have decreased even more. The $S_{(0)}$ decreased to 0.155 and saturation was reached after 1/3ML Au was deposited. No methane evolution (Mr16) was observed which may be due Au stabilising the molecule. However since the signal to noise ratio is quite high and very little acetaldehyde sticking occurred, any methane produced may have been lost in the background noise. Since decomposition was greatly limited after deposition of Au to 1/6ML, it can be concluded that Au has a stabilizing effect

on the molecule. At 1/3ML Au coverage, no decomposition products were seen indicating a total deactivation of decomposition pathways.

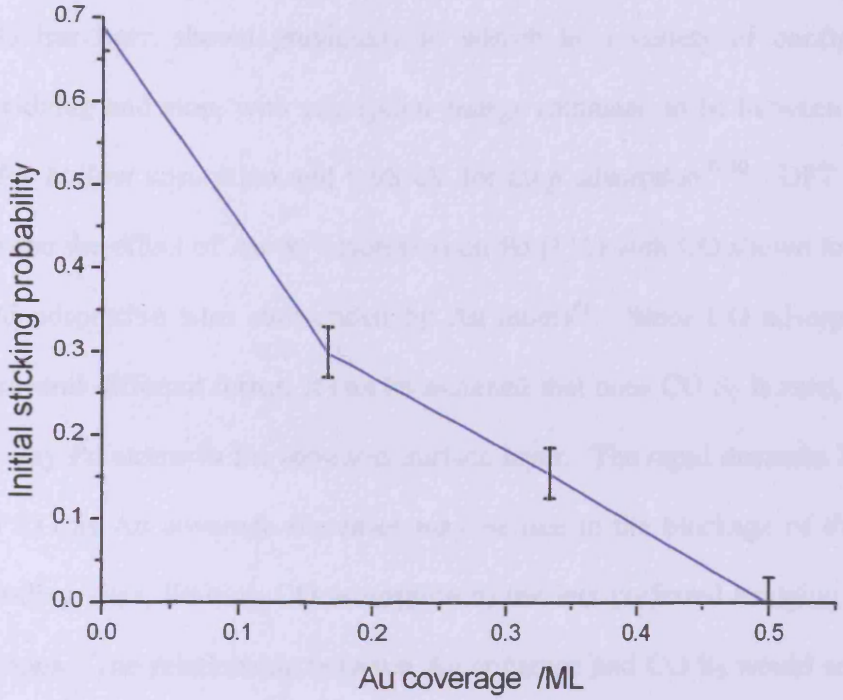

Figure 5.12 Initial sticking probability of acetaldehyde on Pd (111) at 309K as a function of Au deposition time

5.7 Discussion

The experiments probing the effect of different Au coverages on the initial sticking probability of incident molecules have brought to light an interesting feature of adsorption on the Pd (111) surface. For the each of the different molecules studied,

adsorption was suppressed by varying Au coverages, but the extent of suppression was strongly dependant on the molecule used

CO has been shown previously to adsorb in a variety of configurations, hollow, bridging and atop, with adsorption energy estimated to be between 1.47 and 1.54 eV for hollow adsorption and 0.98 eV for atop adsorption[39,40]. DFT has been used to probe the effect of Au on adsorption on Pd (111) with CO shown to prefer to occupy Pd adsorption sites surrounded by Au atoms[41]. Since CO adsorption may occur in several different forms, it can be assumed that once CO S_0 is zero, there are no longer any Pd atoms in the top-most surface layer. The rapid decrease in surface uptake of CO as Au coverage increases may be due to the blockage of the 3-fold-hollow binding sites, limiting CO adsorption to the less preferred bridging and atop configurations. The relationship between Au coverage and CO S_0 would seem to be linear in nature. This is different to CO $S_{(t)}$ as a function of CO uptake shown in chapter 3 which indicated the existence of a CO physisorbed extrinsic precursor state. When gaseous CO molecules collide with associatively adsorbed CO molecules they are blocked from direct chemisorption. However they may become bound to an adsorbate-covered portion of the surface through van der Waals interactions and are free to diffuse laterally, increasing the opportunity to find a free site for chemisorption. When Au is dosed onto the surface, it may be that chemisorption via this extrinsic precursor state is no longer possible and instead, Langmuir type associative adsorption takes place.

O_2 has been shown to dissociate on the Pd (111) surface above 200K with adsorption into a hollow site being the most favourable[42,43]. Deposition of Au onto

the surface was seen to suppress the initial sticking probability with no reactivity observed by 1/3ML. In Chapter 3, the sticking probability of O_2 on Pd (111) as a function of O_2 coverage has been shown. Figure 5.13 compares the effect Au has on the sticking probability of O_2 on Pd (111) with respect to the previous studies. For both systems, uptake of O_2 was prohibited once the concentration of Au or O_2 reached 1/4ML. In this respect, Au atoms are similar to O atoms because they both block adsorption to the same extent, only allowing 1/4ML of surface adsorption to occur. The shape of the two plots is however different, indicating a difference in the way an incoming O_2 molecule interacts with adsorbed Au or O_2 species. The shape of the uptake curve on Au covered Pd is more typical of Langmuir dissociative adsorption while on the O_2 covered surfaces, a precursor mechanism may be happening whereby O_2 molecules physisorb onto oxygen atoms then diffuse away to find a vacant site for dissociative chemisorption to take place.

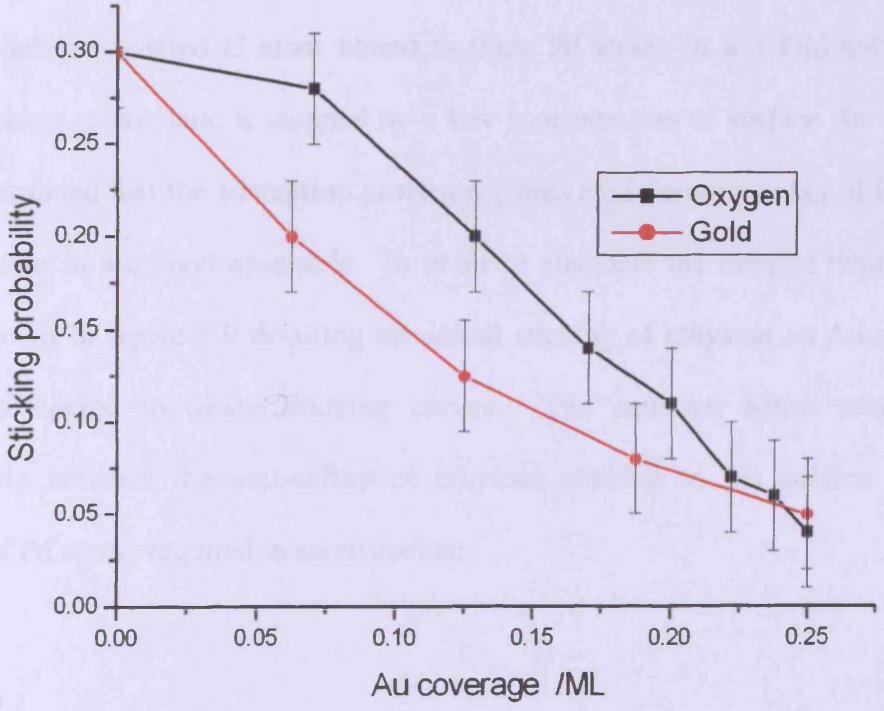

Figure 5.13 O_2 sticking probability on Pd (111) at 373K vs surface contaminant coverage

Ethylene saturates to a coverage of ~0.25ML on clean Pd (111) at 373K with no adsorption of the molecule recorded above this coverage. Au deposition has however been shown to suppress adsorption by 1/8ML. The effect of Au on ethylene adsorption is much more pronounced than its effect on O_2 adsorption where Au can be seen to block surface sites in a similar manner to oxygen atoms. On clean Pd, O_2 dissociatively adsorbs forming oxygen atoms, a relatively simple process. Ethylene however undergoes a more complex process whereby ethylidyne species are formed. Au deposition therefore has a significant effect on the ability of ethylene to adsorb onto the surface and undergo conversion to stable ethylidyne species via vinyl and ethylidene intermediates. The first step of the mechanism involving the dehydrogenation of a di-σ-bonded ethylene group to the vinyl intermediate requires three Pd atoms for binding the vinyl group in a $\eta_1\eta_2$ mode and a 3-fold-hollow site for the dissociated hydrogen atom to migrate to before reattaching to form ethylidene[44,45]. Conversion to ethylidyne then occurs with the C-C bond perpendicular to the surface with the dehydrogenated C atom bound to three Pd atoms in a 3-fold-hollow site. Since sticking of ethylene is stopped by a low concentration of surface Au atoms, it must be assumed that the adsorption process requires a minimum number of Pd atoms to be present in a correct ensemble. In order to elucidate the number required, the results shown in figure 5.9 detailing the initial sticking of ethylene vs Au coverage can be compared to model sticking curves. The equation below models the relationship between the probability of ethylene sticking to the surface and the number of Pd atoms required in an ensemble;

(Eqn 5.1) $S = S_0 (1-(\theta_{Au}/\theta_{max})^N$

S - Initial sticking probability of molecule

S_0 - Initial sticking probability of molecule on clean surface

θ_{Au} - Au coverage

θ_{max} - Maximum adsorbate coverage on clean surface

N - Number of adjacent Pd atoms in ensemble for adsorption to occur

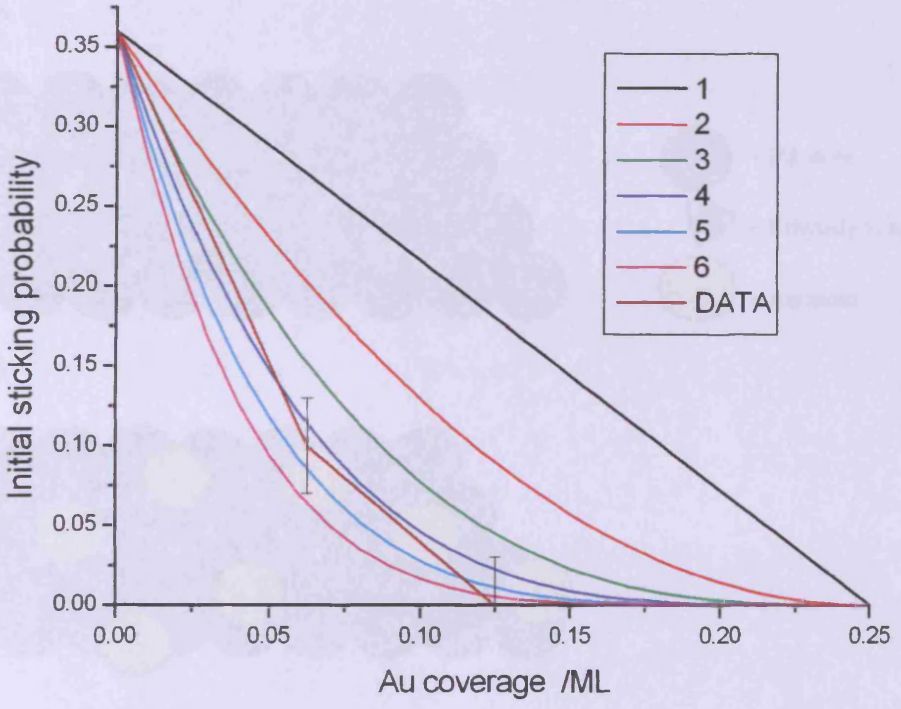

Figure 5.14 A comparison between the number of surface ensemble atoms required and experimental sticking data for ethylene on Au dosed Pd (111) at 373K

The S_0 of ethylene on Pd (111) dosed with different coverages of Au is shown in figure 5.14. Curves 1 to 6 display the effect on sticking Au has upon ethylene when the number of atoms in a Pd ensemble (N) is increased. As would be expected, the larger the ensemble necessary for adsorption, the greater the effect Au has on

sticking. From the plot, it is possible to see that the real data is most similar to the curve generated when N=4. The need for four adjacent Pd atoms may be attributed to the formation of the vinyl intermediate which has also been determined to be the rate determining step for the conversion[33]. In order to probe the significance and validity of this 4-atom ensemble, a model Pd (111) surface was constructed. Different coverages of Au were placed on the model and the effect on possible ethylidyne formation site was examined. The Pd ensemble was assumed to be the similar in shape to the unit cell for the (111) surface.

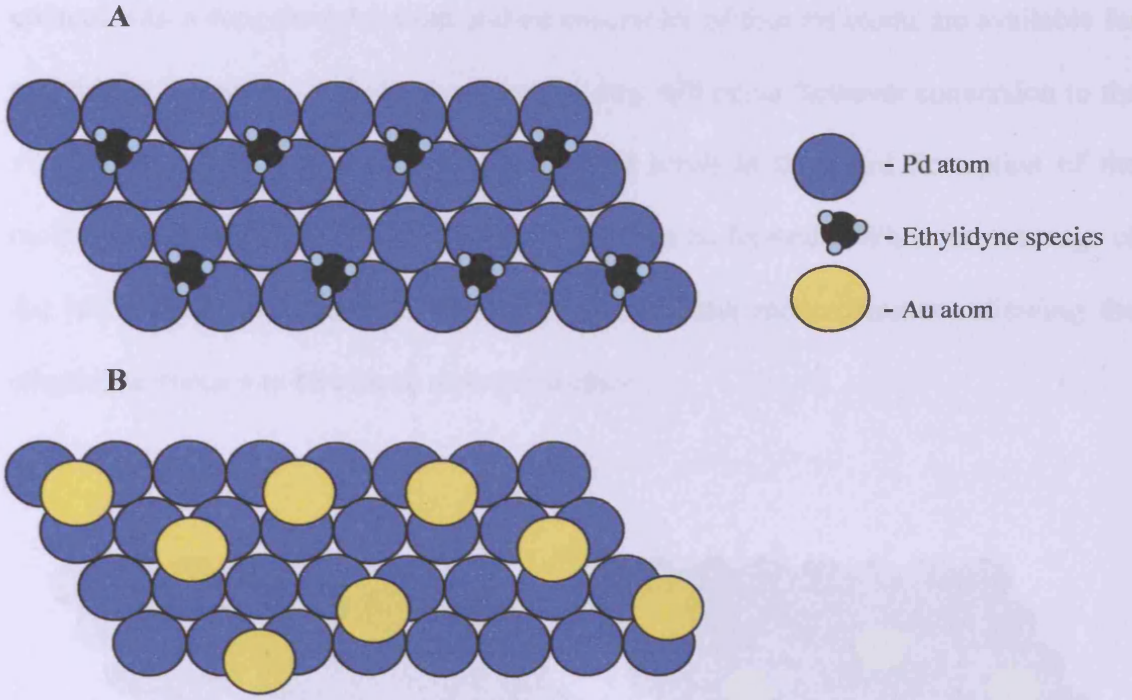

Figure 5.15 **A.** Ordered 0.25ML coverage of ethylidyne species on clean Pd (111); **B.** Deposited Au atoms randomly arranged at 0.25ML coverage

Figure 5.15A shows an ordered array of ethylidyne species bound to the Pd (111) surface at a coverage of 0.25ML. Three Pd atoms are directly bound to the adsorbate with another atom neighbouring the triplet. Figure 5.15B shows a possible

arrangement of Au atoms on the surface at a coverage of 0.25ML. Au overlayers have previously been seen to mimic the substrates surface structure with Au atoms placed in 3-fold hollow sites atop the Pd surface[46]. Layer-by-layer growth has been proposed with Au forming small dendritic islands concentrated around terrace step edges[30]. Due to the small size of these islands, the surface was shown to exhibit a relatively large number of different adsorption sites. Since the surface was only annealed to 523K after deposition to remove contaminants, limited mixing of the metals would have occurred. At this coverage, there are very few Pd atoms not in contact with a deposited Au atom and no ensembles of four Pd atoms are available for ethylidyne formation. Ethylene adsorption may still occur however conversion to the vinyl intermediate is prohibited. This would result in the rapid desorption of the molecule since no stable surface configuration can be formed. When the coverage of Au is lowered, ensembles of four Pd atoms become more common, allowing the ethylidyne species to be placed onto the surface.

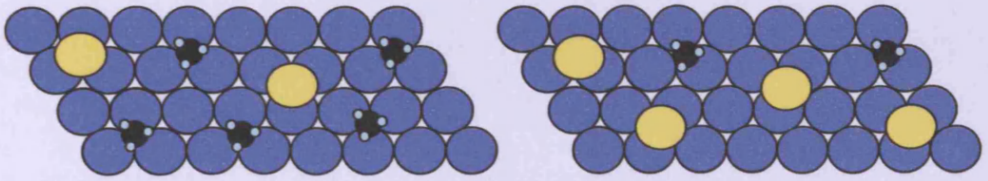

Figure 5.16 (Left) Au of 1/16ML arranged randomly on the surface with ethylidyne species. (Right) 1/8ML Au with ethylidyne

Figure 5.16 above shows the Pd surface deposited with two different coverages of Au. When the surface is dosed with 1/16ML Au, Pd ensembles are available for ethylidyne formation. When the Au coverage is increased to 1/8ML,

there are still sites available for adsorption however the number is far fewer than found on the clean surface. Sticking experiments carried out at this coverage indicated no adsorption however. This lack of reactivity can be attributed to the difficulty in observing the sticking probabilities lower than 0.025 due to the signal to noise ratio

Acetaldehyde has been shown previously to readily adsorb onto the Pd (111) surface at ambient temperatures, decomposing to form methane and CO. This process is thought to occur via the initial binding of acetaldehyde in a η_2 configuration where the carbonyl π orbital overlaps with the Pd d electrons. Dosing the surface with Au decreased the initial sticking probability of the molecule indicating blockage of surface adsorption sites. The decomposition of the molecule was also suppressed by the Au adlayer, in a similar way as seen previously on Zn dosed Pd (111)[48]. Au surface atoms may be inhibiting the surface decomposition pathway by blocking Pd ensemble sites in a similar manner as ethylene discussed previously.

5.8 $Au_{30}Pd_{70}$(111) Alloyed Single Crystal

To further investigate the effect on Pd reactivity by Au, a AuPd (111) single crystal was employed. The bulk concentration of the crystal was a ratio 30:70 Au:Pd. Before each experiment, the sample underwent argon sputtering and an annealing cycle as recommended[47] to ensure cleanliness. Previous studies on the $Au_{30}Pd_{70}$ (111) crystal have been carried out using LEED, AES and LEIS. Surface segregation of Au was seen to occur by heating the surface above 523K. Continued annealing up to 723K resulted in an unreconstructed surface with Au concentration of 75%[47]. The alloy's reactivity was also compared to that of Pd (111) for the hydrogenation of 1,3-butadiene to butane. The alloyed sample exhibited a lower rate of conversion than pure Pd. This was attributed to Au having a blocking effect on reaction sites. However, unlike on Pd (111), the rate of production of butane was very low and the selectivity to butenes reached~100%. The presence of Au may encourage desorption of butenes rather than further hydrogenation.

Hydrogen absorption and oxidation have also been investigated with both Pd (111) and $Au_{30}Pd_{70}$ (111) surfaces in a batch type reactor[49]. The alloyed surface was less efficient in forming water than the pure Pd surface however it didn't deactivate upon exposure to the reactive mixture as pure Pd did. The alloyed sample was also shown to absorb much more hydrogen into the bulk than Pd (111). CO oxidation reactions on this system also yielded less activity on the alloyed surface[50]. On both surfaces, light-off occurs when heating because CO coverage decreases to a critical value allowing oxygen adsorption and dissociation. On the clean Pd (111) surface, after reaction on a fresh surface, a second reaction run exhibited increased production of CO_2. This was attributed to the formation of palladium oxide after light-off. The

rough Pd-O surface exhibited higher activity due to the instability of the oxide indicating the reaction follows the Mars-Van Krevelen mechanism under these conditions[51]. For the alloyed surface, the lack of increase in activity can be ascribed to a gold-induced inhibition of O_2 adsorption and subsequent oxide formation. The surface structure of a Au_3Pd (110) and Au_3Pd (113) alloyed single crystals have also been studied previously using LEED and LEIS[52,53]. The compositions of the topmost layers were shown to be pure Au. The top layer also exhibited no long-range order. The second layer had depleted Au and the third was bulk-like in composition. The lack of reconstruction in the top-layer was attributed to the presence of Pd in the second layer.

CO was exposed to the surface via the molecular beam in order to investigate the change in reactivity and total uptake of the $Au_{30}Pd_{70}$ (111) surface compared to that of pure Pd (111) and the Au dosed Pd (111) surface. Figure 5.17A below shows the beam profile for CO on the $Au_{30}Pd_{70}$ (111) sample at 323K. The initial sticking probability $S_{(0)}$ was 0.32. On clean Pd (111) at 323K a $S_{(0)}$ of 0.54 had been recorded previously. When this 41% drop in initial sticking probability is compared with previous results on Au dosed Pd (111), it is possible to calculate the surface composition to be ~34% Au. Saturation of the surface also occurred much quicker resulting in an equilibrium between the rate of adsorption and desorption of CO molecules. After 146s, the beam flag was raised, stopping the incident molecules from colliding with the surface. As it was raised, a desorption peak can be seen indicating CO molecules leaving the surface. This was because adsorption and desorption were no longer in equilibrium and only desorption occurs.

CO was also background dosed onto the surface and TPD was performed. Figure 5.17B. shows desorption occurring upon heating of the surface and with a

maximum at ~449K. This peak maximum is slightly higher than on clean Pd (111). Even more significant than the decrease in initial sticking between the pure and alloyed Pd surfaces is the decrease in uptake.

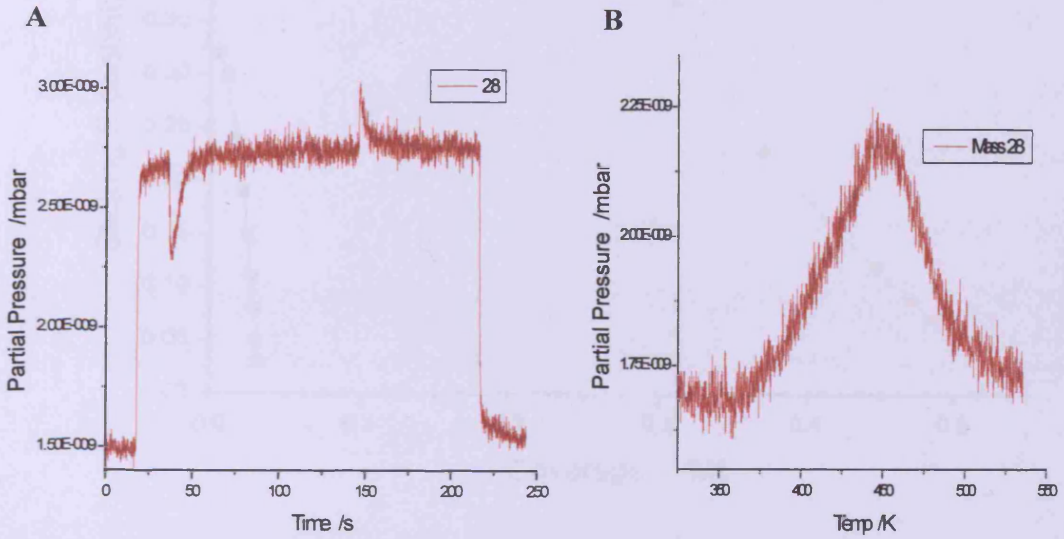

Figure 5.17 A. Beam profile for CO on $Au_{30}Pd_{70}(111)$ at 323K

B. TPD after background dosing 50L CO at 323K

Figure 5.18 shows the change in $S_{(t)}$ as a function of total coverage. For clean Pd, previous studies have shown CO to saturate at this temperature to approximately 0.5ML. For the alloyed surface saturation was reached at a total coverage of 0.032ML, 6.4% of clean Pd. By comparing this drop in CO uptake to results shown previously on the Au dosed Pd (111) surface, this indicates a surface Au composition of ~70%. This is similar to previous studies which concluded a surface concentration of 75% under these annealing conditions[48]. However, with such a high surface Au composition, it is possible that electronic effects from neighbouring Au atoms may alter the reactivity of the isolated Pd atoms.

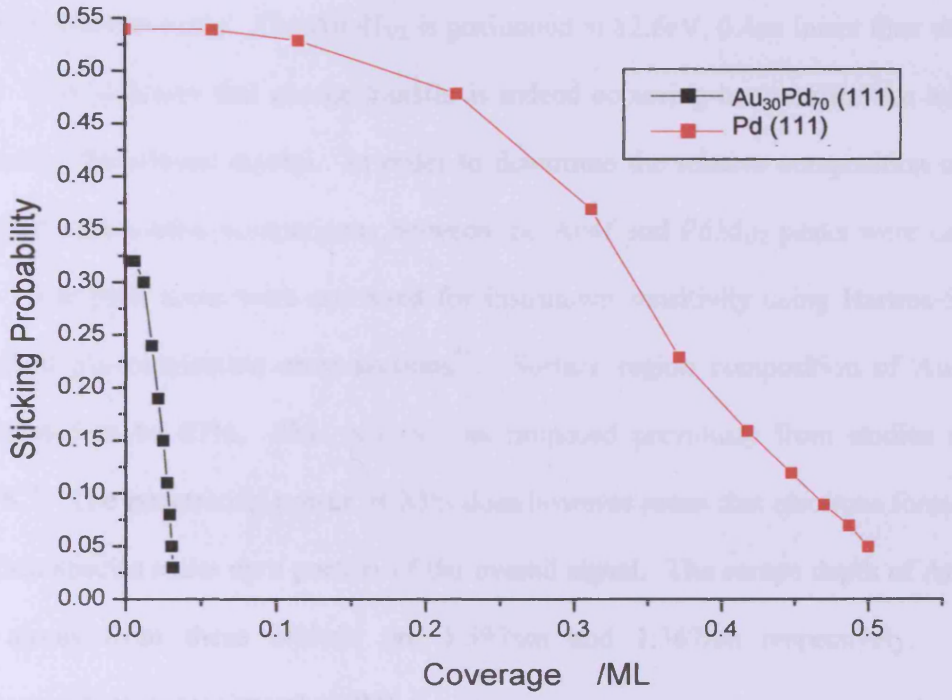

Figure 5.18 Sticking probability vs coverage of CO at 323K on Pd (111) and $Au_{30}Pd_{70}$ (111)

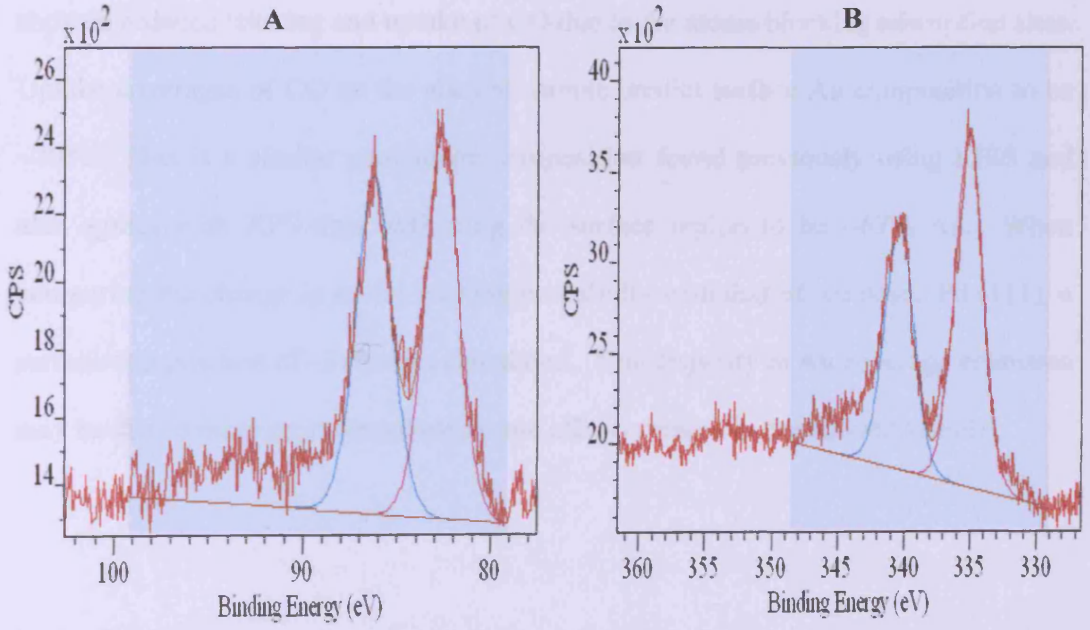

Figure 5.19 ***A.*** XP spectrum of Au4f region ***B.*** XP spectrum of Pd region of $Au_{30}Pd_{70}$ (111)

Figure 5.19 shows XP spectra of the $Au_{30}Pd_{70}$ (111) crystal after a sputter-anneal cleaning cycle. The Au $4f_{7/2}$ is positioned at 82.6eV, 0.4ev lower than atomic Au. This indicates that charge transfer is indeed occurring between the Au and Pd atoms in the alloyed crystal. In order to determine the relative composition of the surface, quantitative comparisons between the Au4f and $Pd3d_{3/2}$ peaks were carried out. The peak areas were corrected for instrument sensitivity using Hartree-Slater subshell photoionization cross-sections[54]. Surface region composition of Au was calculated to be 67%. This is less than proposed previously from studies using LEIS[44]. The penetrating power of XPS does however mean that electrons form sub-surface species make up a portion of the overall signal. The escape depth of Au and Pd atoms from these orbitals are 1.597nm and 1.367nm respectively. This corresponds to approximately 10ML.

Both the $Au_{30}Pd_{70}$ (111) alloyed crystal and the Au dosed Pd (111) surface showed reduced sticking and uptake of CO due to Au atoms blocking adsorption sites. Uptake coverages of CO on the alloyed sample predict surface Au composition to be ~70%. This is a similar percentage composition found previously using LEIS and also agrees with XPS data indicating the surface region to be ~67% Au. When comparing the change in initial sticking probability with that of Au dosed Pd (111), a surface composition of ~34% was calculated. This disparity in Au coverage estimates may be due to more pronounced electronic effects present in the alloyed sample.

5.9 Conclusions

Au was dosed onto the Pd (111) surface at room temperature for different lengths of time and then annealed to 523K in order to remove any adsorbed CO. Once the sample had cooled back down, VAM related molecules (CO, O_2, C_2H_4 and CH_3CHO) were deposited onto the surface using the molecular beam reactor. Since adsorption of these molecules has not been seen to occur on clean Au surfaces at ambient temperatures, it was assumed that depositing Au would decrease their sticking probability. This was found to be true, however the extent to which Au passivated the surface was found to be different for each molecule.

The initial sticking probability of CO was found to decrease proportionally with the coverage of Au on the surface. A dramatic increase in sticking of the molecule was observed once the Au dosed surface was annealed >750K. This indicates that only significant bulk migration of the Au adlayer occurs above this temperature. CO oxidation was also greatly reduced by the deposition of Au due to the suppression of O_2 uptake. Sticking measurements of O_2 on Au dosed Pd (111) shows Au inhibiting adsorption in a similar manner as oxygen atoms on the clean surface.

The reactivity of ethylene was greatly reduced by a low coverage of Au, with no reactivity seen above 1.8ML Au coverage. The large decrease in reactivity at low coverages of Au was attributed to the blocking of Pd ensemble sites needed for adsorption and formation of ethylidyne. The liquid phase mechanism described in chapter 1 shows ethylene reacting with Pd (II) acetate species in the formation of

VAM. Ethylene is not thought to directly interact with Pd metal on the surface of the catalyst in this mechanism. It has also been proposed that the majority of the by-product formation during VAM synthesis results from the decomposition of ethylene. These studies therefore imply that the role of Au in VAM synthesis is to stop the decomposition of ethylene on the catalyst surface, limiting by-product formation and carbidisation. Acetaldehyde decomposition was also limited by the deposition of Au further emphasising its stabilising effect with regard to organic molecules.

5.10 References

1. D. I. Enache, J. K. Edwards, P. Landon, B. Solsona-Espriu, A. F. Carley, A. Herzing, M. Watanabe, C. J. Kiely, D. W. Knight, G. J. Hutchings, *Science.* **311** (2006) 362
2. P. Landon, P. J. Collier, A. J. Papworth, C. J. Kiely, G. J. Hutchings, *Chem. Commun.* **2002** (2002) 2058
3. P. Landon, P. J. Collier, A. F. Carley, D. Chadwick, A. J. Papworth, A. Burrows, C. J. Kiely, G. J. Hutchings, *Phys. Chem. Chem. Phys.* 5 (2003) 1917
4. J. K. Edwards, B. Solsona, P. Landon, A. F. Carley, A. Herzing, M. Watanabe, C. J. Kiely, G. J. Hutchings, *J. Mater. Chem.* **15** (2005) 4595
5. D. T. Thompson, *Platinum. Metals Rev.* **48** (2004) 169

6. J. K. Edwards, B. Solsona, E. Ntainjua, A. F. Carley, A. Herzing, C. J. Kiely and G. J. Hutchings, *Science.* **323** (2009) 1037

7. M. O. Nutt, J. B. Hughes, M. S. Wong, *Environ. Sci. Technol.* **38** (2005) 1346

8. M. Bonarowska, J. Pielaszek, V. A. Semikolenov, Z. Karpinski, *J.Catal.* **209** (2003) 528

9. B. Pawelec, A. M. Venezia, V. La Parola, E. Cano-Serrano, J. M. Campos-Martin, J. L. G. Fierro, *App. Surf. Sci.* **242** (2005) 380

10. L. Prati, A. Villa, F. Porta, D. Wang, D. Su, *Catal. Today.* **122** (2007) 386

11. M. M. Pohl, J. Radnik, M. Schneider, U. Bentrup, D. Linke, A. Brückner, E. Ferguson, *J. Catal.* **262** (2009) 314

12. N. Macleod, J. M. Keel, R. M. Lambert, *App. Catal. A.* **261** (2004) 37

13. D. Kumar, M. S. Chen, D. W. Goodman, *Catal. Today.* **123** (2007) 77

14. D. Kumar, M. S. Chen, C. Yi, D. W. Goodman, *Science.* **310** (2005) 291

15. D. W. Goodmam, *Nature.* **424** (2008) 948

16. M. Chen, D. W. Goodman, *Chin. J. Catal.* **29** (2008) 1178

17. S. Nakamura, T. Yasui, *J. Catal.* **17** (1970) 366

18. B. Samanos, P. Boutry, *J. Catal.* **23** (1971) 19

19. F. Maroun, F. Ozanam, O. M. Magnussen, R. J. Behm, *Science.* **293** (2001) 5336

20. P. Han, S. Axnanda, I. Lyubinetsky, D. W. Goodman, *J. Am. Cham. Soc.* **129** (2007) 14355

21. K. Lou, T. Wei, C. W. Yi, S. Axnanda, D. W. Goodman, *J. Phys. Chem. B.* **109** (2005) 23517

22. M. S. Chen, K. Lou, Z. Wei, Z. Yan, D. Kumar, C. W. Yi, D. W. Goodman, *Catal. Today.* **117** (2006) 37

23. M. Bowker, C. Morgan, *Catal. Lett.* **94** (2004) 131

24. R. M. Ormerod, C. J. Baddeley, R. M. Lambert, *Surf. Sci.* **259** (1991) L709

25. C. J. Baddeley, R. M. Ormerod, A. W. Stephenson, R. M. Lambert, *J. Phys. Chem.* **99** (1995) 5146

26. C. J. Baddeley, M. Tikhov, C. Hardacre, J. R. Lomas, R. M. Lambert, *J. Phys. Chem.* **100** (1996) 2189

27. Z. Li, F. Gao, Y. Wang, F. Calaza, L. Burkholder, W. T. Tysoe. *Surf. Sci*, **601** (2007) 1898

28. B. Gleich, M. Ruff, R. J. Behm. *Surf. Sci.*, **386** (1997) 48

29. T. G. Owens, T. E. Jones, T. C. Q. Noakes, P. Bailey, C. J. Baddeley, *J. Phys. Chem. B*, **110** (2006) 21152

30. L. L. Kesmodel, J. A. Gates, *Surf. Sci.* **111** (1981) L747

31. M. Sock, A. Eichler, S. Surnev, J. N. Anderson, B. Klötzer, K. Hayek, M. G. Ramsey, F. P. Netzer, *Surf. Sci.*, **545** (2003) 122.

32. L. V. Moskaleva, Z. X. Chen, H. A. Aleksandrov, A. B. Mohammed, Q. Sun, N. Rosch, *J. Phys. Chem. C.*, **113** (2009) 2515

33. D. Stacchiola, W. T. Tysoe, *J. Phys. Chem. C.*, **113** (2009) 8001

34. D. Stacchiola, W. T. Tysoe, *Surf. Sci.* **513** (2002) L431

35. J. L. Davis, M. A. Barteau, *J. Am .Chem. Soc.* **111** (1989) 1782

36. J. L. Davis, M. A. Barteau, *Surf. Sci.* **235** (1990) 235

37. M. A. Henderson, Y. Zhou, J. M. White, *J. Am .Chem. Soc.* **111** (1989) 1185

38. E. Jeroro, J. M. Vohs, *J. Phys. Chem. C.*, **115** (2009) 1486

39. A. M. Bradshaw, F. M. Hoffman, *Surf. Sci.*, **72** (1978) 513

40. X. Guo, J. T. Yates, *J. Chem. Phys.*, **90** (1989) 6761

41. P. Liu, J. K. Norskov, *Phys. Chem. Chem. Phys.*, **3** (2001) 3814

42. X. Guo, A. Hoffman, J. T. Yates Jr, *J. Chem. Phys.*, **10** (1989) 5787

43. M. K. Rose, A. Borg, J. C. Dunphy, T. Mitsui, D. F. Ogletree, M. Salmeron, *Surf. Sci.*, **561** (2004) 69

44. V. Pallassana, M. Neurock, V. S. Lusvardi, J. J. Lerou, D. D. Kragten, R. A. Van Santen, *J. Phys. Chem. B.*, **106** (2002) 1656

45. V. Pallassana, M. Neurock, *J. Catal.*, **191** (2000) 301

46. D. Fenske, D. Greshnykh, S. Neuendorf, D. Hoogestraat, H. Borchert, K. Al-Shamery, *Surf. Sci*, **602** (2008) 2101

47. Y. Kuk, L. C. Feldman, P. J. Silverman, *Phys. Rev. Lett.* **50**, (1983) 51112

48. L. Piccolo, A. Piednoir, J.C. Bertolini, *Surf. Sci.*, **592** (2005) 169.

49. L. Piccolo, A. Piednoir, J.C. Bertolini, *Surf. Sci.*, **600** (2006) 4211

50. A. Piednoir, M.A. Languille, L. Piccolo, A. Valcarcel, F.J.C.S. Aires, J.C Bertolini, *Catal Lett.* **114** (2007) 110

51. B.L.M. Hendriksen, S.C. Bobaru J.W.M. Frenken, *Surf. Sci.* **552** (2004) 229

52. J. Kuntze, S. Speller, W. Heiland, *Phys. Rev. B.* **60** (1999) 1535

53. M. Aschoff, G. Piaszenski, S. Speller, W. Heiland, *Surf. Sci.* **770** (1998) 402

54. J. H. Scofield, *J. Electron Spectrosc. Relat. Phenom.* **8** (1976) 129

6. *Conclusions and Future Work*

6.1 Introduction

The studies detailed in the previous chapters have been successful in providing models for the adsorption and decomposition of VAM related molecules on specific Pd-based catalysts under UHV conditions. These results can be related to the mechanism for industrial production of VAM and should enhance the understanding of the processes taking place. There are, however significant differences between the conditions used industrially and those used in these studies and these need to be considered and addressed. In Chapter 1, the areas of VAM synthesis not fully understood were discussed posing the following questions; what are the surface intermediates present, what is the nature of the active catalytic site, how are by-products formed and how does Au affect the catalytic properties of Pd? This study has helped in providing relevant new information regarding these aspects of VAM synthesis.

6.1.1 Interactions with Pd (111)

In Chapter 3, various molecules related to VAM synthesis were introduced to the Pd (111) surface and their reactivity was monitored using XPS and MS techniques. It was determined that oxygen adsorbed dissociatively with an initial sticking probability of ~0.3 at 373K. At ambient temperatures, O_2 surface adsorption was seen to saturate the surface inhibiting uptake above a coverage of 0.25ML. At higher temperatures however, evidence of sub-surface oxygen was observed with the continual uptake of O_2 implying bulk diffusion of surface oxygen atoms is occurring.

The interactions of various organic molecules related to VAM were also studied on the Pd (111) surface. Ethylene, acetaldehyde and acetic acid all readily undergo adsorption at ambient temperatures, saturating the surface. At higher temperatures however decomposition products were observed and steady-state reactivity was seen to occur. This was attributed to the migration of carbon into the bulk of the crystal. It was possible to remove this deposited carbon and to draw carbon from the bulk via oxygen clean-off beam experiments. Despite these organic molecules exhibiting interesting chemistry on the Pd (111) surface, with regards to VAM synthesis these decomposition reactions are highly unfavourable and highlight the potentially destructive nature of the Pd surface.

6.1.2 Interactions with Au/Pd (111)

In chapter 4, Au adlayers were deposited onto the Pd (111) surface via MVD and XPS was employed to observe the growth. Annealing the surface resulted in dissolution of Au into the sample which agrees with previous findings which showed alloying to be a favourable process due to the negative heat of formation[1]. Au adlayers were shown to be unaffected by annealing cycles up to 550K allowing subsequent experiments to be carried out on stable surfaces below this temperature.

Chapter 5 discussed the effect of Au on the reactivity of the Pd (111) surface. Molecules studied previously in Chapter 3 were beamed onto the surface dosed for different coverages of Au. The extent to which the coverage of Au affected the initial sticking probability was strikingly different for the various molecules. For CO,

surface Au atoms inhibited uptake in a similar manner as adsorbed CO. This was also the case for oxygen beam experiments. Au atoms blocked adsorption sites in a similar manner to oxygen atoms. The reactivity of ethylene however was greatly reduced by only a small coverage of deposited Au, which inhibited the adsorption and subsequent decomposition of the molecule. Carbidisation of the surface was therefore inhibited. This finding would seem to be of significance regarding VAM production since the prevention of feedstock decomposition is important in providing optimum yields. The role of Au in the manufacture of VAM may therefore be to prevent the decomposition of reactants and products by passivating the destructive Pd surface.

6.2 UHV vs High Pressure

There are many differences between the industrial VAM synthesis and the molecular beam experiments performed in this study using UHV conditions. One of the main differences is that the industrial catalyst has Au and Pd is dispersed as nanoparticles on a silica support. These nanoparticles have been predicted to display facets with fcc (111) atomic arrangements[3]. Structurally then, UHV studies on Pd (111) may reflect the reactions occurring on such nanoparticles, although in general practical studies on many systems have found that particles do not exhibit specific planes. There is however a large difference in scale between the Pd (111) crystal used in these studies and the much smaller Pd and Au nanoparticles. This would imply that saturation of Pd to Pd carbide by the formation and dissolution of surface carbon may be more pronounced in the industrial case where the particles are only of the order of 100 Pd atoms, and thus do not have significant volume for carbon dissolution. The

nature of the interaction of Pd and Au in the nanoparticles is also of importance and may not reflect the Au/Pd (111) structures used in this study. More information is required on the structures both of the nanoparticulate system and the Au/Pd (111) systems in order to appreciate their differences.

The influence of high pressures in the industrial synthesis, compared to the very low pressures of UHV has the implication that synthesis is less likely in UHV as suggested by Le Chatelier's principle and entropy laws. Recent work by Goodman on VAM synthesis showed a surprisingly low turnover frequency for VAM on Pd suggesting that VAM synthesis, and hence the probability of reaction between oxygen, ethene and acetic acid will be much lower in UHV where the beam pressure is many orders of magnitude lower than in the industrial synthesis[3].

6.3 Future studies

Despite the significant amount of interest in VAM synthesis in recent times, there are still questions which remain unanswered. Based on the findings in this study, there are several opportunities for future work. The direct reaction of ethylene and acetic acid on the Pd (111) surface using the molecular beam reactor was shown not to result in the formation of VAM. It was concluded that the initial preadsorption of oxygen could facilitate this reaction. An attempt should therefore be made to synthesise VAM in UHV by introducing a mixed beam of ethylene and acetic acid to the Pd (111) surface preadsorbed with oxygen. Care would have to be taken when analysing the results since the amount of VAM produced would probably be minimal

in comparison to the extent of by-products formation. These experiments could be monitored across a variety of surface temperatures in order to elucidate the optimum conditions for VAM production.

The growth of Au and the effect of annealing the surface were studied in Chapter 4. Further studies regarding the growth mode and presence of surface structures could be carried out using techniques such as LEED and STM. These studies would help clarify the nature of the surface with regards to molecular adsorption. Restructuring of the surface could also be observed as the surface is annealed and Au diffuses into the bulk. Similar STM and LEED studies could also be employed to analyse the formation and diffusion of surface carbon from the decomposition of organic molecules. Careful studies could shed light on the nature of the stable sub-monolayer carbon coverage observed across a range of temperatures. Further studies of ethylene dosed on low coverages of Au could be carried out using RAIRS or HREELS to examine the bonding of the molecule to different adsorption sites.

The formation of the Au dosed Pd (111) surface is a model representing how the two metals may interact on the real catalyst. Since this representation may be different from the actual Au and Pd interactions on the real catalyst, an attempt to mirror the real system more closely would be of interest. This could be carried out by producing Pd and/or Au nanoparticles on a silica surface and carrying out similar experiments regarding VAM related molecules. Titania could also be used as a Au and Pd nanoparticle support allowing easier analysis with STM. Any changes in size and distribution of these particles after annealing the surface at different temperatures

could be monitored using imaging techniques and any changes in reactivity could also be examined using the molecular beam reactor. The addition of a support material may also introduce SMSI effects into the surface processes which may have a significant effect on surface reactivity.

Potassium acetate is employed as a promoter in the industrial production of VAM, however there are few studies investigating the interaction of K on Au or Pd surfaces. The role of K could be explored with regards to its effect on the relative stability of surface intermediates. In order to examine its effect on the surface, K could be evaporated onto the surface in a similar way to the MVD approach used for Au deposition.

6.4 References

1. H. H. Shih, E. Bauer, H. Poppa, *Surf. Thin Solid Films* **88** (1982) L21
2. B. Samanos, P. Boutry, R. Montarnal, *J. Catal.*, **23** (1971) 19
3. E. M. McCash, 'Surface Chemistry' ISBN 0-19-850328-8
3. Y. F. Han, D. Kumar, C. Sivadinarayana, D. W. Goodman, *Abstr. Papers Am. Chem. Soc.*, 227: 37 – Petr, Pt. 2 (2004).